

Development and Evaluation of two Methods for a standardized
Quantification of global and regional Information in
Nuclear Radioisotope Studies.

Dissertation to obtain
the Doctor's Degree
of the
Albert Szent-Györgyi
Medical University
Szeged, Hungary

by
Rolf Weller



Ulm, 1991

Index

1	Introduction.....	1
2	New methods.....	3
2.1.	Onion-skin-method.....	3
2.1.1	Introduction.....	3
2.1.2	Mathematical derivation and algorithm for onion-skin-background.....	3
2.1.3	Mathematical derivation and algorithm for onion-skin-EF.....	8
2.1.4	The linear regression and the error bandwidth of the algorithm.....	13
2.1.5	Method validation.....	16
2.1.6	Materials and results.....	18
2.1.6.1	Mathematical model and results.....	18
2.1.6.2	Physical model and results.....	21
2.1.7	Discussion.....	24
2.1.7.1	Mathematical model.....	24
2.1.7.2	Physical model.....	25
2.1.8	Onion-skin-method conclusion.....	25
2.2	Circle reference method.....	26
2.2.1	Introduction.....	26
2.2.2	Principle of the method.....	27
2.2.3	Reversibility.....	29
2.2.4	Improvements.....	31
2.2.5	CRF-method conclusion.....	32
3	Radio-Nuclide-Ventriculography.....	35
3.1	Method.....	35
3.2	Application of Onion-skin-method in RNV.....	36
3.2.1	Method and result verification on angiographic data.....	36
3.2.2	Creation of normal EF-values and statistics.....	38

Index

3.2.3	Discussion of the results.....	39
3.3	Application of CRF-method in RNV.....	42
3.3.1	Creation of normal pattern and statistics.....	42
3.4	Definition of defect-pattern.....	45
3.5.	Recent and published application of the CRF-method.	47
4	Gated-spect radionuclide ventriculographie (Gaspect).....	50
4.1	Introduction.....	50
4.2	Data-acquistion.....	50
4.3	Conventional Data-processing.....	51
4.4	Gaspect processing.....	52
4.4.1	Flash-Spect-method.....	52
4.4.2	Coefficients-reconstruction-theory.....	52
4.4.3	Reconstruction-procedure.....	54
4.4.4	Reorientation due to heart axis.....	55
4.4.5	Replanarisation.....	58
4.4.6	Creation of four heart-axis-related Ventriculograms.....	65
4.5	Global values evaluation.....	68
4.5.1	Global values results.....	70
4.5.2	Global values discussion.....	73
4.6	Application of CRF-method for detection of RWMA....	74
4.7	Recent and published applications of the method....	75
5	Brain perfusion studies with HMPAO.....	77
5.1	Introduction.....	77
5.2	Acquisition.....	77
5.3	Data processing.....	78
5.3.1	Reorientation of the tomographic data-set.....	79
5.3.2	Axial normalization.....	80
5.3.3	Application of CRF-method in brain spect studies...	81
5.3.4	The standardization of the data set.....	82

Index

5.3.5	Creation of normal pattern and statistics.....	83
5.3.6	The error of the method.....	85
5.3.7	ROI definition in circle reference data set.....	86
5.4	Application of the method in an individual study...	92
5.5	Recent and published applications of the method....	95
6.	Conclusion.....	97
7.	Abbreviations.....	100
8.	Acknowledgments.....	101
9.	References.....	102

1 Introduction

From the beginning, nuclear medicine has been a discipline featuring the cooperation between physicians, physicists and engineers. Standard mathematical algorithms like Fourier-analysis, Factor-analysis and others have been made available for data-processing by this cooperation. A multitude of processing options do exist and will bring its own variation to the presentation of the results and to the results themselves. However, each method leading to a presentation covers only one aspect of the data, representing the connection between physiology and the physical method on one side, and between measurement and the resulting presentation on the other side.

The aim of this paper is the presentation of two new methods, their comparison to conventional methods and the description of their potential application.

The first, the "onion-skin method", is an algorithm which quantifies the contamination of count rates (or derived values) by a special way of observation techniques. The contamination rate is being assessed as function of the size of the ROI. The sampling process itself is the so called onion skin method, illustrating the peeling of the once defined ROI skin by skin. The relation of the measured count rate to the continuously decreased ROI, expressed by a mathematical function, can be used to quantify contamination values.

The second, the "circle reference method", serves to quantify regional parameters. This algorithm removes the influence of different shapes and forms of several scans, by

a reversible transformation to a circle. It can be used to create databases of normal pattern and to compare individual scans against it.

The methods, tested by mathematical and physical models have found entrance in our routine work recently. As far as the clinical application of the method in patients is concerned, it is clear that the studies have been done under the responsibility of a nuclear physician.

2 New methods

2.1. Onion-skin-method

2.1.1 Introduction

Since the introduction of radionuclide ventriculography the determination of left and right ventricular ejection fraction was subject of many studies and improvements (Ref. 1,2,3,4,6). Most of these efforts resulted in sophisticated edge-detection algorithms to optimize ROI definition for enddiastolic/endsystolic left and right ventricular and background regions. However, due to statistical limitations and the geometric count distribution the determination of the true background remains uncertain. Aim of this study was the introduction of a new method whereby the EF and background could be calculated without defining the endsystolic and background region. It is furthermore insensitive to enddiastolic region definition. When applying this algorithm to a single image from any other study the calculation of background in a defined region is inherently possible.

2.1.2 Mathematical derivation and algorithm for onion-skin-background

The routinely used standard method for the determination of over- or underlying background is the calculation of mean counts in a defined background region (Ref. 9,39). The mean counts measured in this region are expected to be the mean contaminating counts in the region of the interesting organ as well. In the past the statistical error of the background and its influence on derived values has been evaluated (Ref. 31). However the relevance of the

chosen ROI to be projected to the interesting region remains subject of personell skill and training. This new approach allows the observation not only of the statistical but also of the systematical errors of background evaluation.

The method for calculation of background requires:

OCO Object counts
 BGO Background contamination of the object in counts
 BG_i Background in individual ROI in counts
 AR_i Area of individual ROI in pixel
 CM_i Counts measured in an individual ROI
 BGM Mean background in the ROI in counts per pixel

It is obvious if a background contaminated object is measured in a region of interest the resulting counts are:

$$CM_i = OCO + BG_i \quad [I]$$

In the defined region of interest there is a mean background contamination per pixel:

$$BGM = BG_i / AR_i \quad [II]$$

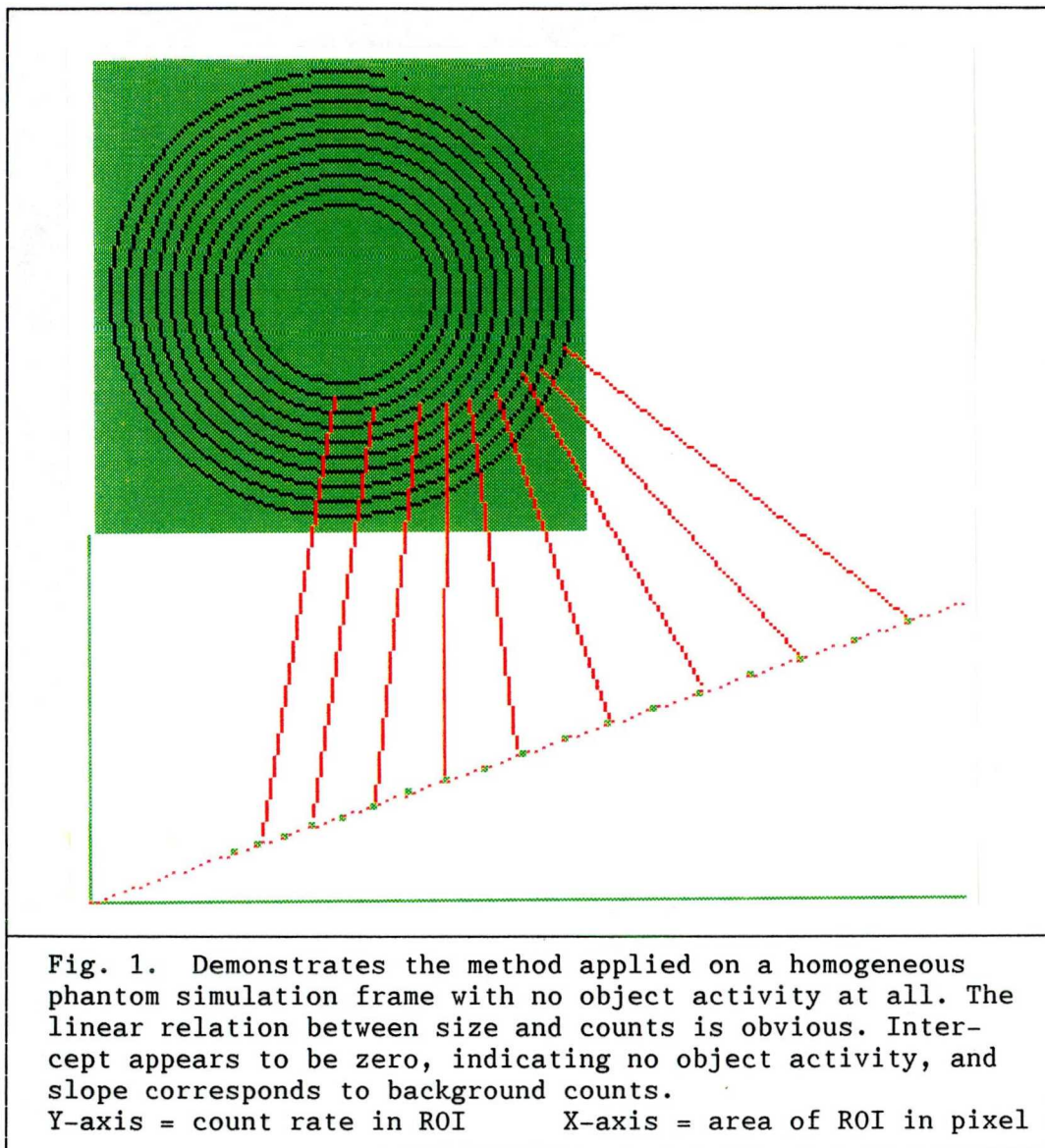
this mean background value is the mean background value of a reasonable defined ROI outside the real object area, and is generally expected to be the mean valuable background value for the object as well. This observation represents the basis of the commonly used method for background subtraction.

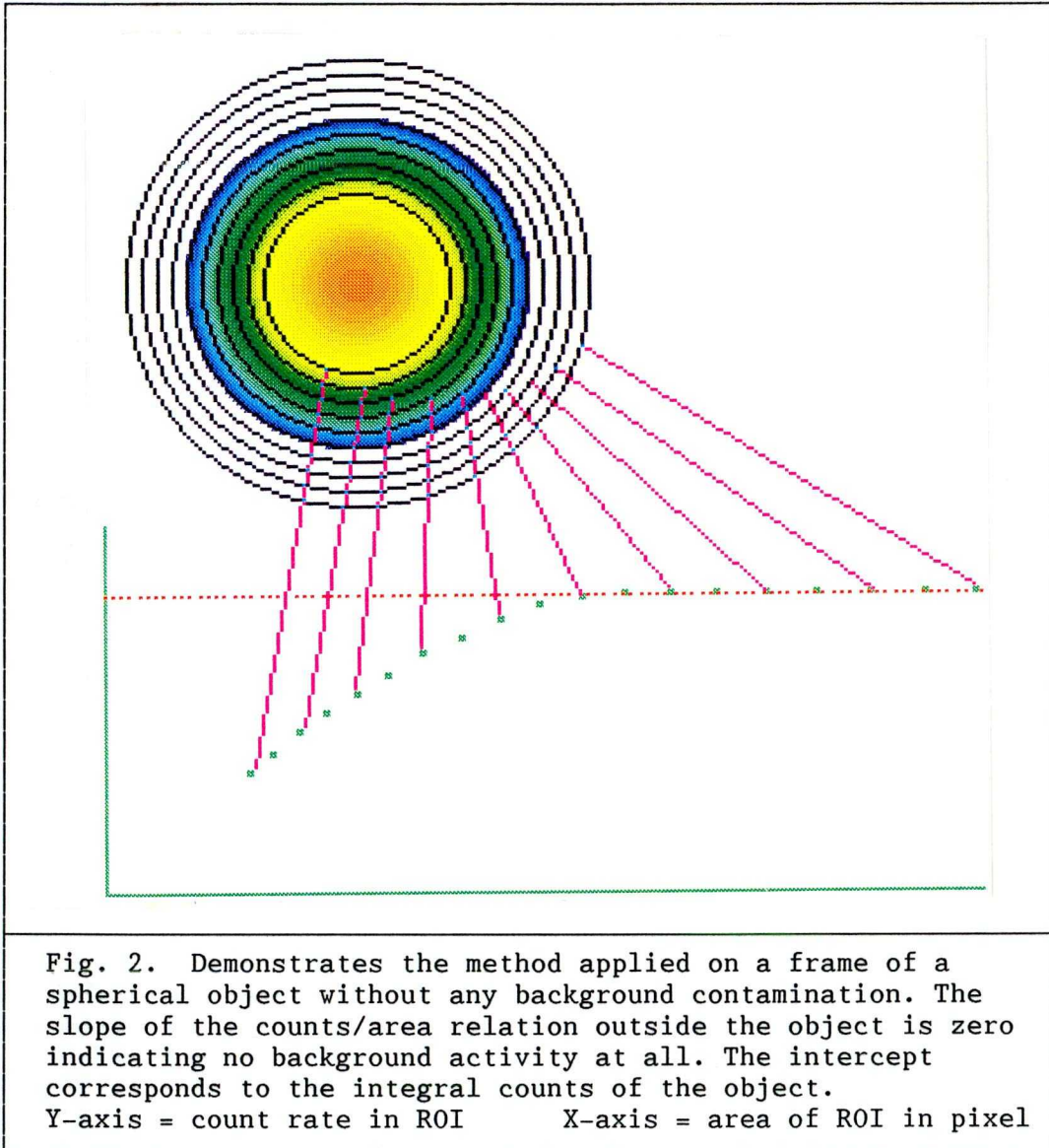
By inserting [II] in [I] the resulting equation unmaskes its straight line character.

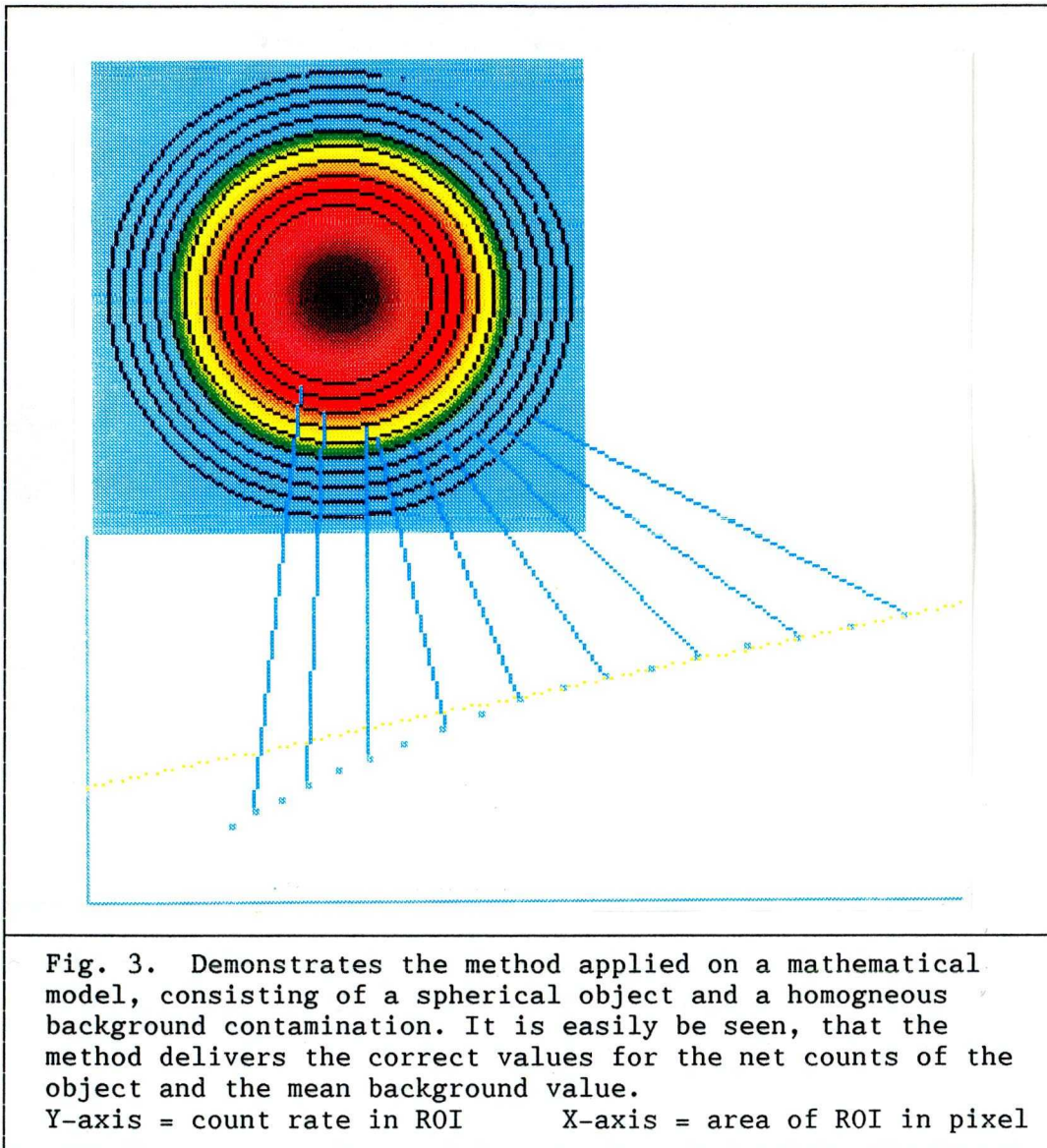
$$CM_i = OCO + BGM * AR_i \quad [III]$$

This formula leads to the simple algorithm:

A generously defined ROI around the object is reduced in size in an onion skin manner. As long as the ROI is defined outside the real object the relation between the measured, background contaminated counts CM_i and the size of ROI AR_i is linear and can be described by a straight line fit. This fit results in an intercept and a slope of the straight line. Where the intercept corresponds to the net counts of the object and the slope corresponds to the mean background counts.







2.1.3 Mathematical derivation and algorithm for onion-skin-EF

The idea of quantification of the influence of contamination values has been applied on the technique of ejection fraction calculation. Thereby a new method for calculation of true ejection fraction (EFT) was developed and requires:



EDV	Enddiastolic volume
ESV	Endsystolic volume
EDC	True ventricular enddiastolic counts
BGD	True ventricular enddiastolic background
ESC	True ventricular endsystolic counts
BGS	True ventricular endsystolic background
EDM	Measured ventricle enddiastolic counts
ESM	Measured ventricle endsystolic counts
IV	Intermediate variable (dummy ejection fraction)
FD	Endiastolic number of pixels
FS	Endsystolic number of pixels

The formula for the calculation of the true ejection fraction (EFT) is familiar:

$$\text{EFT} = \frac{\text{EDV} - \text{ESV}}{\text{EDV}} \quad [1]$$

If there is a linear relation between true counts and volume, the correct formula for the calculation of EFT is:

$$\text{EFT} = \frac{\text{EDC} - \text{ESC}}{\text{EDC}} \quad [2]$$

A new variable dummy ejection fraction IV is calculated, regardless of any background contamination:

$$IV = \frac{EDM - ESM}{EDM} \quad [3]$$

A closer look at this formula leads to understanding of the background contamination:

$$IV = \frac{(EDC+BGD) - (ESC+BGS)}{(EDC+BGD)} \quad [4]$$

Remove the brackets and rearrange, then

$$IV = \frac{EDC - ESC + BGD - BGS}{EDC + BGD} \quad [4a]$$

Divide the numerator and denominator by EDC:

$$IV = \frac{\frac{EDC - ESC}{EDC} + \frac{BGD}{EDC} - \frac{BGS}{EDC}}{1 + \frac{BGD}{EDC}} \quad [4b]$$

Insert equation [2] :

$$IV = \frac{EFT + R - \frac{BGS}{EDC}}{1 + R} \quad [5]$$

introducing variable

$$R = \frac{BGD}{EDC} \quad [5a]$$

Therefore

$$EDC = \frac{BGD}{R} \quad [5b]$$

$$IV = \frac{EFT + R - \frac{BGS}{BGD} * R}{1 + R} \quad [6]$$

If assuming the same homogenous background in enddiastole and endsystole, the quotient BGS/BGD can be replaced by the quotient of the endsystolic/endeddiastolic areas or the quotient of the respective number of pixels FS/FD. On rearranging, equation [6] becomes:

$$IV = \frac{EFT + R}{1 + R} - \frac{R}{1 + R} * \frac{FS}{FD} \quad [7]$$

i.e. the straight line

$$Y = A + B * X$$

with

$$A = \frac{EFT + R}{1 + R}; \quad B = -\frac{R}{1 + R}; \quad X = \frac{FS}{FD} \quad [8]$$

It is obvious that for any given x value the function value y can be calculated. This fact leads to a procedure, which allows the calculation of several points on the straight line:

to this effect the above function can be plotted by varying the ratio of the enddiastolic/endsystolic areas ($X=FS/FD$). Take care to be outside of the obvious end-systolic ventricular boundary. The relation of IV to the quotient FS/FD should be linear and the coefficients of the straight line equation bear the information of EFT. The coefficients A and B can be evaluated by a simple linear regression. With that information, true ejection fraction EFT can finally be evaluated.

From equations [8] :

$$EFT = A*(1 + R) - R \quad [9a]$$

Inserting from [8]

$$EFT = A*\left(\frac{1 + B - B}{1 + B}\right) + \frac{B}{1 + B} \quad [9b]$$

which yields for the true ejection fraction:

$$EFT = \frac{A + B}{1 + B} \quad [10]$$

Also,

$$\text{EDM} = \text{EDC} + \text{BGD} \quad [11]$$

With division by BDG and equation [5a]

$$\frac{\text{EDM}}{\text{BGD}} = \frac{1}{R} + 1 \quad [12a]$$

$$\text{BGD} = \text{EDM} * \frac{R}{1 + R} = \text{EDM} * (-B) \quad [12b]$$

2.1.4 The linear regression and the error bandwidth of the algorithm

The calculation of the straight line parameters is relatively simple and is done in a standard manner (Ref. 5). Aim of the method is to define a straight line of the form

$$y = A + B * x$$

as a so called line of best fit or sample regression line. The method can be understood geometrically: If we measure the distance between a point (x_i, y_i) and a line $y = A + B * x$ vertically by $D_i = |y_i - (A + B * x_i)|$, then the regression line is that one which minimizes the sum of the squared distances to the n points. The mathematical solution for this problem is:

$$B = \frac{\sum (x_i - \bar{x}) * (y_i - \bar{y})}{\sum (x_i - \bar{x})^2}$$

and

$$A = \bar{y} - B * \bar{x}$$

where

$$\bar{x} = (1/n) \sum x_i, \text{ and } \bar{y} = (1/n) \sum y_i$$

The quality of the linear regression fit to the data resulting from the area ratio outside the endsystolic region depends on the compliance of each data point with the mathematical theory. For the resulting regression line a confidence interval can be calculated, describing the area wherein probable regression lines are possible. Intercept and slope are the relevant parameters for the calculation of EF and background and consequently their errors determine the error bandwidth of EF and background. Because the slope of the regression line is always negative, maximal intercept and the most negative slope for the upper error threshold on the one hand and minimal intercept and the most positive slope for the lower error threshold on the other hand will be the relevant parameters. The regression analysis describes the error of intercept as (Ref. 5):

$$ERR_A = s * t_{n-2} \left(\frac{\alpha}{2} \right) * \left(\frac{1/n + \bar{x}^2}{\sum (x_i - \bar{x})^2} \right)^{\frac{1}{2}}$$

and the error of the slope as (Ref. 5):

$$ERR_B = s * t_{n-2} \left(\frac{\alpha}{2} \right) * \left(\sum (x_i - \bar{x})^2 \right)^{\frac{1}{2}}$$

n = number of points

s = uniformly minimum variance unbiased estimate of σ
(Ref. 5)

t = student distribution

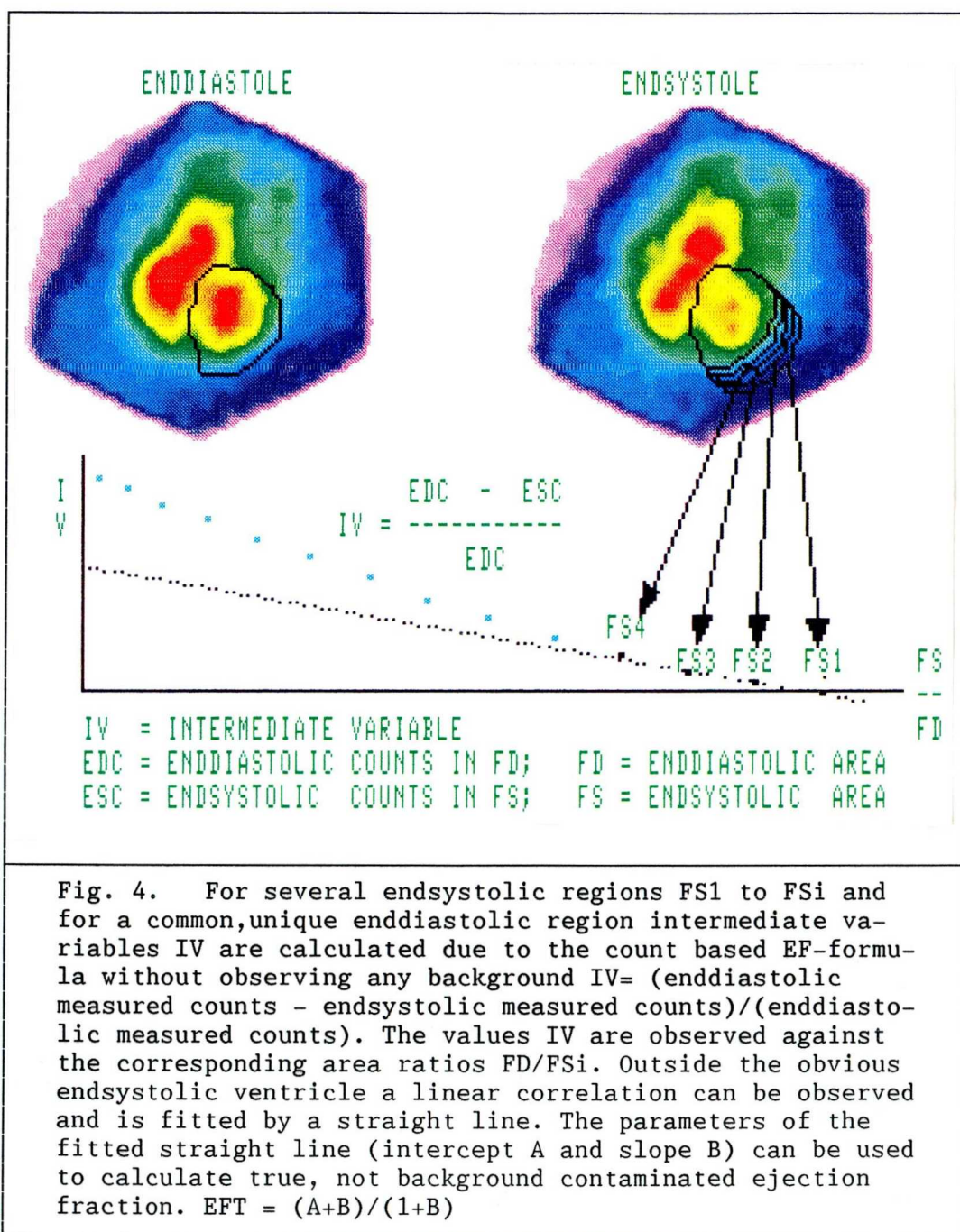
The EF error bandwidth is defined as:

$$EF_{\max} = \frac{A + ERR_A + B - ERR_B}{1 + B - ERR_B}$$

$$EF_{\min} = \frac{A - ERR_A + B + ERR_B}{1 + B + ERR_B}$$

2.1.5 Method validation

The mathematical derivation described leads to a simple and easy to use algorithm. The RNV-study is acquired and processed in a standard manner (Ref. 3,6). The processing results in an enddiastolic and an endsystolic image, and in a left ventricular enddiastolic region defined by Fourier analysis of the cyclic motion of the heart. This enddiastolic region is expanded to the lateral wall and to the apex by 3 pixels. Starting with this area as endsystolic region, several intermediate variables (IV) were calculated, according to the count based EF-formula without background consideration, reducing the endsystolic region step by step in an onion-skin manner (see Fig. 4). These intermediate variables were observed against the area quotient of endsystolic and enddiastolic regions and show a linear correlation according to the mathematical theory. This linear correlation is only true outside the endsystolic ventricle, therefore only values which fulfill this condition are processed by a linear regression fit (Ref. 5). The parameters of this fit, intercept and slope, allow the calculation of ejection fraction and background according to the formulae [10,12b].



2.1.6 Materials and results

2.1.6.1 Mathematical model and results

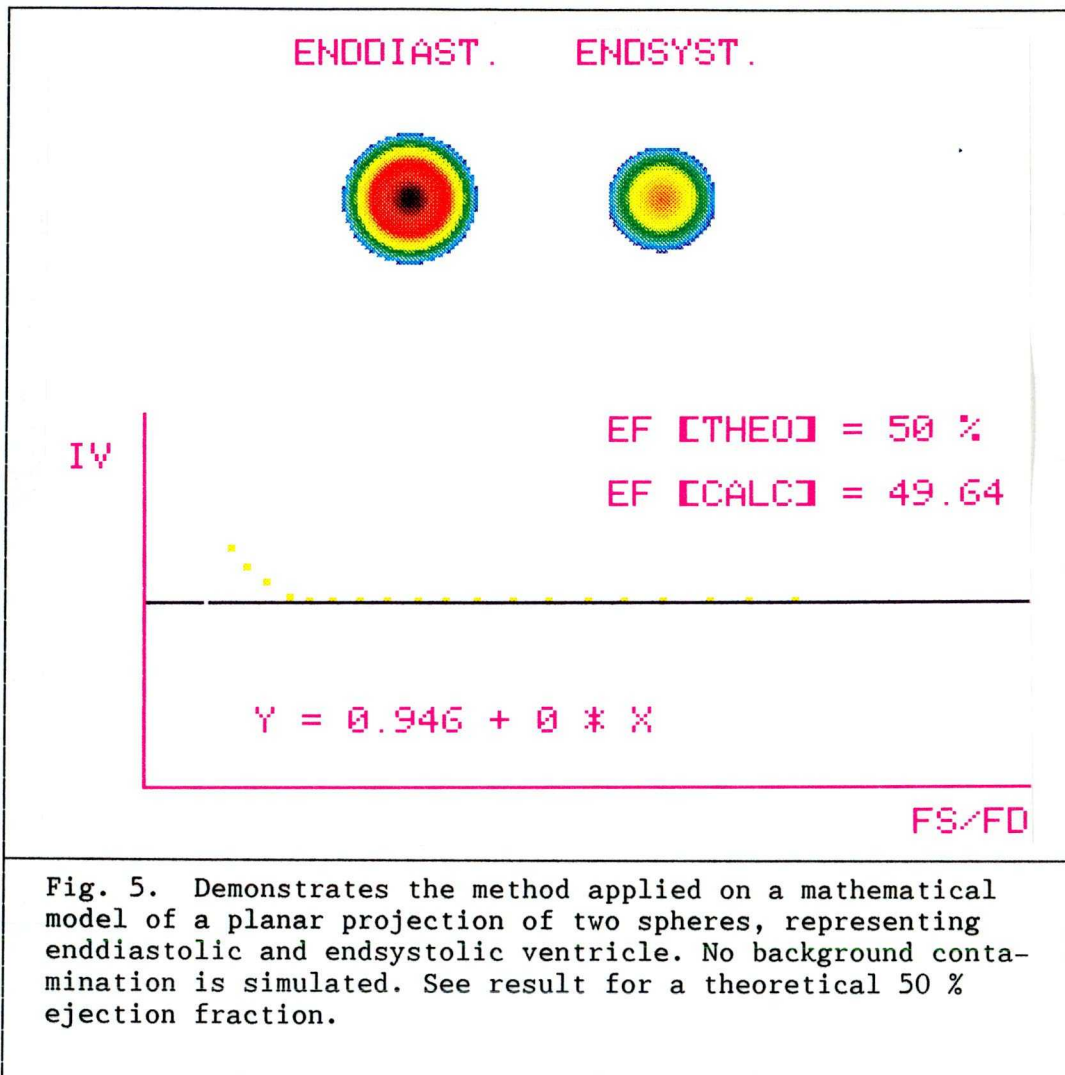
As a first step the procedure is applied to a mathematical model. The model describes the planar projection of two spherical sources of radioactivity simulating an isolated ventricle in enddiastole and endsystole. The volumes of the spheres are chosen so that theoretical ejection fractions between 10 and 90 percent can be simulated. These theoretical ejection fractions are compared with those calculated, see Tab. 1 for results. This is done with a correct enddiastolic region as well as with an enddiastolic region which is far too big, demonstrating the independence of the method to a non correct diastolic region. The planar projections are subsequently background overlaid by addition of a homogeneous phantom image, to demonstrate the ability of the method to evaluate background contamination of region counts.

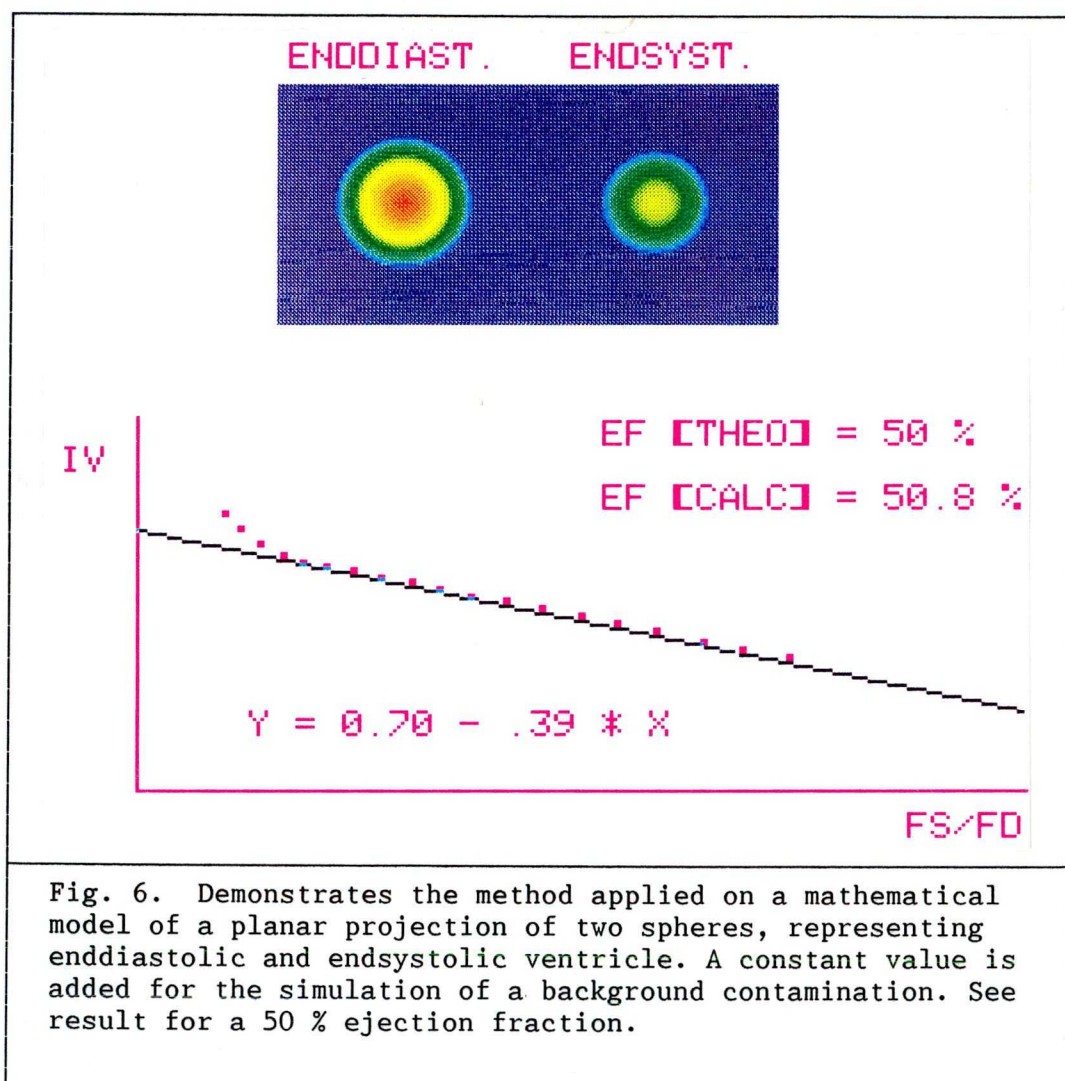
TABLE 1

Calculated EF versus theoretical EF with correct and enlarged enddiastolic region in a mathematical model.

Theoretical E F	C a l c u l a t e d E F (E F T)			
	ED-ROI enlarged		ED-ROI correct	
	w/o BG	with BG	w/o BG	with BG
10	9.773	9.661	9.643	9.784
20	19.856	19.725	19.663	20.041
30	30.233	29.744	29.638	30.363
40	40.072	39.733	39.584	40.498
50	50.025	49.837	49.643	50.759
60	59.945	59.739	59.502	60.944
70	69.989	69.764	69.483	71.014
80	80.015	79.771	79.446	81.309
90	90.009	89.747	89.378	91.446

All EF values in [%]





2.1.6.2 Physical model and results

As a second step five glass balls with different volumes are filled with the same activity concentration. The spheres with 250, 100, 50, 25 and 10 ml are counted in various enddiastolic and endsystolic combinations (Tab. 2) with and without background contamination simulated by a homogeneous phantom. From the combinations of those images all possible ejection fractions are calculated.

The background counts resulting from a flood phantom in the full field of view were 51959 counts and the prevailing background was 543 counts.

The counts in the whole field of view correlated to the volumes of the balls with a regression of $y = 1255x + 9426$ and a correlation coefficient $R^2=0.999$ in the study w/o background contamination. In the study with background contamination the regression line was $y = 1294x + 57817$ and the correlation coefficient $R^2=0.999$.(Fig. 7)

The background contaminated ejection fractions are listed in Tab. 2 and correlated to $y = 1.013 x + 2.703$ with a correlation coefficient $R^2=0.999$.

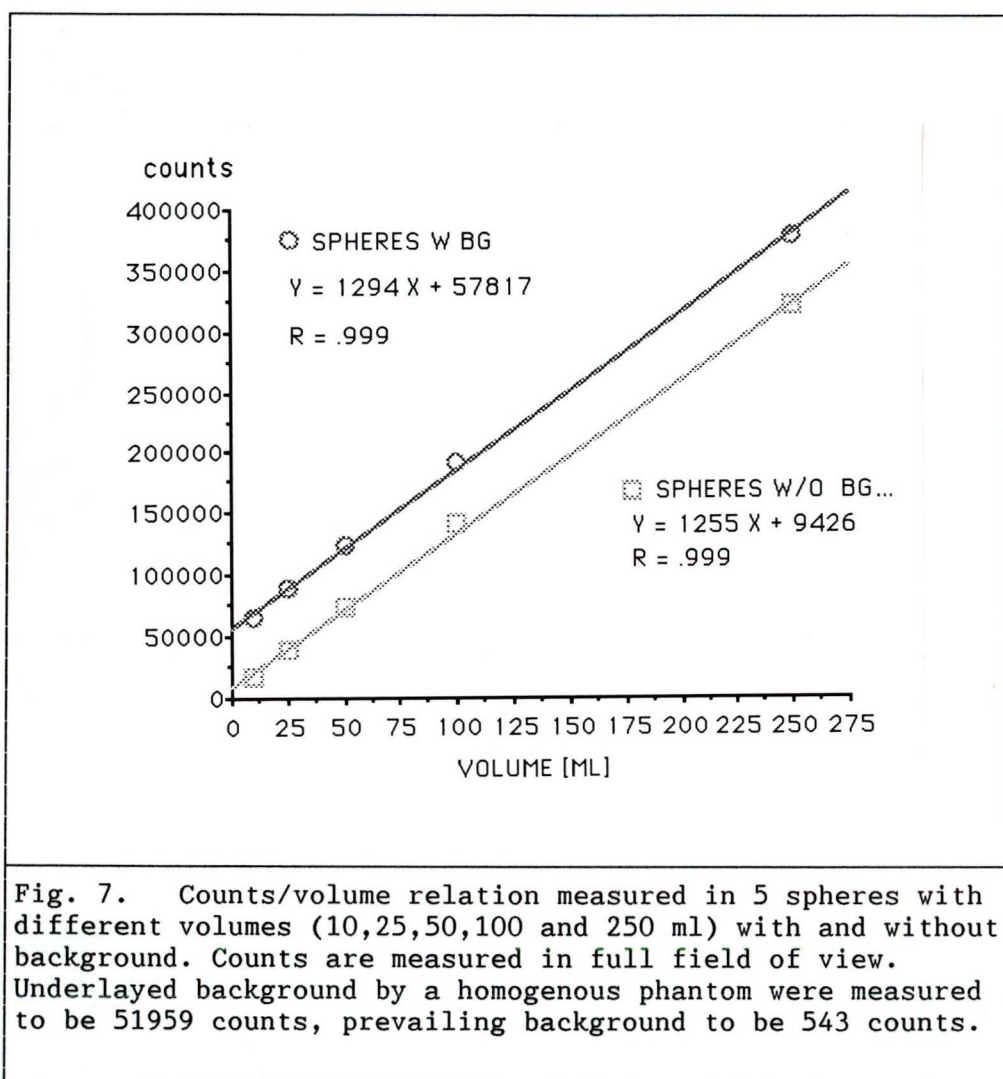
The non background contaminated ejection fractions (Tab. 2) correlated to $y = 1.017 x + 3.179$ with a correlation coefficient $R^2=0.998$.

TABLE 2

Theoretical EFs are derived from the combination of 5 spheres.
 EFs were calculated in studies with and without background
 contamination

		Theoretical	C a l c u l a t e d EFT	
ED.Vol.	ES. Vol.	EF	w/o Bckgrd	with Bckgrd
250	100	60	56.415	56.977
250	50	80	77.07	77.553
250	25	90	88.078	88.414
250	10	96	95.027	95.063
100	50	50	47.605	48.037
100	25	75	72.886	73.332
100	10	90	88.705	88.665
50	25	50	48.574	48.982
50	10	80	78.621	78.399
25	10	60	58.546	57.944

All volumes in [ml], all EF values in [%]



2.1.7 Discussion

2.1.7.1 Mathematical model

The evaluation of the method with a mathematical model serves to verify the algorithm and programme. The deviation of the results is within the range of calculation precision. In this model, the results are completely independent of enddiastolic region definition. Obviously, this is only partly due to the completely homogenous back-

ground and the single ventricle model, chosen for the experiment. In practice, therefore it is also expected that the method will be rather insensitive to endiastolic edge detection variations.

2.1.7.2 Physical model

The counts in the total field of view show, with and without background contamination, an excellent linear correlation. However, the intercept of both correlations show an error offset of 9425 counts, which in this case represents approximately 8 ml in volume. This has to be explained by differing internal absorption in the spheres and by the fact that there may be some relevant information, especially for the larger spheres, lost outside the field of view. The different ejection fraction values, with and without background, correlate highly significantly to the given model values. The slopes with values of respectively 1.013 and 1.017 are approximately equal to unity and the intercept offsets of respectively 2.703 and 3.179 can be explained by the overall count/volume relation as discussed above in terms of internal absorption and the lost counts effect.

2.1.8 Onion-skin-method conclusion

Subject of this method is the quantification of contamination values. The algorithm constructs a linear influence of such values so that they can be described mathematically by a linear regression fit. With the information of the parameters obtained from the regression analysis all derived values can be recovered without background contamination. The method was tested and verified in mathematical and physical models and in patient data and

showed good correlations of EF and background values to those of contrast medium ventriculography and to those of nuclear medicine standard procedure. In fact, the background of any static image can be evaluated, when choosing the same image for "enddiastolic" and "endsystolic" region, with implications to be further studied. Because of its insensitivity to variations in ROI definition variations this method yields highly reproduceable values and could commendably be applied to fully automated procedures.

2.2 Circle reference method

2.2.1 Introduction

Although most of the radionuclide studies of various organs are digitized nowadays and lend themselves to quantification, for example by ROI-techniques, it is nearly impossible to establish reference matrices of a normal count density distribution pattern which would allow quantitative comparison of the individual study against that normal matrix. This shortcoming is due to the wide variation of shape, size and position of human organs and, accordingly, of the radionuclide scans. Thus, individual studies cannot be superimposed accurately enough for computing an organ or scan related normal matrix. Only recently, a pixel matrix of normal for the distribution of Tl-201 in myocardium during exercise on a polar coordinate display of SPECT studies was established (Ref. 10) and further developed for quantification of washout (Ref. 11) and extended to resting blood flow distribution with display of an ischemia image (Ref. 12,13) and attempts were undertaken to create reference matrices, for example for planar brain studies (Ref. 14) in the past. Here, a new and simple procedure is presented that allows

the transformation of essentially any digitized nuclear medicine study into a standard reference matrix without losing information. The same procedure can be used to compute - out of a normal data base - a normal reference image against which the individual studies can be compared in terms of significantly abnormal regional count distribution. This procedure is illustrated using the amplitude heart image as a first application.

2.2.2 Principle of the method

The objective of this method is the transformation of an individual scan into a standard sized reference circle matrix. The algorithm was programmed on a common Nuclear Medicine computer system. The point of gravity inside the left ventricular ROI on the amplitude scan was determined. From this point, the count density profiles of the radii, which are of various length, were obtained in 720, 360, 180 or 72 sampling angles and were transformed into a 128 by 128 matrix, with the diameter of the standard circle being 120 pixel in size as shown in Fig. 8. 720 angle steps as upper limit was chosen because the number of pixels on the outer circumference of a 120-pixel diameter circle is more than 400. The radii were 1 pixel thick, and the profiles of each angle were transferred into the equivalent radius profile of the reference circle by simple linear interpolation to fit the individual profile to the radius of the reference circle as also illustrated in Fig. 8. The different number of sampling angles was chosen to determine the minimum number of angles needed to cover all pixels of the outer edge of the left ventricular ROI. Thus, the whole information of the unevenly shaped left ventricular region is transformed radius by radius into the reference circle. The total counts of the reference circle were normalized to 1500 K for standardization.



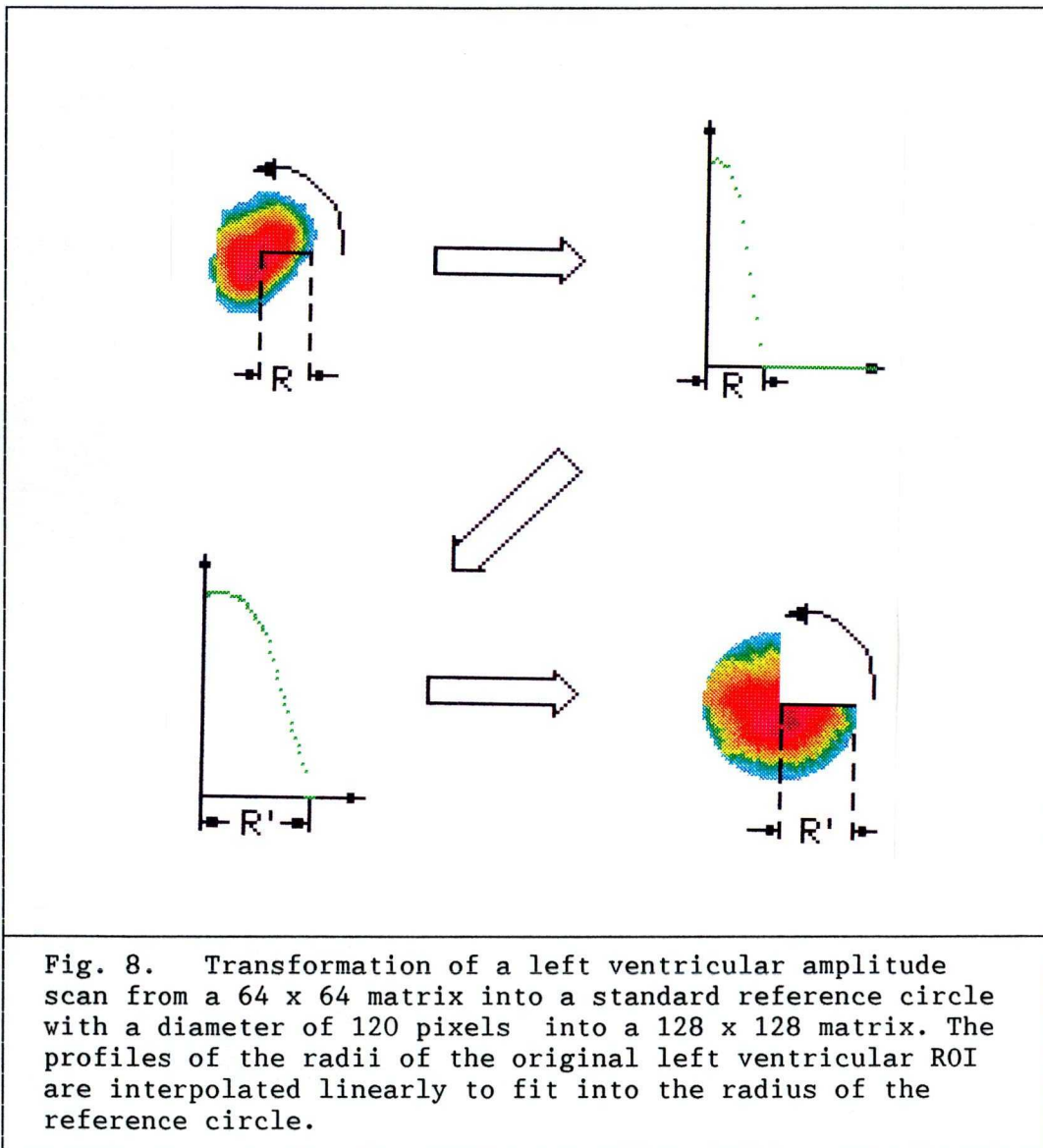
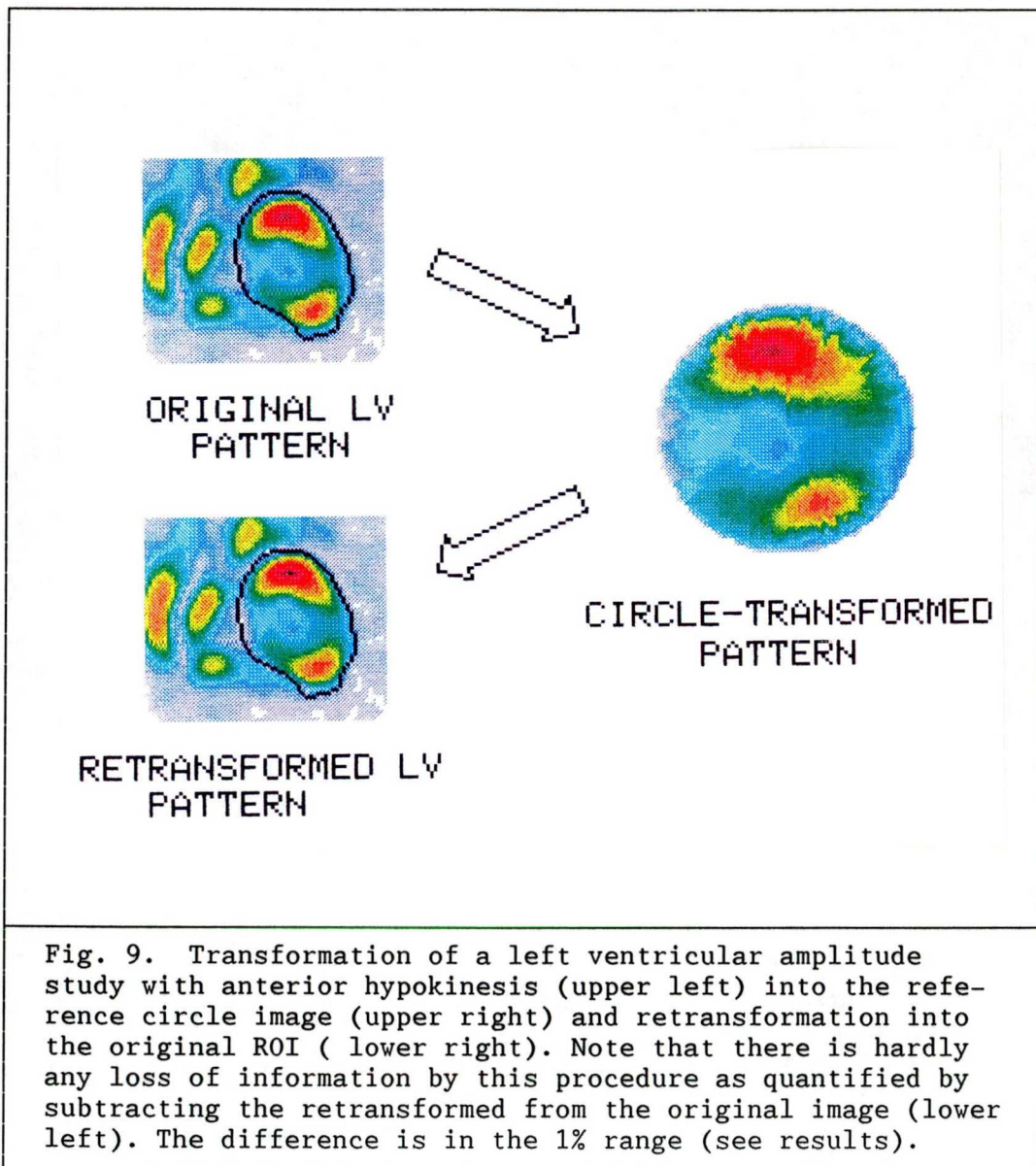
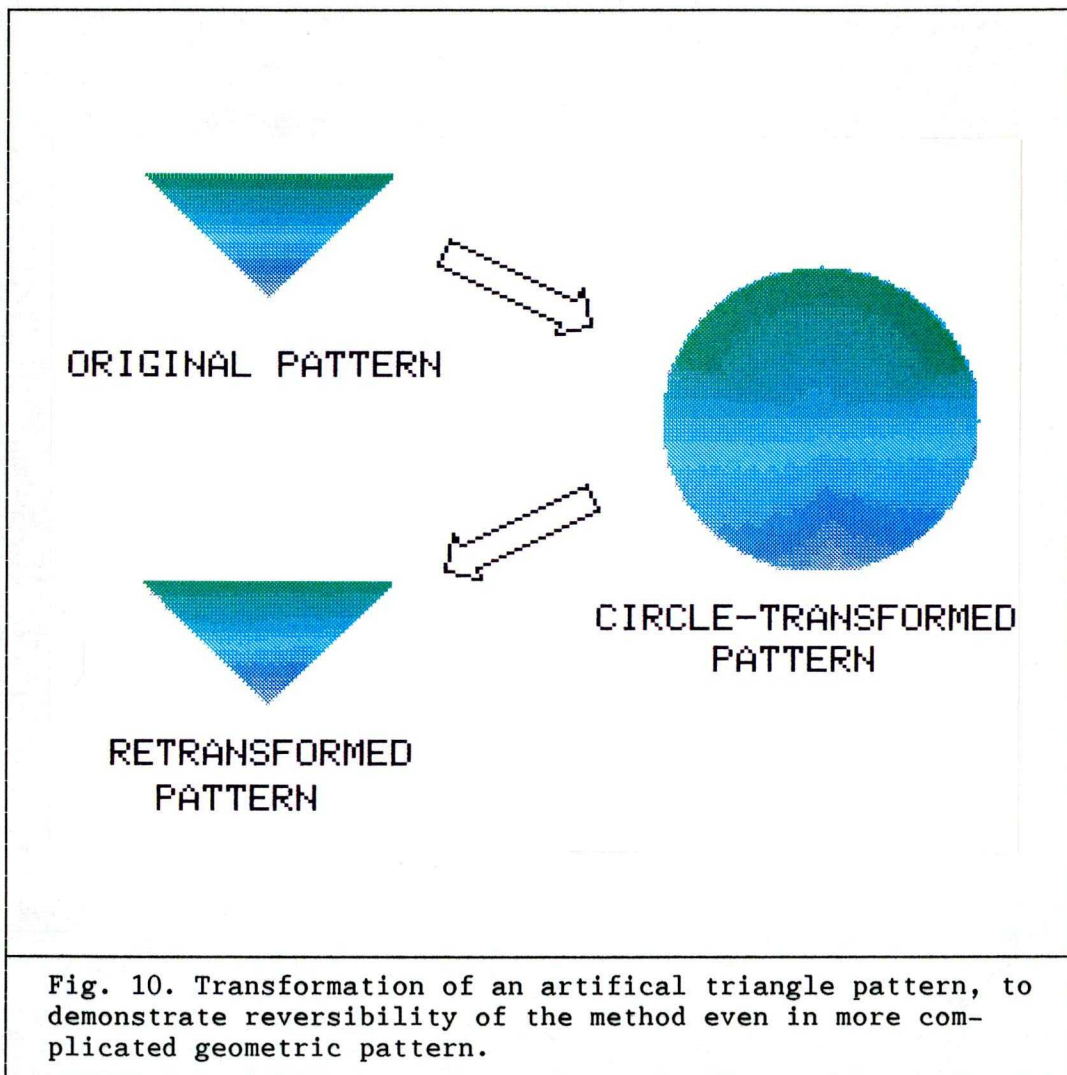


Fig. 8. Transformation of a left ventricular amplitude scan from a 64×64 matrix into a standard reference circle with a diameter of 120 pixels into a 128×128 matrix. The profiles of the radii of the original left ventricular ROI are interpolated linearly to fit into the radius of the reference circle.

2.2.3 Reversibility

The whole procedure is completely reversible without loss of information as shown in Fig. 9 in a study with a decreased amplitude in the anterior myocardium. The reversibility and, thus, the accuracy is documented quantitatively by subtracting the retransformed image from the original image. Averaging this differences of all images retransformed and subtracted from their originals in this study, i.e. 20 normals and 1 example, resulted in only 1.2±0.4 % normalized to the original image for the 720-angle transformation, in 1.0±.3 % for 360-angle sampling, in 0.9±0.5 % for the 180-angle steps but in 5.9±6.4 % for the 72-angle transformation. The latter was significantly ($p < 0.001$) different to 720-, 360- and 180-sampling. Although 360- or 180-sampling angles were sufficient in most instances in two cases with dilated left ventricles - and thus larger outer ROI circumferences - only 720-sampling did cover the whole information and was thus used for all further processing.





2.2.4 Improvements

The transformation procedure described in the chapter 2.1.2 has the disadvantage that the points near the center are multiply determined. To handle that situation, the information which ever comes last is taken. As far as the retransformation is done by the same philosophy the results are consistent. However it is more elegant and perhaps even less time consuming, not to proceed in angle-steps but in pixel-steps.

2.2.5 CRF-method conclusion

Objective interpretation of nuclear medicine studies is a desired goal as shown by the useful application of parametric images, such as amplitude and phase images of heart studies, factor analysis images and polar coordinate images of myocardial perfusion studies. However, all these parametric images were designed for processing very specific studies and no procedure is available so far that would allow to compare any digitized nuclear medicine study with another quantitatively or to create a standard reference image of normal with the exception of the polar coordinate image, the so called bull's eye display (Ref. 10,11,12,13).

The simple approach described allows the transformation of any irregularly shaped and variably sized organ scan into a standard sized image, which is a circle in the example used in this paper. By this easy to perform and easy to program transformation algorithm essentially no information is lost; the transformation step is fully reversible, with an error of approximately only 1% if using more than 180 sampling angles. 720 angle steps might be recommended to be on the safe side in cases of very large ventricles.

This new technique was applied first for objectively quantifying regional wall motion abnormalities because the objective definition of a wall motion abnormality from gated heart studies is still difficult. Since there is no standard heart amplitude image many approaches have been postulated, such as regional ejection fraction (Ref. 17) and regional decrease of amplitude (Ref. 18,19,20). However, most of the proposed methods have the shortcoming of dividing the left ventricle into a definite number of sectors (Ref. 17,18,19,20).

If a wall motion abnormality extends substantially into two adjacent sectors, it might escape detection when the sector size is large in relation to the size of the wall motion abnormality, and increasing the number of sectors decreases the count statistics for each sector. Our approach allows the computation of a normal amplitude image as shown in Fig. 16. This "intelligent" normal image is encoded with the statistical information to decide whether an individual patient's amplitude image contains areas of significantly depressed wall motion. Each radionuclide laboratory is able to define its own normal matrix out of a normal data base retrospectively, and it would be possible to compare the normal matrices of various laboratories worldwide despite different techniques used and definition of a wall motion abnormality could become common standard.

Other ways than the radial transformation such as the Cartesian conversion of a left ventricular ROI to the circle are conceivable. Further, in the case of the left ventricle or tomographic brain studies a standard ellipse could be used instead of a circle to minimize the magnitude of potential distortion.

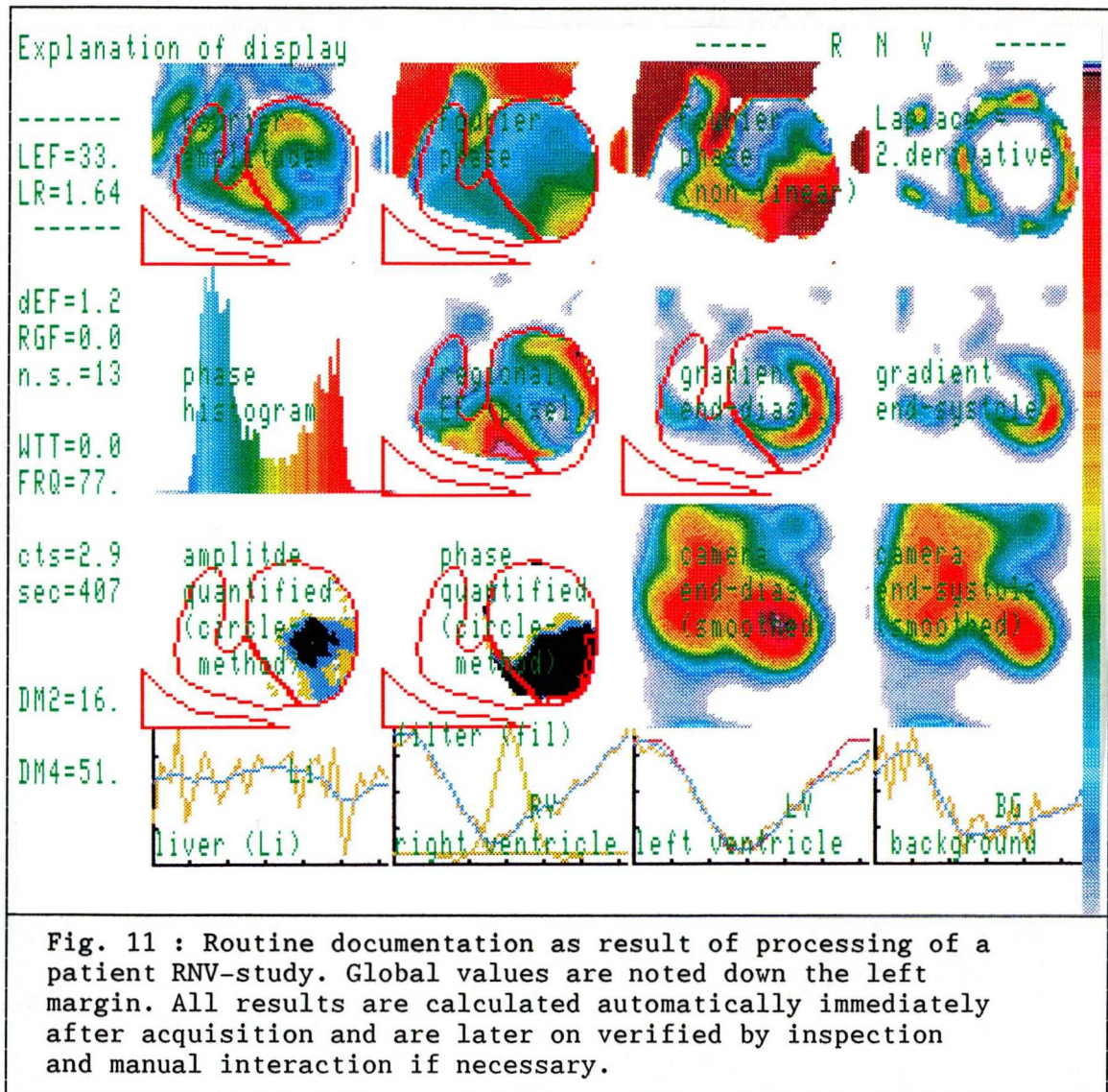
Finally it should be mentioned that this method can be applied to any organ scan, such as brain SPECT and PET studies, since there is no standard so far for a normal count distribution in the individual Tc-99m HMPAO, I-123 Amphetamine or F-18 FDG studies. Like in the heart, many approaches with hand-drawn ROI's (Ref. 21) or multiple squared ROI's (Ref. 22) have been proposed to normalize or quantify regional brain uptake, especially important for scientific studies. The same approach as described above for the heart, shown in Fig. 16 and Fig. 18 can be performed using Tc-99m HMPAO studies, and one example for this applications based on data of 10 normals is shown the corresponding chapter.

Other potential applications might be establishing a normal lung perfusion and ventilation matrix and definition of a normal phase matrix of gated heart studies. This method also allows the transformation and superimposition of radionuclide scans with other digitized images obtained with ultrasound, NMR or x-ray organ studies, for example from the thyroid, coronary angiography, brain CT or NMR tomograms, etc, for quantitative comparison and computation of correlative functional images. The latter might gain major attention with the forthcoming installation of picture archiving and communicating systems (PACS).

3 Radio-Nuclide-Ventriculography

3.1 Method

The procedure used routinely in our laboratory has been described in detail. (Ref 3,26). Briefly, a tracer dose of 740 MBQ of ^{99m}Tc -labeled erythrocytes are injected intravenously. After the tracer has distributed homogeneously, 32 frames per cardiac cycle are obtained in a 32 x 32 matrix in a septum optimized LAO projection. The acquisition is done with a buffered beat acquisition mode technique. Loss in acquisition time for the last images due to variations of the heart rate are corrected by a time-ratio approach. Calculation of the phase and amplitude images are then performed. Ventricular and atrial ROI's are delineated using the amplitude and phase data, with a Laplacian filter for defining the interventricular septum. The automatically defined regions can be verified interactively by help of isocontours in enddiastolic and endsystolic gradient images thus overcoming the problem of nonsignificant amplitudes in hypokinetic regions. The parametric data of phase and amplitude are then normalized for mean amplitude, heart rate, and for the ventricular ejection fraction, thus facilitating interindividual comparison. The phase data are normalized to the ventricle that contracted first. Regional WMA can be quantified from eight sectorial amplitude and phase data. This sectorial phase and amplitude data are related to the mean of our normal group and their deviations are expressed as standard deviations of normal. Global values like ventricle volumes, ejection fraction, stroke volume etc. are calculated automatically. Finally the left ventricle curve is analysed to evaluated characteristic time marks during the representative heart cycle.



3.2 Application of Onion-skin-method in RNV

3.2.1 Method and result verification on angiographic data

A group of patients with anterior or posterior wall infarction were investigated. All of these patients underwent biplane contrast medium ventriculography. Left ventricular ejection fraction was calculated according to

Simpson's rule and had EF values in the range from 34.8 % to 86.9 %. In that group of patients 19 RNV studies were acquired and processed in a standard manner resulting in an enddiastolic and an endsystolic image, and in a left ventricular enddiastolic region defined by Fourier analysis of the cyclic motion of the heart. The LVEF was calculated by the method described here. The correlation to angiographic data was highly significant and the correlation coefficient was determined by $r = 0.945$ (Fig. 12). The mean error of the results were calculated to ± 2.02 % (Table 3)

TABLE 3
Left ventricle ejection fraction from biplane ventriculography and planar RNV in a group of patients with infarction

Pat.#	EF Biplane	EF Onion	\pm Abs. Error
P1	34.9	19.0	2.10
P2	56.6	36.6	2.55
P3	61.5	37.5	0.95
P4	67.6	45.2	3.70
P5	49.2	29.2	3.60
P6	86.9	47.3	0.80
P7	79.4	52.2	1.40
P8	47.3	31.9	1.75
P9	57.7	35.0	3.10
P10	59.0	40.4	1.15
P11	56.6	38.0	2.85
P12	61.5	36.8	0.80
P13	67.6	40.6	4.20
P14	86.9	52.9	1.30
P15	79.4	51.7	1.35
P16	47.3	28.5	1.80
P17	57.7	39.6	2.20
P18	61.5	35.0	1.15
P19	47.3	32.7	1.80

All Values in [%]

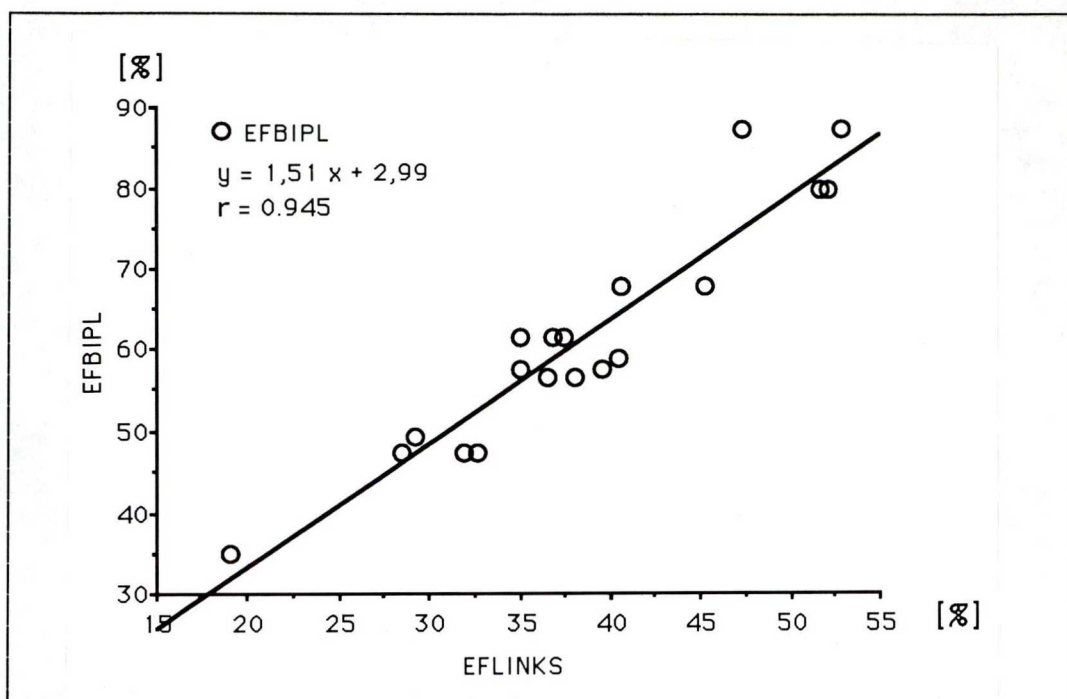


Fig. 12 : 19 patients with anterior or posterior infarction underwent x-ray ventriculography and had their EF calculated in biplane mode according to Simpson's rule. The correlation to the results of the onion skin method appears to be excellent.

3.2.2 Creation of normal EF-values and statistics

To obtain normal values a group of high probability normal patients was investigated. The values were corrected by the regression coefficients to angiographic data to give the cardiologists comparable values. The quality and ranges of the normal values depend to a great extent on the definition of the normal group; it is clear, that these results, especially concerning the right ventricle have to be verified in clinical studies. But it is clear, too, that the values, especially in the relation rest to stress, and right ventricle to left ventricle are physiologically realistic (Ref. 8).

The data of the 19 normal studies were analyzed by the

algorithm. For that group of patients (n=19) LVEF, corrected by the appropriate regression coefficients (Fig. 12) to angiographic data, resulted in a mean of $63.6 \% \pm 11.4$ during rest and 76.5 ± 16.62 during stress, thus defining the normal range of the values. The right ventricular ejection fraction was also calculated by the onion-skin-method from this data and resulted in a mean value of $47.8 \% \pm 8.5$ during rest and in $56.8 \% \pm 8.6$ during stress. Tab 4.

TABLE 4
Left ventricle ejection fraction of a group of normal patients calculated by standard EF-method and by onion-skin-method.

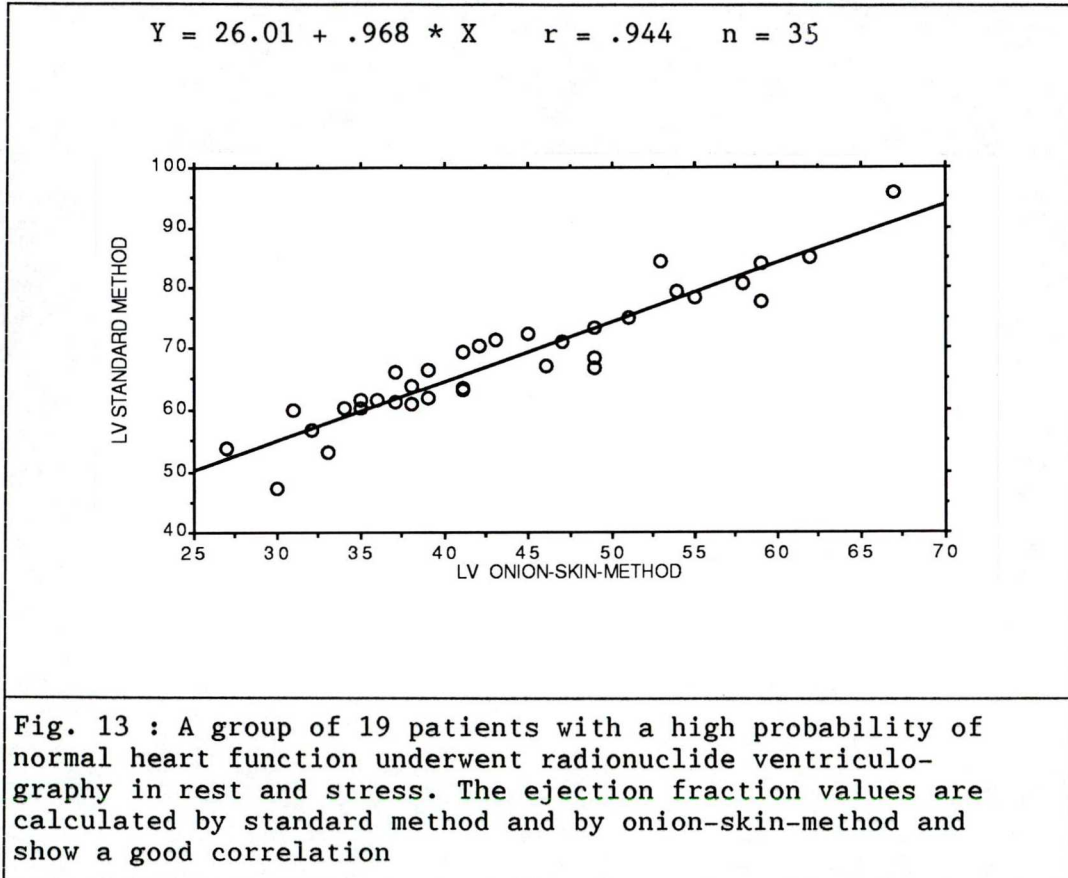
Pat.#	L E F T V E N T R I C L E				R I . V E N T R I C L E			
	Stand. Meth. rest	Meth. stress	Onion-S-Meth. rest	Onion-S-Meth. stress	Stand. Meth. rest	Meth. stress	Onion-S-Meth. rest	Onion-S-Meth. stress
PA1	60.3	69.5	34.0	41.0	31.2	34.8	26.0	31.0
PA2	53.9	61.6	27.0	36.0	23.3	27.3	27.0	36.0
PA3	66.9	77.7	59.0	49.0	32.7	39.7	34.0	43.0
PA4	67.2	-----	46.0	-----	25.9	-----	33.0	-----
PA5	66.6	71.4	39.0	43.0	26.2	28.8	28.0	32.0
PA6	72.5	66.31	45.0	37.0	34.0	33.9	25.0	27.0
PA7	60.4	60.0	35.0	31.0	23.5	23.4	28.0	33.0
PA8	61.9	84.0	39.0	59.0	19.5	35.4	21.0	34.0
PA9	63.5	79.2	41.0	54.0	20.1	33.9	31.0	36.0
PA10	61.7	-----	35.0	-----	32.3	-----	40.0	-----
PA11	61.3	71.3	37.0	47.0	27.3	33.9	25.0	31.0
PA12	73.6	84.9	49.0	62.0	30.7	40.0	34.0	41.0
PA13	70.5	84.1	42.0	53.0	28.6	33.5	37.0	42.0
PA14	47.3	61.0	30.0	38.0	19.5	31.5	22.0	28.0
PA15	56.8	63.8	32.0	38.0	32.2	42.5	27.0	33.0
PA16	53.0	-----	33.0	-----	28.8	-----	26.0	-----
PA17	78.3	95.6	55.0	67.0	26.6	36.2	55.0	46.0
PA18	68.6	80.6	49.0	58.0	30.3	38.1	38.0	42.0
PA19	63.3	75.0	41.0	51.0	20.6	33.4	24.0	32.0

3.2.3 Discussion of the results

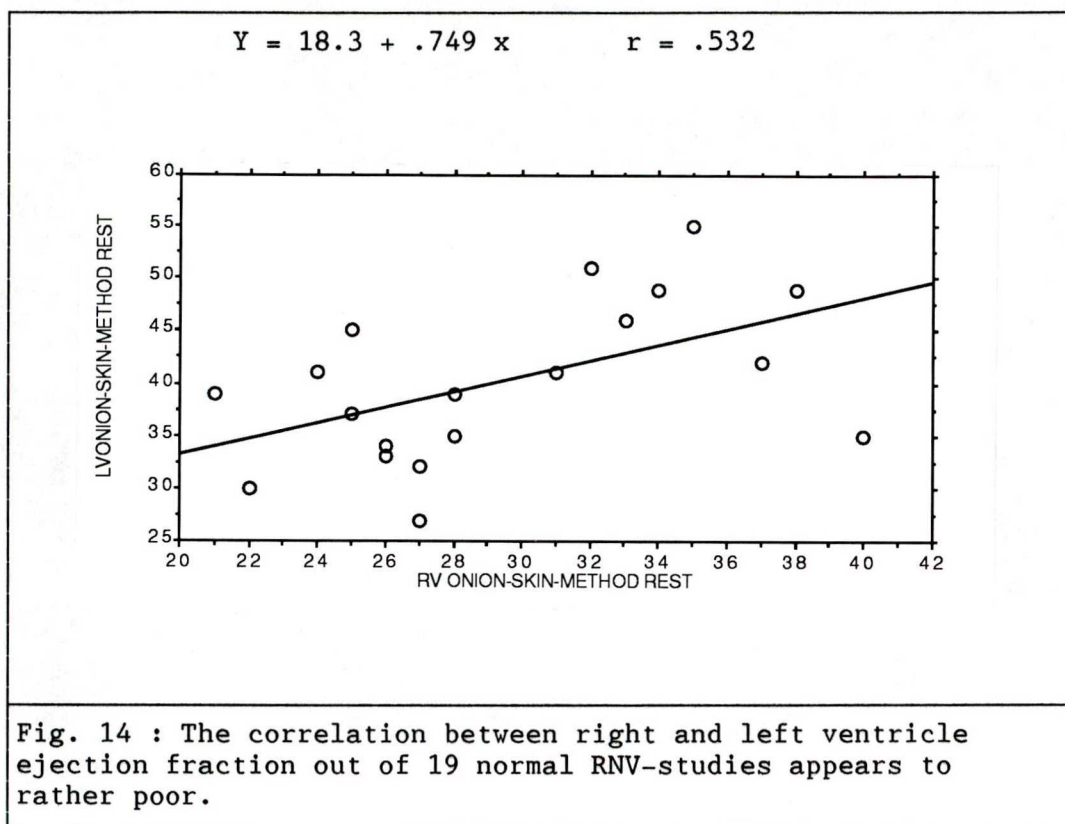
Although the clinical interpretation of the result is beyond the scope of this paper there are some interesting aspects which should be mentioned.

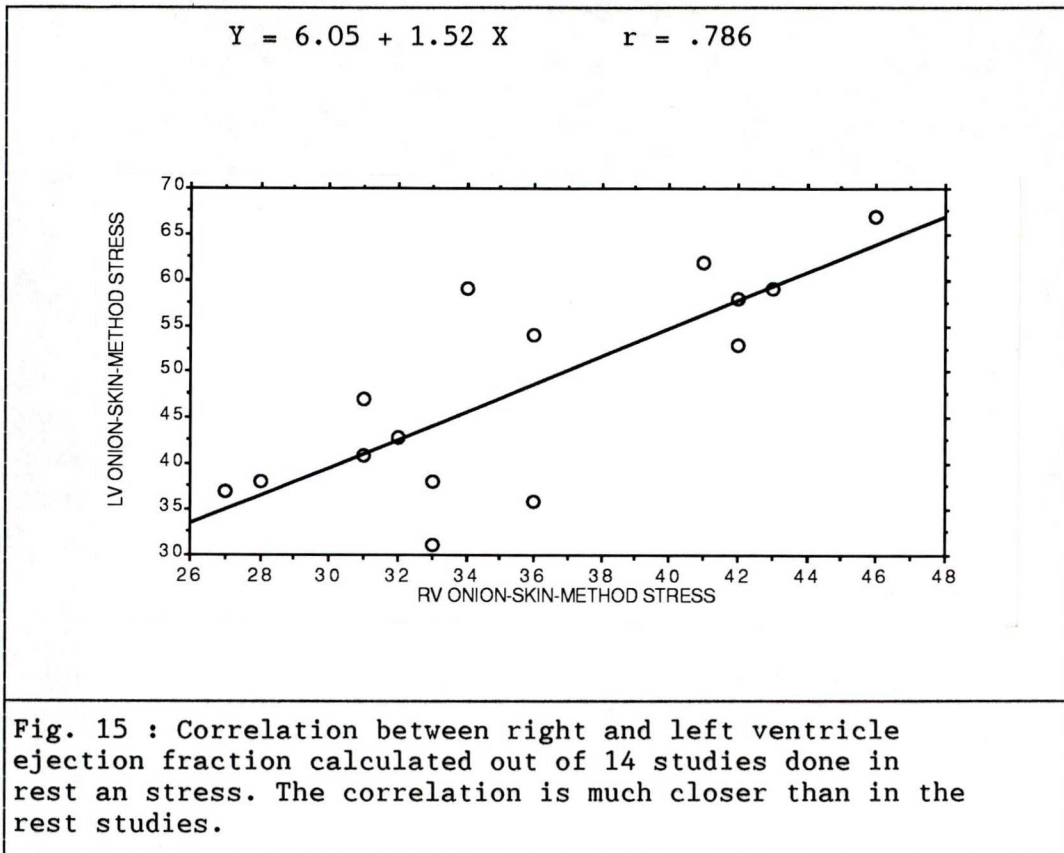


Like in the patient group discussed in chapter 3.2.1 the correlation between standard nuclear medicine method and new onion-skin-method proved to be excellent. (Fig. 13).



The increase in ejection fraction of 12.9 % between rest and stress for the left ventricle and of 9.0 % for the right ventricle is expected and corresponds to physiology. The correlation between left and right ventricle ejection fraction during rest showed a very poor correlation $p = 0.158$. (Fig. 14). The correlation between ejection fraction during stress between right and left ventricle showed a significantly closer correlation $p = .0005$ (Fig. 15)





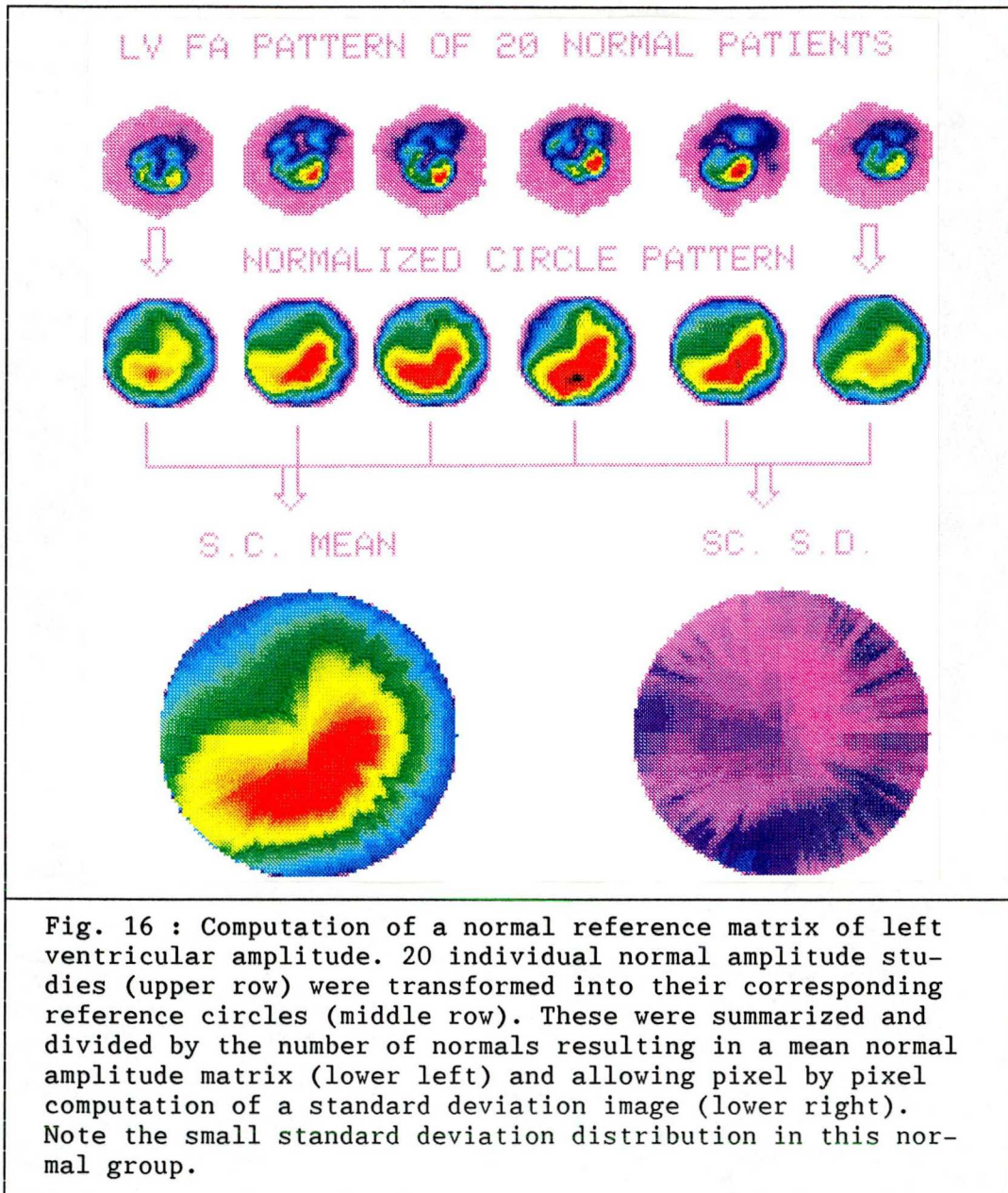
3.3 Application of CRF-method in RNV

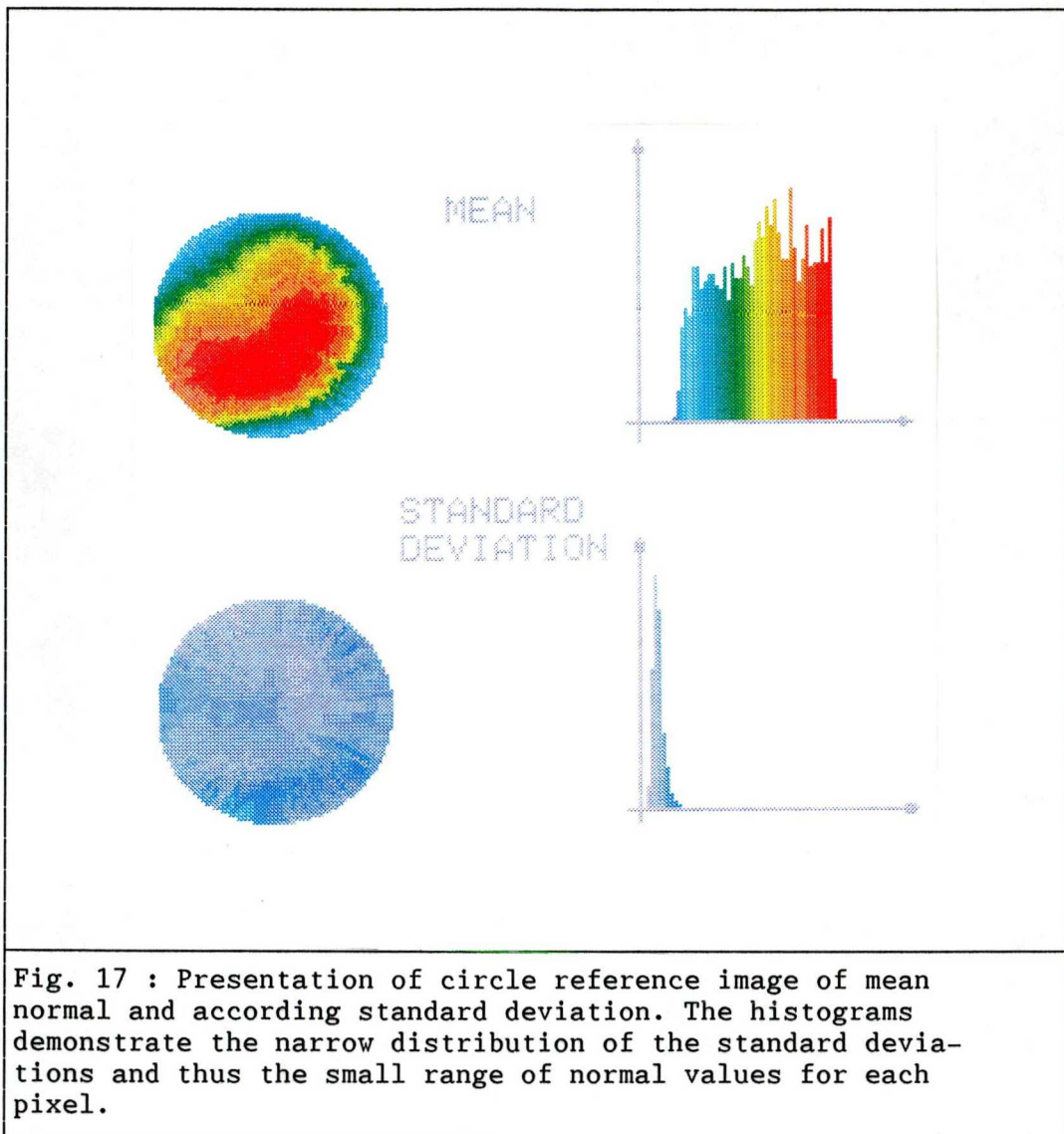
3.3.1 Creation of normal pattern and statistics

Computation of a normal amplitude image matrix: Out of our normal data base 20 LAO resting studies were used to create a normal reference. The Fourier amplitudes in the left ventricle regions were transformed to its circle presentation. These circle pattern were added pixel by pixel and the resulting values were divided by the number of normal subjects resulting in a pixel by pixel "mean" image. Likewise the standard deviation of each transformed pixel is calculated for the number of normal subjects, describing the statistical property and thus the normal range of the

normal reference circle image. (Fig. 16)

The relative standard deviation of the mean values is an important indicator for the compliance of the method. If there are common structures within the amplitudes of left ventricle in the normal subjects and if it is possible to overlay them in a reasonable manner than the relative standard deviations should minimize. Fig. 17 proves that standard deviation is in the mean round 7 % on a pixel by pixel base. Thus sensitive discrimination of depressed amplitudes is expected.





3.4 Definition of defect-pattern

The great value of the normalization procedure described in this paper in terms of objectively identifying regional wall motion abnormalities is illustrated in a patient study with anterior infarction shown in Fig. 18 . There is now a normal value for each amplitude on a pixel by pixel base and likewise important a normal range for each pixel.

Any pixel having an amplitude value below normal will show up and can, in addition, be color-coded. This was accomplished in our algorithm in a way that all pixels with counts below 1 to 2 standard deviations were color-coded in yellow, below 2 to 3 standard deviations in blue and below 3 standard deviations in black. This statistically encoded reference circle of the original study was then retransformed into the original ROI thereby displaying the extent and the magnitude of a significantly depressed wall motion in the original scale. With this information LV-amplitudes of each individual patient transformed to its circle reference is compared and quantified against the normal. This is done regionally as demonstrated in Fig. 18 . and globally. For that purpose the amplitudes having values which are depressed more than two standard deviations with respect to the normal reference are summed up in the LV - ROI and put in relation to the amplitude integral in the normal circle reference image. The result is a defect score which quantifies the size and the amount of amplitude depression in the LV.

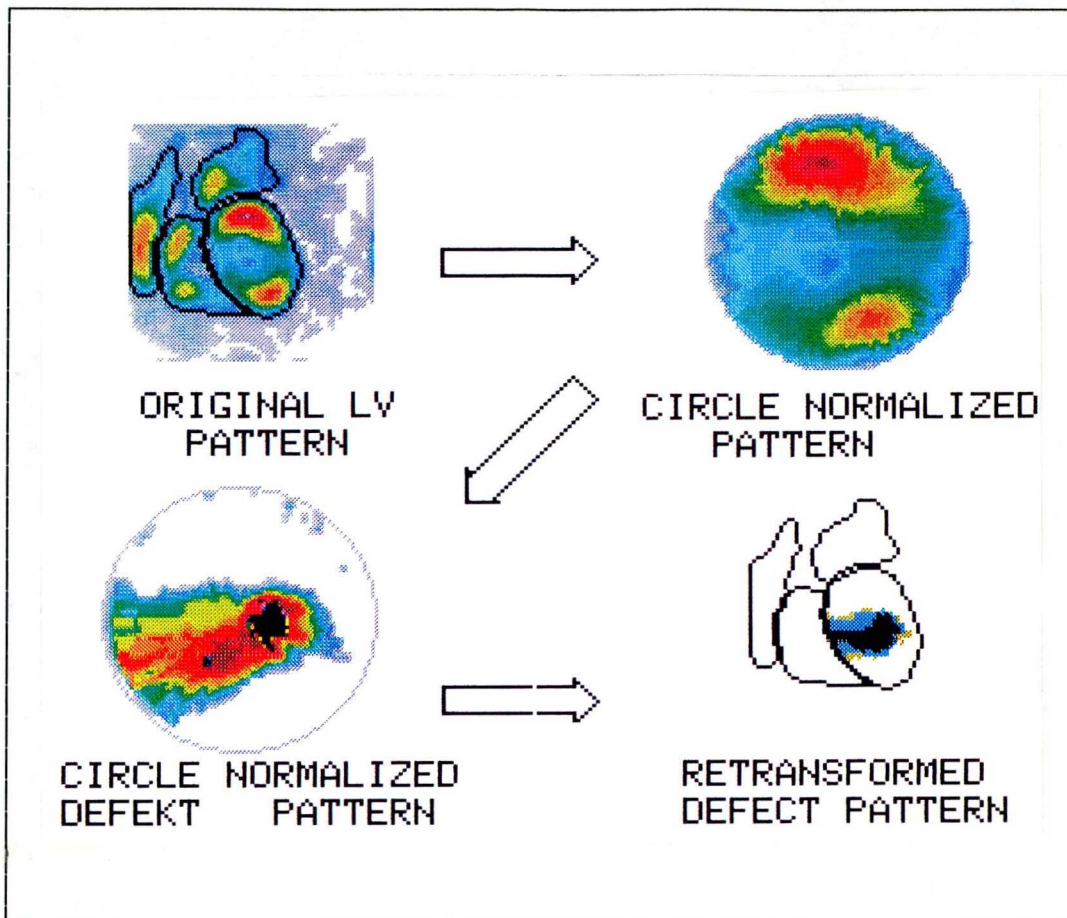


Fig. 18 : Application of the normal reference circle technique for verifying and quantifying a regional wall motion abnormality. First, the individual study (upper left) is transformed into its reference circle image (upper right) and compared to the normal circle matrix (Fig. 17) by subtracting the mean normal matrix and dividing the difference by the standard deviation matrix (out of Fig. 17). This results in a color-coded circle image that shows all pixels below 1-2 SD in yellow, below 2-3 SD in blue and below 3 SD in black. This coded circle image can be retransformed into the original ROI (lower right) thereby displaying the size and magnitude of the wall motion abnormality quantitatively in the original LAO projection.

3.5. Recent and published applications of the CRF-method

Mester et. all used the CRF method to analyze amplitude scans of 25 patients with aortic regurgitation. Patients with aortic insufficiency exhibited a significantly larger

amplitude defect-score (DM) as normals. A value of 2.0 was declared to be the upper limit of normal values for DM. Sensitivity and specificity of the method were found to be .80 and .79 respectively. (Ref. 30)

A further application of the method in a clinical study was done by Tarkowska et al. (Ref. 36). The reference circle method was used to measure distribution of Fourier amplitudes obtained from the ECG-gated equilibrium radio-nuclide ventriculography in 20 normal subjects (Nm) and in 55 patients with myocardial infarction (MI). Amplitude decrease was measured pixel-by-pixel and expressed in standard deviation units (SDU). The defect-score DM as described in chapter 3.4 was used to quantify global amplitude depression. In the normal group amplitude decrease equal to SDU-1 was found in 13.72 % of the LV-area and equal to SDU-2 in 0.89 %. None of those subjects showed abnormality greater than SDU-2. DM amounted to 0.85 %. In patients with MI these values were significantly greater than in Nm. The highest values of those indices were found in patients with aneurysm, a less pronounced FA reduction was observed in anterior wall infarction and the lowest in posterior wall infarction. The sensitivity of the CRF method in detecting regional hypokinesis was 85.2 %, specificity 100 % and accuracy 85.4 %. In patients with regional hypokinesis, the visual evaluation of the statistically encoded image revealed a sharply outlined, easy to detect area. It is concluded that the CRF method enables regional hypokinesis to be detected, localized and quantified accurately. (Ref 36).

One step further went Bitter et al., when applying this method on data of several groups. Characteristic pattern of geometrical amplitude distribution were calculated to describe posterior wall infarction, anterior wall infarc-



tion, aneurysm, moderate aortic stenosis and severe aortic stenosis. The difference in the characteristic scans has been quantified by the euclidian distance, which is the square root of the integral of the squared pixel-by-pixel differences. By this value significant differences could be found between the groups. Good results could be achieved in reclassifying the patient with help of that value. (Ref. 40)

4 Gated-spect radionuclide ventriculographie (Gaspect)

4.1 Introduction

Planar radionuclide ventriculography is the state of the art method in nuclear medicine for the detection of regional wall motion abnormalities and for the evaluation of global heart performance. (Ref. 41). However, due to the planar data acquisition technique the method has some disadvantages in detecting posterior wall problems and in separating left and right ventricle and atrial information. With the implementation of Spect it was obvious to combine the possibilities of RNV and SPECT to a method that overcomes all of these problems. (Ref. 42,43,44,46)

4.2 Data-acquisition

The acquisition of data in gated Spect mode is performed by a rotating scintillation-camera. After in vitro labeling of the erythrocytes is performed with 740 MBq Tc-99m the data are acquired in 32 positions over 180 degrees from right anterior oblique view to left posterior oblique view. Care is taken for stable positioning of the patient on the SPECT table to avoid any motion artifacts. For each position a standard radionuclide ventriculography is performed, the gating is two-thirds forward and one-third backward, resulting in 8 images of a 64x64 matrix distributed across the cardiac cycle. A mechanism allows the repetition of an acquisition of the recent projection if not enough cycles due to varying heart rates could be acquired. From the clinical point of view there is a strong demand for short acquisition times, to minimize stress by medicinal interaction and to maintain the possi-

bility to investigate under standardized stress conditions in the future. In the present state acquisition times per projection are down to 30 seconds per projection, resulting in an effective acquisition time of 16 min, however the time for storing the information is another 8 min. The elapsed time for the study is then round 24 min. The mean heart rate is acquired once before the acquisition of all projection data. It is desirable to store the acquired data after the acquisition of all projection to minimize the idle state of the acquisition programm.

4.3 Conventional Data-processing

Data processing starts with corrections for camera inhomogeneity, center of rotation, and for differences in effective acquisition time per angle due to an inconsistent number of discarded cycles.

Conventional data processing of Gaspect-studies, then, is usually performed as the extraction of wall motion abnormalities observed in the transverse slices and as the calculation of ejection fraction by geometrically based algorithms.

By this method, the original projection data are back-projected time-step by time-step to transverse slices. As a result, for 8 images per projection 8 three dimensional tomographic data sets are constructed. These data sets undergo edge detection algorithm to evaluate the border of the heart in each of the time states and in each of the slices. By analyzing the movement of the border of the heart dis- or akinetic regions of the ventricles can be detected. Ejection fractions of the heart chambers are calculated routinely by a geometric evaluation of the volumes in the short axis slices. The disadvantages of the method are mainly the heavy influence of the poisson statistic in the relatively poor acquisition data, the prob-

lem in the detection of the edges of the heart in the transverse slices and the extensive calculation expense. (Ref. 42,43,44)

4.4 Gaspect processing

4.4.1 Flash-Spect-method

The idea to compress the projection data by breaking up the information in its Fourier-coefficients is recently published in the Journal of Nuclear-medicine. (Ref. 45). The basic idea is to reconstruct the sinus and cosinus coefficients to transverse slices images instead of backprojecting original data. One has to be aware not to handle with amplitudes and phases because these data are not created by linear procedures and are therefore lacking interchangeability.

In detail, following acquisition the projection data sets, consisting of 8 images per view, are Fourier transformed each. The result consists of mean level images, looking like an untriggered study, of cosine and sine matrices for the first harmonic and of cosine and sine matrices for the second. After correction for homogeneity, center-of-rotation and constant acquisition time per view, transverse slices from each of the 5 projection data sets are calculated.

4.4.2 Coefficients-reconstruction-theory

This chapter gives an instant mathematical prove for the demand to reconstruct cosine and sine coefficients instead of amplitude and phase.

Let o be the object and p the projection-data, and let P be the Projection and B a SPECT-Reconstruction-operator. So B and P are linear Transformations.

$$B(ap_1+bp_2) = B(aP(o_1)+bP(o_2))$$

and because of the linearity of P

$$B(P(ao_1+bo_2))=ao_1+bo_2$$

because always is

$$B(P(o)) = o$$

and

$$ao_1+bo_2 = aB(p_1) + bB(p_2)$$

Now for example the sinus-coefficient is

$$S = \sum_{i=0}^{n-1} o_i \sin \frac{i2\pi}{n}$$

where o_i is the object during the i . time step.

We know $o_i = b(p_i)$, therefore

$$\sum_{i=0}^{n-1} o_i \sin \frac{i2\pi}{n} = \sum_{i=0}^{n-1} B(p_i) \sin \frac{i2\pi}{n}$$

because the sinus value is constant for all projections
and because of the linearity of B

$$= B\left(\sum_{i=0}^{n-1} p_i \sin \frac{i2\pi}{n}\right)$$

and finally sinus- and cosinus-coefficients can be calculated as SPECT-reconstructions of the projections. From these coefficients Fourieramplitudes and phases can then be calculated in the well known manner.

4.4.3 Reconstruction-procedure

The reconstruction of the five projection files is done by means of backprojection algorithm. The projection data are filtered by a count-dependent Metz filter, i. e. a filter which takes in account the modular transfer function of the camera computer system. By this geometric filtering the noise due to the poisson statistic is depressed in such a way, that the projection data can be backprojected by a simple ramp type filter. When reconstructing sine and cosine coefficients however another problem emerges: most of the Spect-reconstruction program packages are not able to reconstruct negative values. The sine and cosine coefficients are defined however as being negative and positive. This problem is overcome by adding a homogeneous constant to the coefficient data to be projected. Hereby, the coefficients are brought to always positive values. The addition of the constant has the effect of an addition of a parabolic offset to the transverse slice information. This effect is calculated by an isolated reconstruction of that constant. In the transverse domane the effect can be subtracted, resulting in pure data of sine and cosine coefficients.

4.4.4 Reorientation due to heart axis

The angulation of the three Fourier-coefficients are done corresponding to three manually given axis. These three axis are defined at the data of the 0. Fourier-coefficient which is in fact the mean value over one representative heart cycle. The reorientation is done by manipulation of one slice-representation after the other. First the transverse slices are reoriented to reposition the projection of the long axis in this view from its left inclination to a matrix-lined position. Then the deviated sagittal slices are manipulated to rotate the heart information in a horizontal position, than the deviated coronal slices are handled in the same way. (Fig. 20).

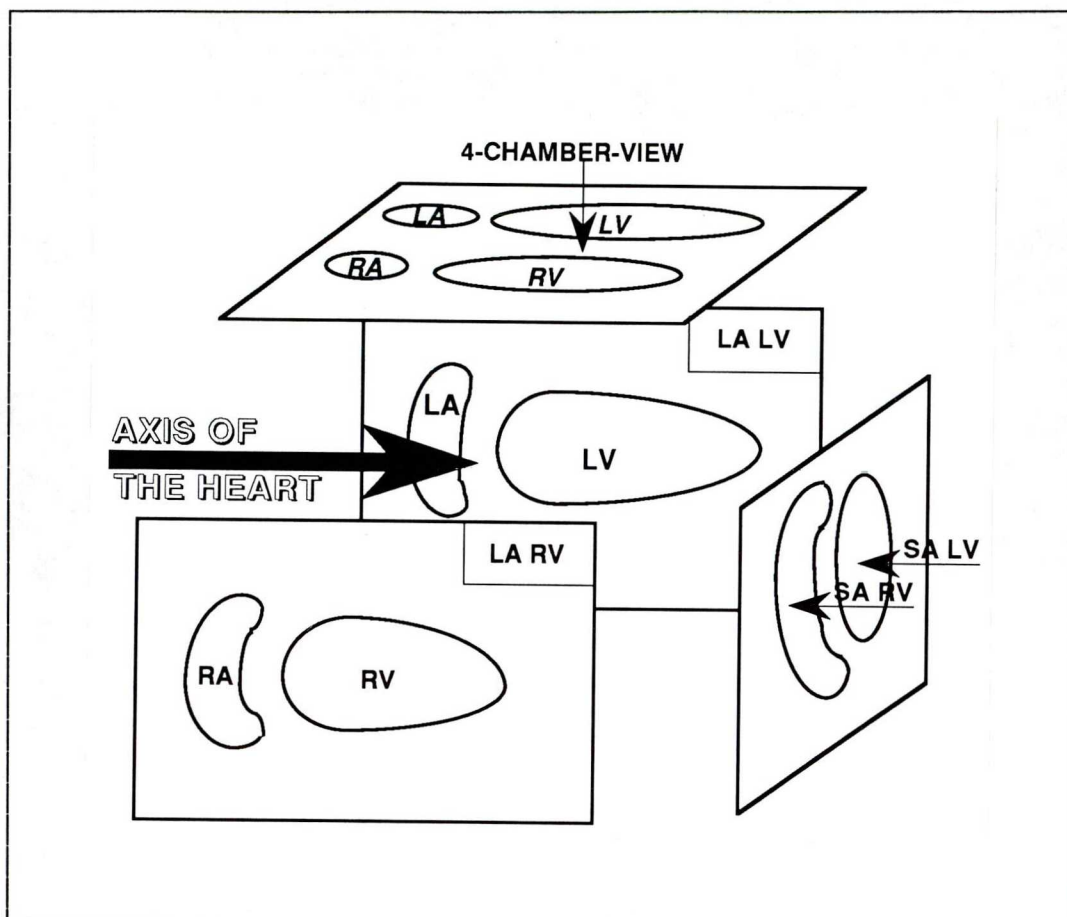


Fig. 19 : Schematic display of the 4 views in double-angulated Gaspect. All views are oriented according to the long axis of the heart: short axis view (SA), long axis view for right (RV-vLA) and left ventricle (LV-vLA), and 4-chamber view (4CH).

The reposition algorithm of the information is based on a linear mapping of points in one frame to points in another frame. This mapping is such that two points (x_1, y_1) and (x_2, y_2) , in the original frame will map directly to the two corresponding points (x_1', y_1') and (x_2', y_2') in the result frame.

The coefficients A to D are calculated to satisfy the following set of equations:

$$x1 = Ax1' + By1'$$

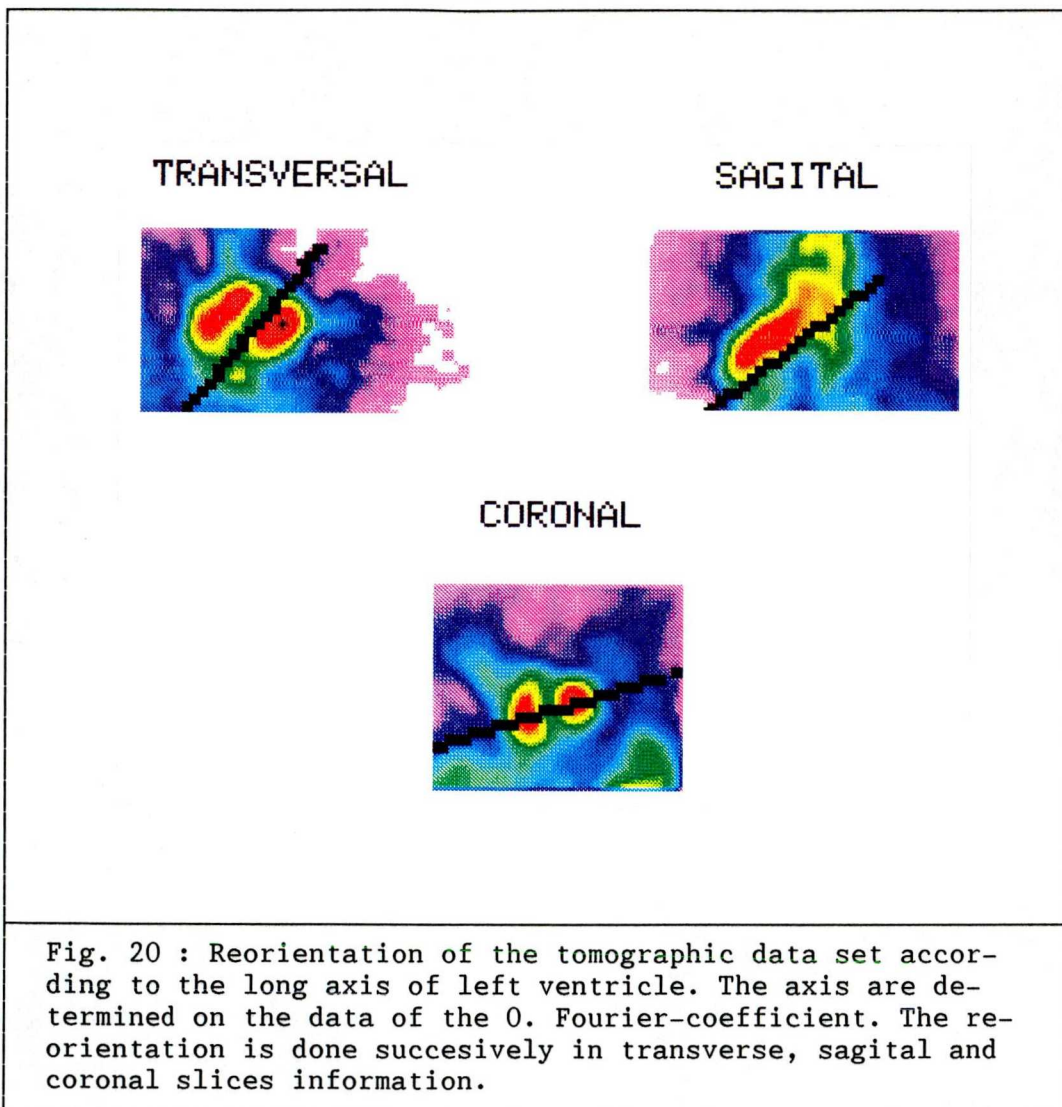
$$y1 = Cx1' + Dy1'$$

$$x2 = Ax2' + By2'$$

$$y2 = Cx2' + Dy2'$$

The coefficients A through D are the increments needed to get from one point to the next point in the original image when incrementing to the corresponding point in the result image. For example, when incrementing Y from the start of one line to the start of the next line in the result image, the coefficients B and D are the X and Y increments needed to get to the corresponding point in the original image. Any pixels in the resulting image that fall outside the boundary of the original frame are set to zero. The pixels that do map within the frame boundary are each calculated from their nearest neighbors in the original image using bilinear interpolation.

After reorientation of the 0. Fourier-Coefficient the first and the second Fourier-parameters are reoriented by the previously manually given axis in the same way.



4.4.5 Replanarisation

After reorientation, the information aligned according to the heart axis, can easily be handled by program. Amplitude and phase can be calculated to display extent and time of heart kinetics in each slice. Fig. 21 shows an example of a set of data which represents kinetic of the heart by the short axis slice Fourier amplitude information of a heart.

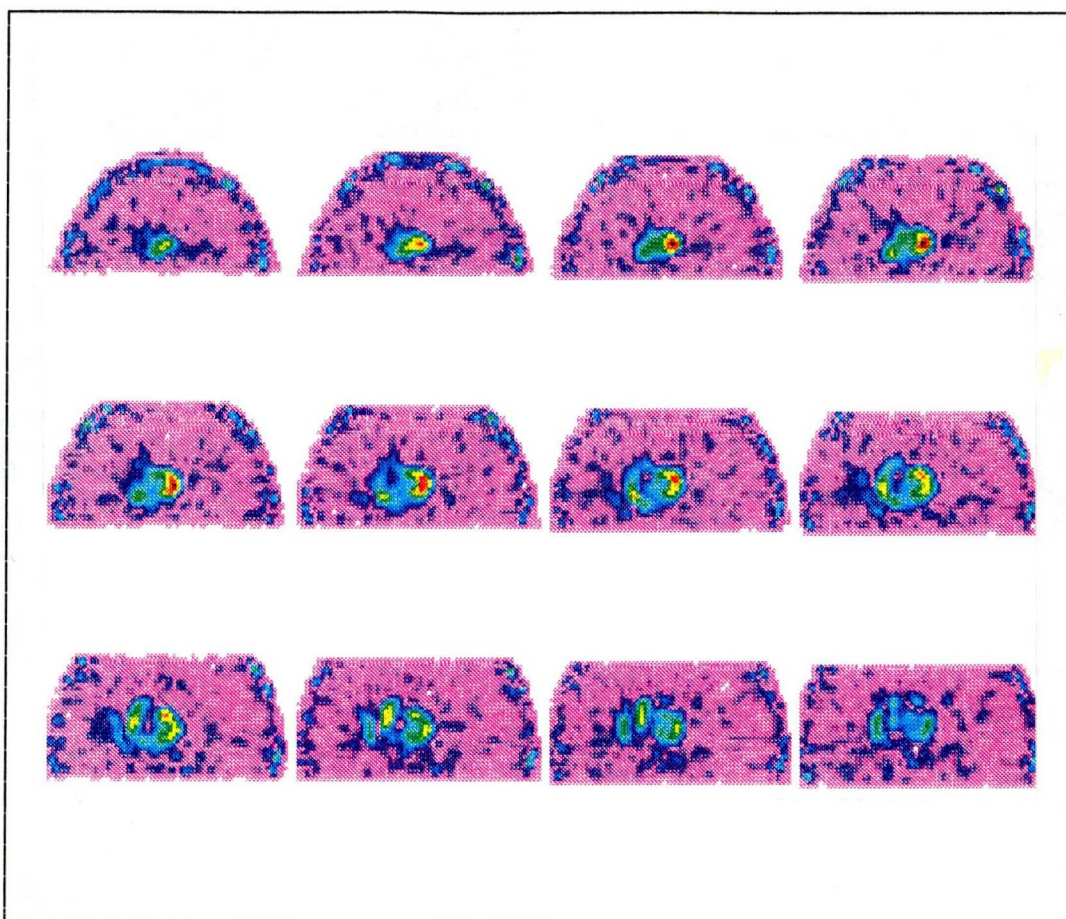
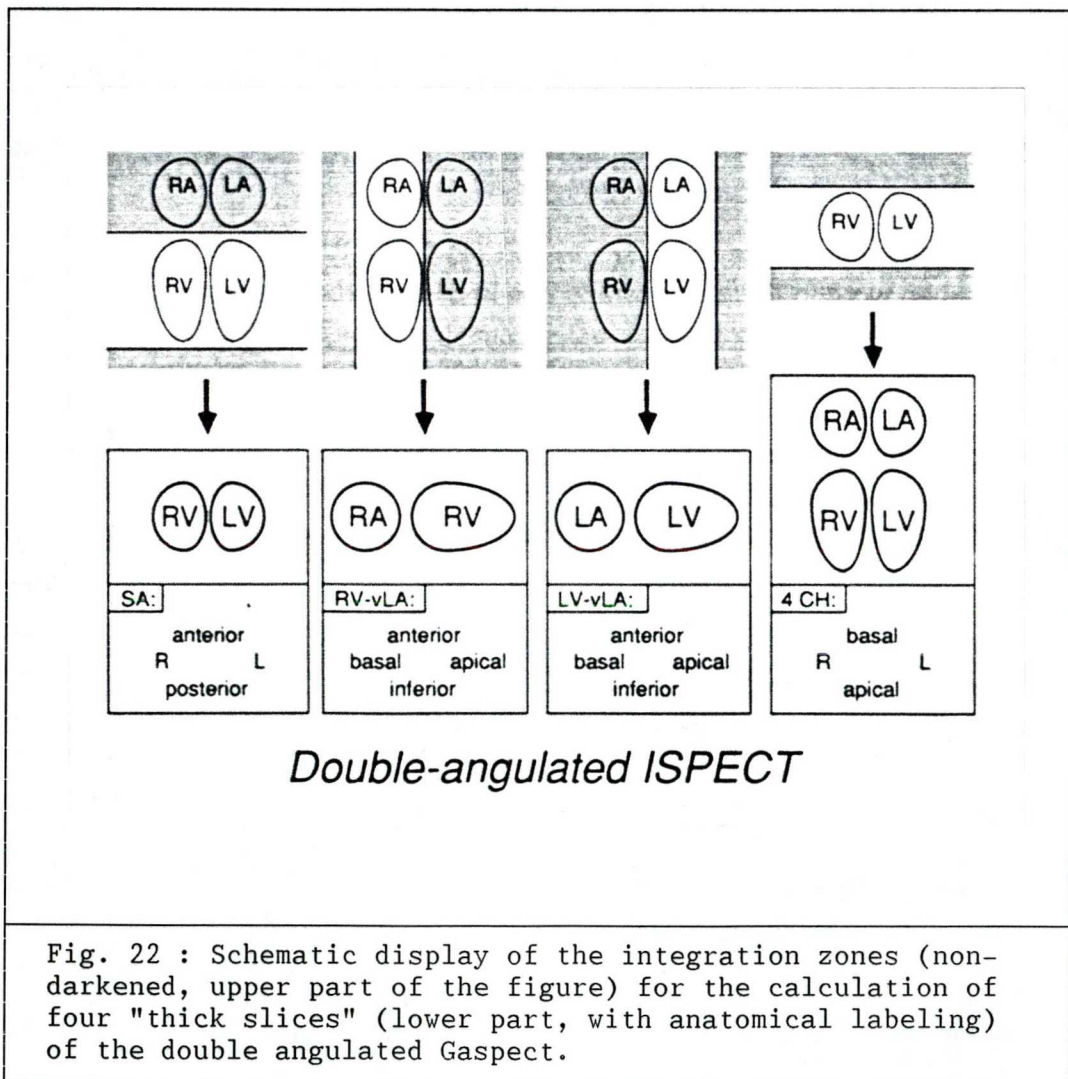


Fig. 21 : Examples of a set of Fourier amplitudes from the apex to the base of the heart. The data are very noisy. The pattern shown a ring structure because the remaining end-systolic blood volume is not moved at all.

This example demonstrates, that in gated radionuclide ventriculography the demands on the count statistics are rather high, since the data are spread not only over the cardiac cycle but over all angle steps as well. To improve count statistics Fourier analysis is implemented, however, even when including this stabilizing and concentrating mathematical instrument the resulting information is rather noisy. This requires additional smoothing procedures, thereby decreasing geometric resolution, or further intel-

ligent data processing procedures, which are overcoming the problem of count statistics. An special way of data processing, the technique of thick slices, first introduced by Itti et. al. (Ref. 47) is used to maintain a clinically feasible presentation of results.



For that reason the Fourier-coefficients, aligned with respect to the heart axis, are integrated in slices. This is done for all 5 parameters, for the mean the cosine and sine of the first Fourier harmonic and the cosine and sine of the second. The borders of the heart are defined rectangularly in each view with help of the mean parameter, maintaining a cubic region of integration. As a result of the integration procedures four planar sets of 5 parameters are produced.

The first set represents the integrated information of the 5 parameters from the valve plane to the apex, the so called short axis view.

The second set represents the integrated information of the 5 parameters from the septum to the right lateral border, the right ventricle long axis view.

The third set represents the integrated information of the 5 parameters from the septum to the left lateral border, the left ventricle long axis view.

Finally the fourth set represents the integrated information of the 5 parameters from the anterior to the posterior wall of the heart, the so called four chamber view.

Although this information contains relevant information as shown in Fig. 23. where the data sets are displayed column by column, amplitude and phase have to be calculated now, to make the kinetic information visible. (Fig. 24)

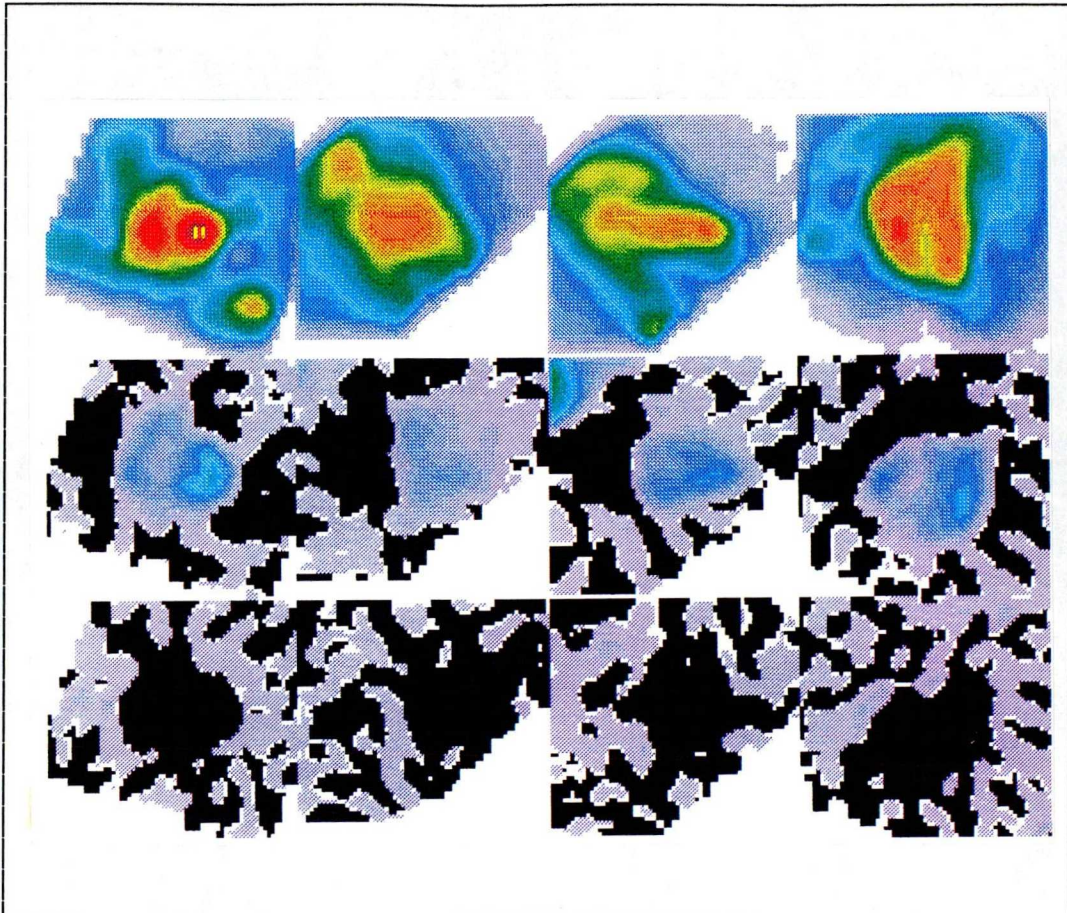
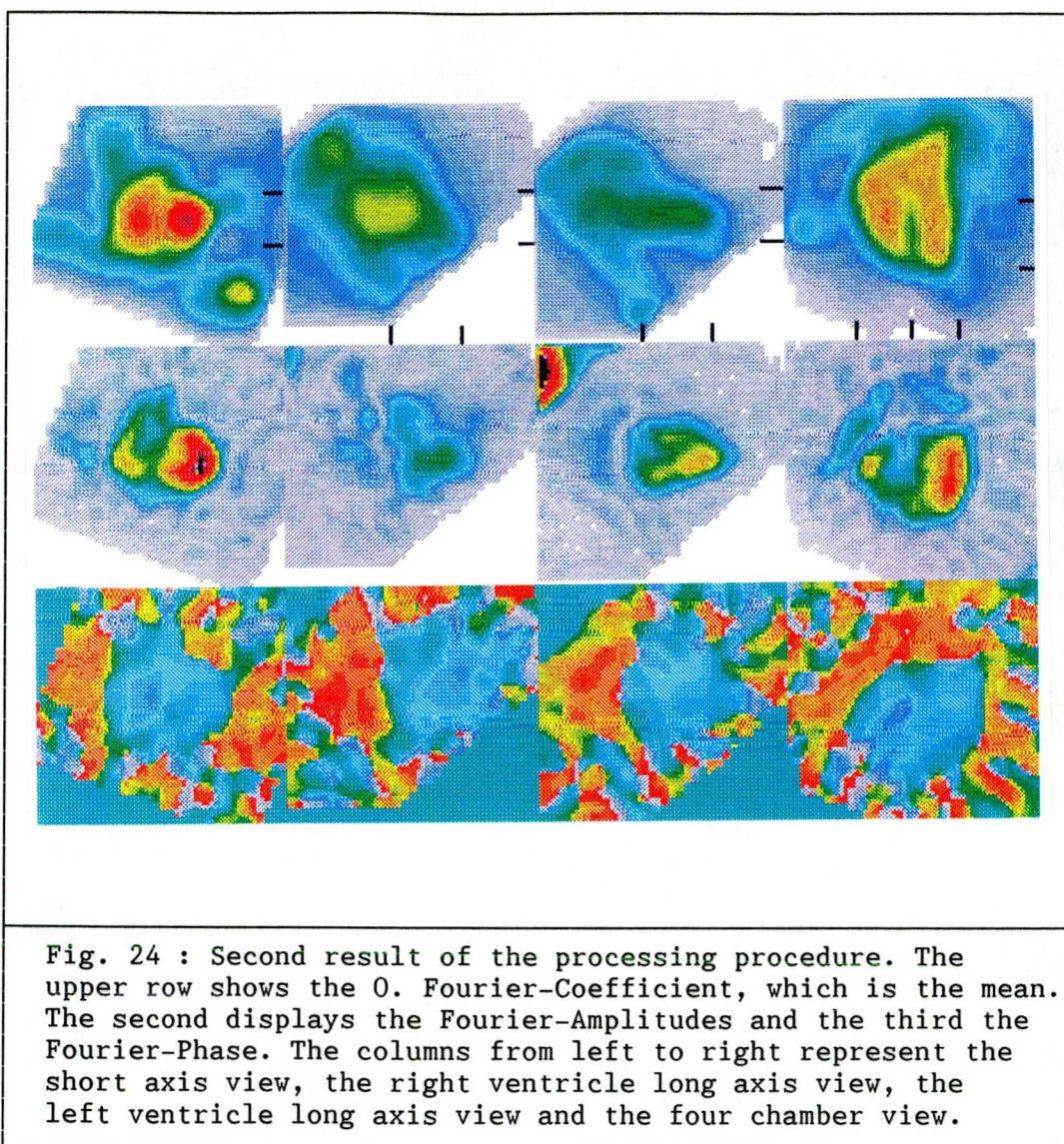


Fig. 23 : As a first result 4 sets of data are calculated, representing four views in columns 1 to 4. In the first row the mean Fourier parameter is shown, in the second and third the cosine and sine parameter of the 1. harmonic is displayed. The 1. harmonic contains positive and negative values, so information cannot be analysed visually.

The first aim of this study was the facilitation of the anatomic location of regional wall motion abnormalities and of the areas of first contraction. This was established by providing Fourier-amplitudes and Fourier-phases information in four independent views. Amplitude and phase analysis can take place to evaluate geometrically well defined findings.



A possibility to define ventricle and atria interactively in the different views is included. The interesting information is masked and a normalization of the information is done. For that purpose in each view the pixel of maximal amplitude in the right or left ventricle is found. The phase information in the image is normalized so that the phase value of this pixel is shifted to $+\pi/2$. This procedure will result in a consistent phase display which allows phase analysis and comparison in different views.

The forth row of the screen can be used to display relevant information. This can be e.g. phase histogram, gradient image or others.

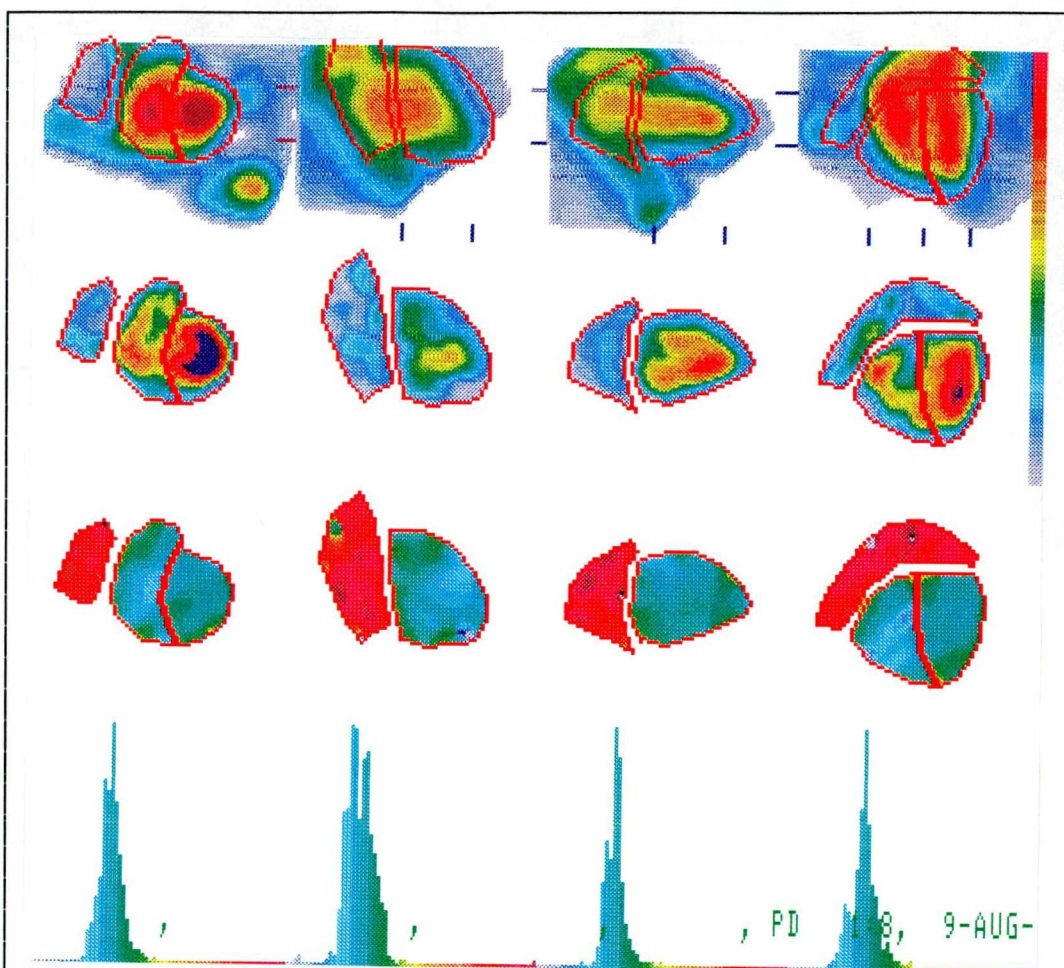


Fig. 25 : Third result of the processing procedure. The interesting information in the interactively defined ROIs is unmasked of the background noise. Phase histogram is displayed in the forth row, other information can be put to disposal at that place.

Although the method was intentionally created to follow up regional heart kinetic in patients with exitation and posterior wall problems by observation of Fourier-Coefficients, the calculation of global function values remained desirable. Consequently the ventricle volumes in different

views were evaluated according to Simpson's rule and the L/R ratio of the Fourier-Amplitudes was calculated to differentiate valve insufficiency. Ejection fraction however, the most valuable global parameter could in this state not be calculated. Therefore a further step to the method was included.

4.4.6 Creation of four heart-axis-related Ventriculograms

With the processed Fouriercoefficients it is possible to recreate ventriculograms consisting of a set of images, describing the movement of the heart during a revolution. This data sets can be processed like a standard radio-nuclide ventriculography, whereby the region defined on Fourier-Amplitude and Phases, as shown in Fig. 25 , are accepted.

Consequently, a programm is provided, that resynthesizes planarized Fourier-coefficients. By that procedure four standard RNVs for four views are obtained. For that resyntheses the program includes beside the mean parameter information of two more Fourier-Coefficients. Because only mean and two additional Fourier-Coefficients are used for the reconstruction the study appears to be moderately smoothed, but the essential information should be present. The reconstructed information of these data sets delivers a smoothed but fair description of the kinetic in each of the corresponding pixels. RNV is calculated with 16 images and with the standard RNV processing algorithm global ejection fraction, geometric volume in enddiastole and endsystole and several characteristic time marks on the left ventricle volume curve can be calculated.

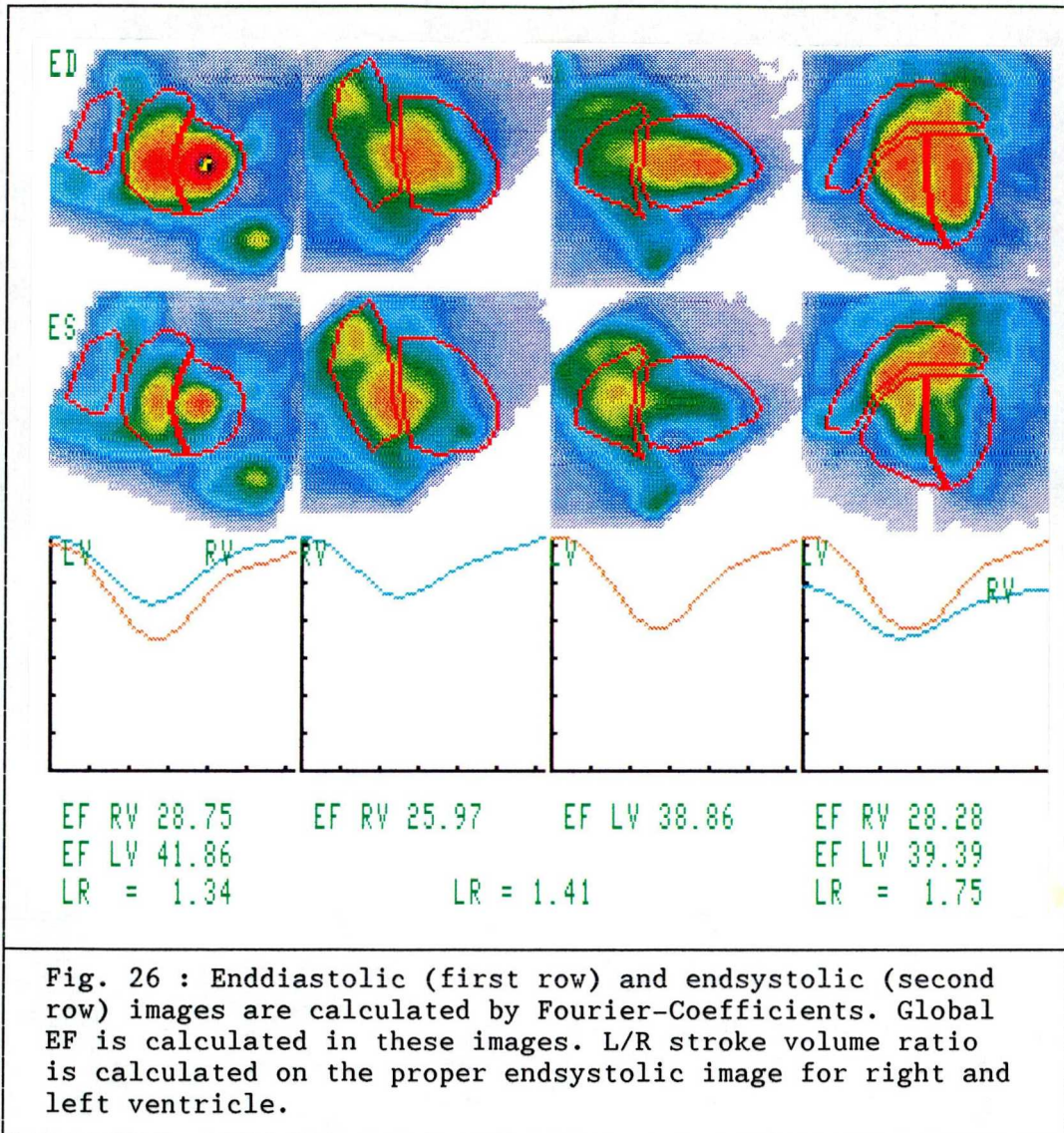


Fig. 26 : Enddiastolic (first row) and endsystolic (second row) images are calculated by Fourier-Coefficients. Global EF is calculated in these images. L/R stroke volume ratio is calculated on the proper endsystolic image for right and left ventricle.

The resulting data set presents enddiastolic and endsystolic images and the possibility to define ventricular and atrial regions. In a first group of patients, processed by the program, there was evidence that the time of endsystole varied between right and left ventricle, due to heavy excitation problems. Thus, a movie of all four views was presented and the L/R stroke volume ratio was determined by means of the global ventricle curves. (Fig. 26).

After working with the program it turned out that a dual ROI technique may lead to further findings, so this possibility was included as well. After all the method and so the program has grown in an evolutionary way and the development has not yet come to an end.

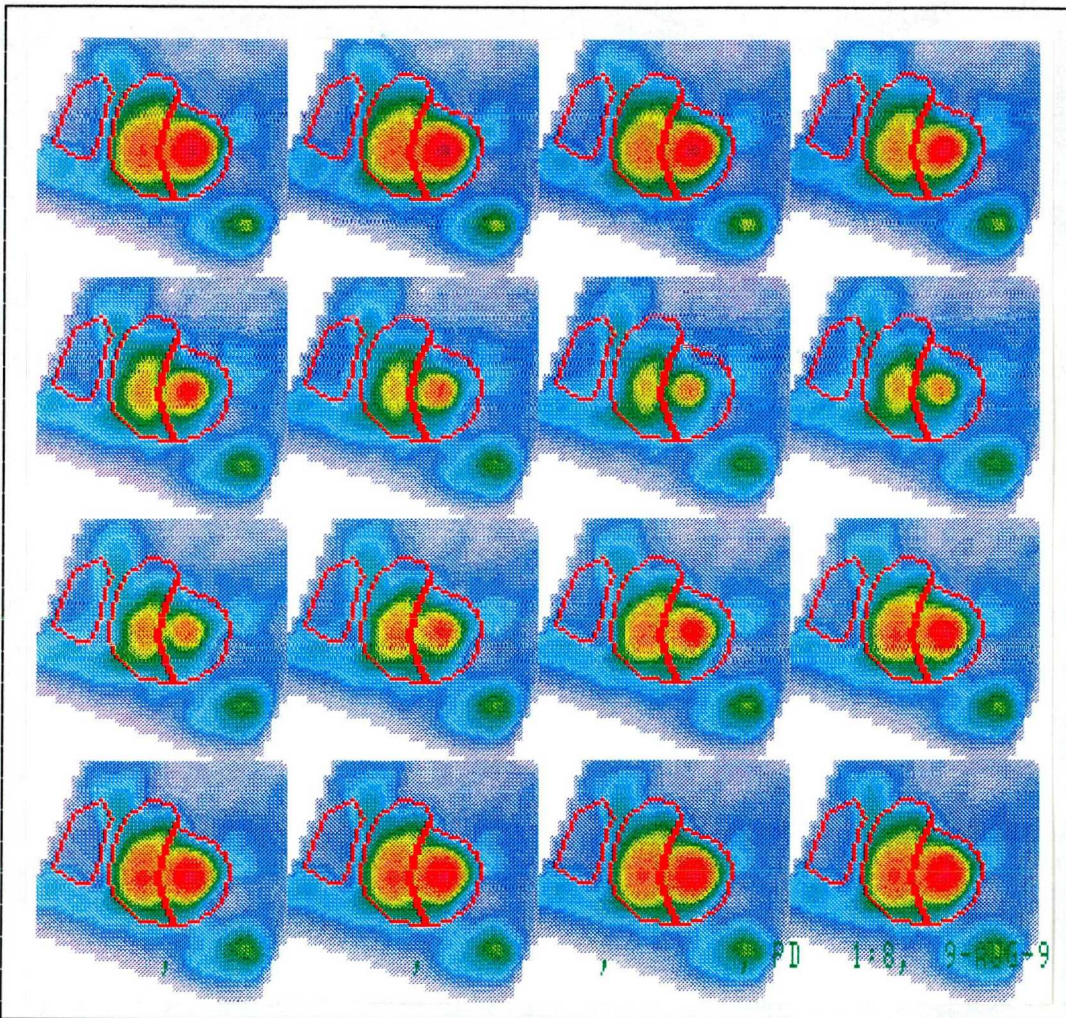


Fig. 27 : Set of 16 images reconstructed from Fourier-Coefficients of short axis view information. Movie information can be provided by long axis view and four chamber view as well.

4.5 Global values evaluation

14 patients with various cardiac problems were investigated by gated spect method. The right and left ventricle ejection fractions and LR-ratios were evaluated. EF is calculated in a first step by assuming no background contamination at all. This assumption is made due to the special integration method which allows depression of counts resulting from areas before or behind the heart. The consistency of the method is checked by relating the results in different views.(Tab. 5). Then an attempt is made to take into account the slight contamination of the real object counts by various effects. Therefore the EF was calculated by new onion-skin method. The LR-ratio was determined in three different views. (Tab. 6). All 14 patients underwent planar radionuclide ventriculography as well. The ejection fractions from these studies were evaluated as well by the new method. With this proven values the Gaspect EF-values were correlated.

T A B L E 5

Ejection fraction without background observation

Pat. #	E j e c t i o n Right Ventr.			F r a c t i o n Left Ventr.			L / R R a t i o		
	SA	LA	4CH	SA	LA	4CH	SA	LA	4CH
AH	33.5	30.6	33.4	12.0	11.8	12.4	1.15	0.81	1.01
BH	25.4	25.2	23.9	41.5	41.4	41.4	1.82	1.86	2.12
CT	19.1	19.1	21.1	38.9	42.7	41.4	2.55	2.04	3.00
EJ	23.4	30.1	24.5	17.3	15.9	16.9	1.29	1.33	1.50
ER	21.5	26.2	29.8	15.3	14.2	14.3	1.27	0.89	1.04
FG	14.7	22.2	21.6	11.0	10.7	10.8	1.94	1.85	1.81
GW	16.9	15.2	11.9	29.3	29.8	29.9	1.04	1.05	1.91
HK	23.5	23.3	20.1	52.7	55.8	51.6	1.99	2.00	3.58
HR	28.7	29.9	29.9	40.4	42.6	42.7	1.26	1.14	1.38
HR1	37.6	33.7	30.0	50.6	47.5	51.5	1.07	1.08	1.53
HE	26.7	21.5	30.4	46.6	49.3	55.7	1.05	1.93	1.47
HRo	37.9	36.2	38.4	17.4	17.8	16.7	1.02	1.23	0.91
JP	24.1	22.7	20.3	36.0	32.8	35.7	1.94	1.73	2.17
KA	31.2	36.5	38.7	25.5	27.2	27.1	1.55	1.68	2.06

T A B L E 6

Ejection fraction calculation by onion skin method

Pat.#	E j e c t i o n Right Ventr.			F r a c t i o n Left Ventr.			planar RNV	
	SA	LA	4CH	SA	LA	4CH	LV	RV
AH	53.7	33.3	38.3	16.4	14.4	16.2	13.9	43.7
BH	55.8	34.7	30.6	49.2	49.8	51.1	39.6	49.2
CT	19.1	28.7	31.1	54.2	49.9	50.3	50.9	42.6
EJ	49.6	34.3	28.3	27.5	21.6	22.7	21.0	32.4
ER	52.8	34.8	40.8	20.0	17.7	20.4	19.7	37.1
FG	38.3	31.8	30.2	15.2	15.5	13.8	11.7	18.2
GW	27.0	16.9	14.7	36.9	34.2	37.5	23.4	21.6
HK	62.6	28.8	24.4	73.8	75.4	68.6	67.3	40.2
HR	46.3	38.1	38.6	48.9	49.7	47.1	37.6	65.9
HR1	53.4	40.1	60.6	63.2	52.6	60.6	41.4	52.5
HE	62.2	31.9	48.3	78.1	55.7	68.1	55.2	66.3
HRo	99.0	36.2	55.9	21.2	21.9	20.8	14.6	47.7
JP	24.1	22.7	26.7	53.2	40.0	49.2	49.1	30.3
KA	84.2	43.9	55.8	31.0	34.8	31.4	31.2	54.2

4.5.1 Global values results

The basic aim of this part of the study was to verify the global value results, especially the ejection fraction values of the Gaspect studies. The first requirement was to maintain comparable values in all three views (SA, LA and 4 chamber view). The ejection fraction values were checked against each other for the left and right ventricle. (see Tab. 7).

TABLE 7

Gaspect view to view EF consistency check

Correlation	Correlation coefficient r	
	left ventricle	right ventricle
shor axis to 4 chamber view	.988	.789
long axis to 4 chamber view	.987	.864
long axis to short axis view	.991	.832

The values were then correlated to the ejection fraction values from planar RNV studies. These data were acquired undependently of the Gaspect study. To this well proven ejection fraction values (see chapter 3.2.3) the Gaspect ejection fraction of all views were correlated. (Tab. 8).

TABLE 8

Gaspect EF to planar RNV EF correlation

Correlation	Correlation coefficient r			
	without BG		with BG	
	LV	RV	LV	RV
shor axis to RNV	.934	.644	.947	.476
long axis to RNV	.922	.456	.941	.617
4 chamber to RNV	.906	.643	.942	.655

To include observation of background contamination new onion-skin method was used to calculate from each of the three views for right and left ventricle ejection fraction values. Under this aspect the values of the correlation coefficients improved at least for the left ventricle. (Fig. 28 - 31)

The enddiastolic-endsystolic left to right ratio of the count differences as an equivalent of stroke volume ratio of left to right ventricle was calculated as well. Because this value is background independent the counts were evaluated in the original data. The values correlated in different views of the Gaspect study with $r = 0.707$ to 0.915 to the planar RNV LR values. (Tab. 9).

TABLE 9

LR value correlation from Gaspect to RNV

Correlation	Correlation-coefficient r
shor axis to RNV	0.806
long axis to RNV	0.915
4 chamber view to RNV	0.707

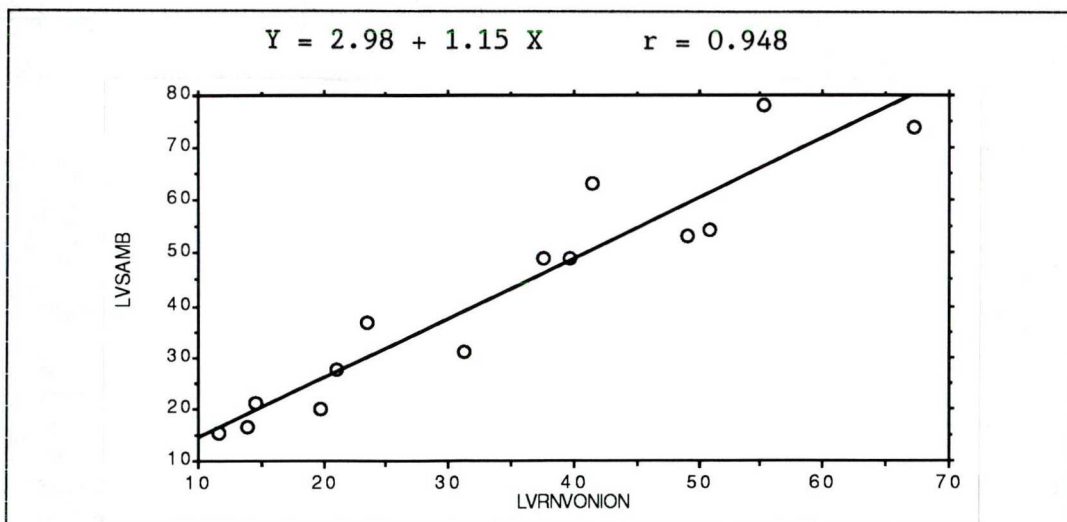
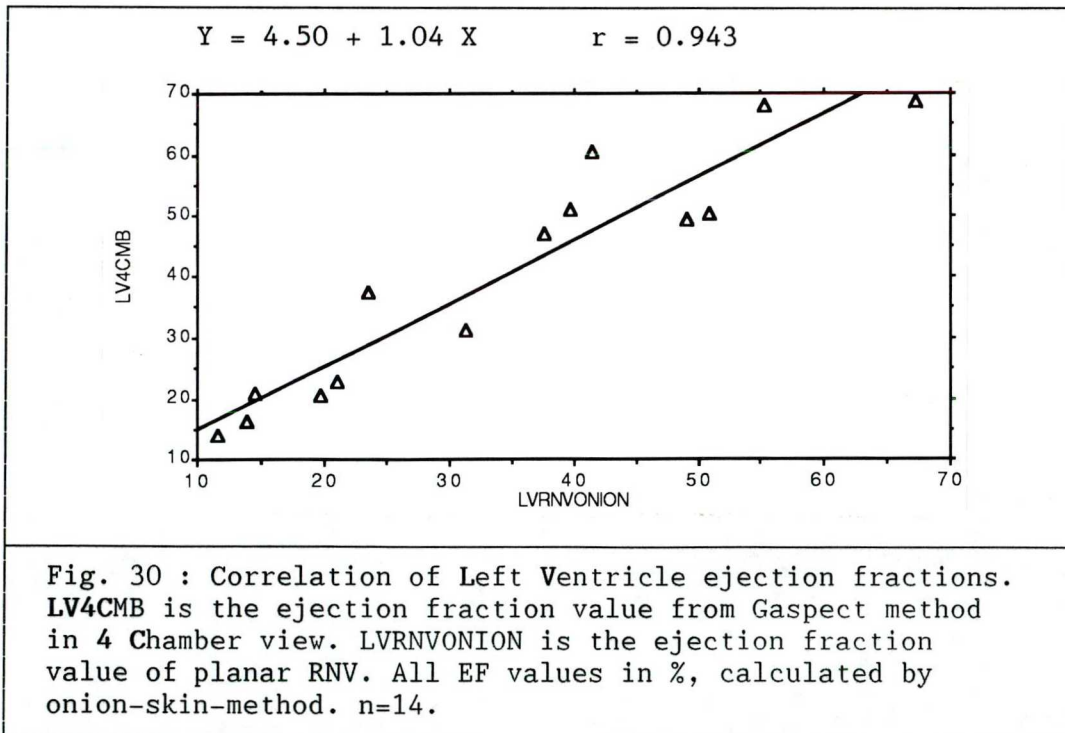
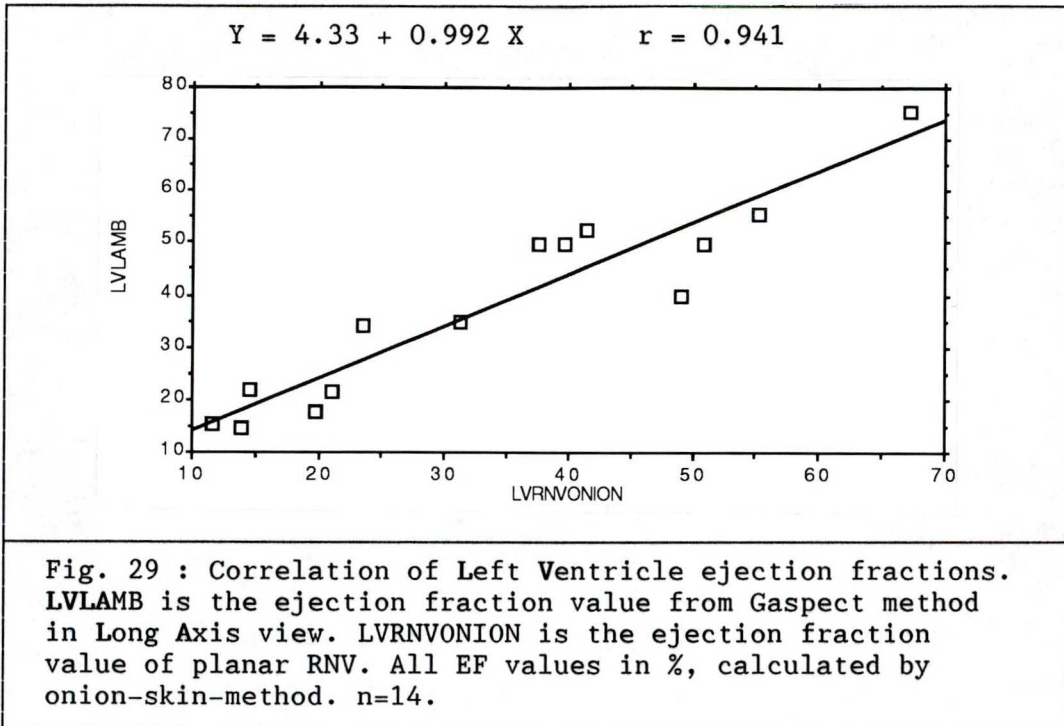
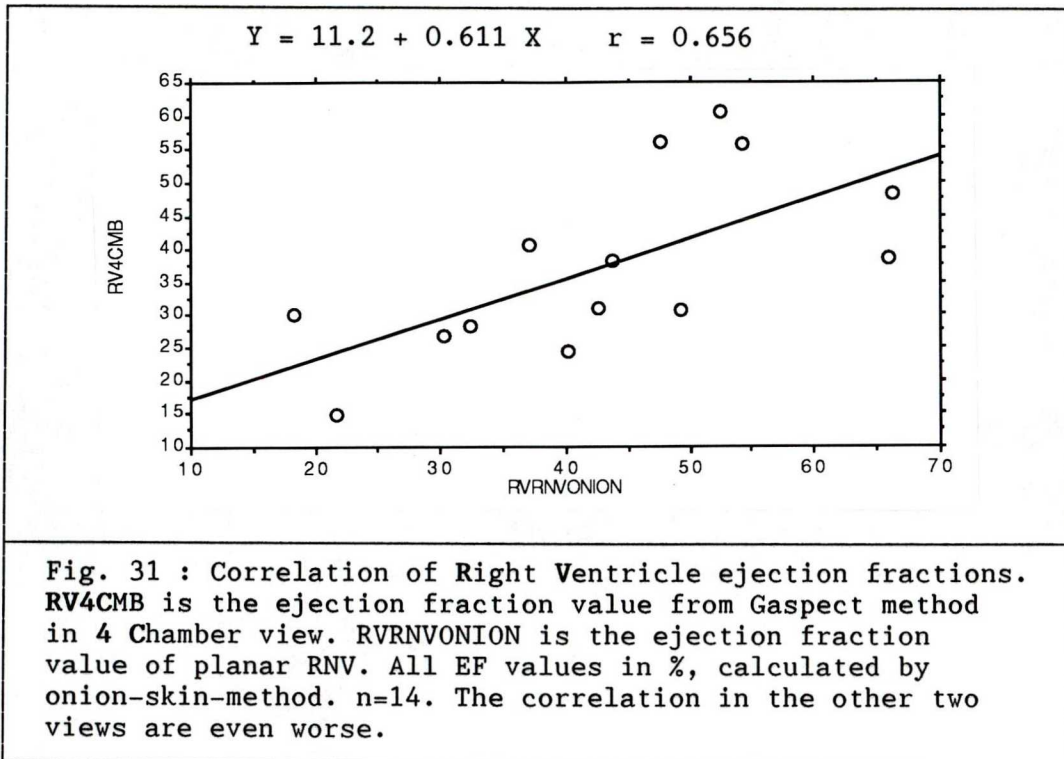


Fig. 28 : Correlation of Left Ventricle ejection fractions. LVSAMB is the ejection fraction value from Gaspect method in Short Axis view. LVRNVONION is the ejection fraction value of planar RNV. All EF values in %, calculated by onion-skin-method. n=14.





4.5.2 Global values discussion

The correlation of the ejection fraction values from view to view especially in the left ventricle appeared to be excellent.(Tab. 7). Thereby demonstrating that the method can deliver consistent results. The ejection fraction values from Gaspect to planar RNV showed in all three views excellent correlation to the left ventricle, documenting reasonable result in comparison to routinely used values (Tab. 8,9). When observing the background contamination the results were even better. (Fig. 28 - 31) The background contamination can be explained first of all by the cubic integration technique, which overlaps to the elliptic structure of the heart especially in the corners some nonobject counts. This results make clear that the method can deliver reasonable values, comparable to planar

RNV, as far as it concerns ejection fraction values. On the other hand the LR values did not come up with comparable close correlations to planar RNV, beside perhaps the short axis view result. This might be due to a different, significant movement of the valve plane in both ventricles. This would explain why the short axis view which corresponds best to the planar RNV view showed best correlation. In a work in progress a dual ROI-technique is applied to overcome the problem of the up and down moving valve plane. However manual definition of that borders remains difficult.

4.6 Application of CRF-method for detection of RWMA

5 patients out of the group of 14 were defined by visual inspection of the parametric scans to be without severe heart problems. The left ventricle amplitude pattern of the 4 chamber view was used to create as an example a normal reference. This was done analogous to the procedure for planar RNV. (see chapter 3.3.1). The four chamber view amplitude scans of 14 Gaspect studies underwent circle reference method. The derived regions of wall motion abnormalities were quantified as described in chapter 3.4. The defect score was correlated to the defect score of the planar RNV. (see Fig. 32). This examples of RWMA quantitation demonstrates the possibility of the application of that method.(Fig. 33). The crucial point is the acquisition of a number of normal studies to maintain a statistically significant database of normal amplitude distribution, then valuable normal references could be calculated for each of the three views and for left and right ventricles.

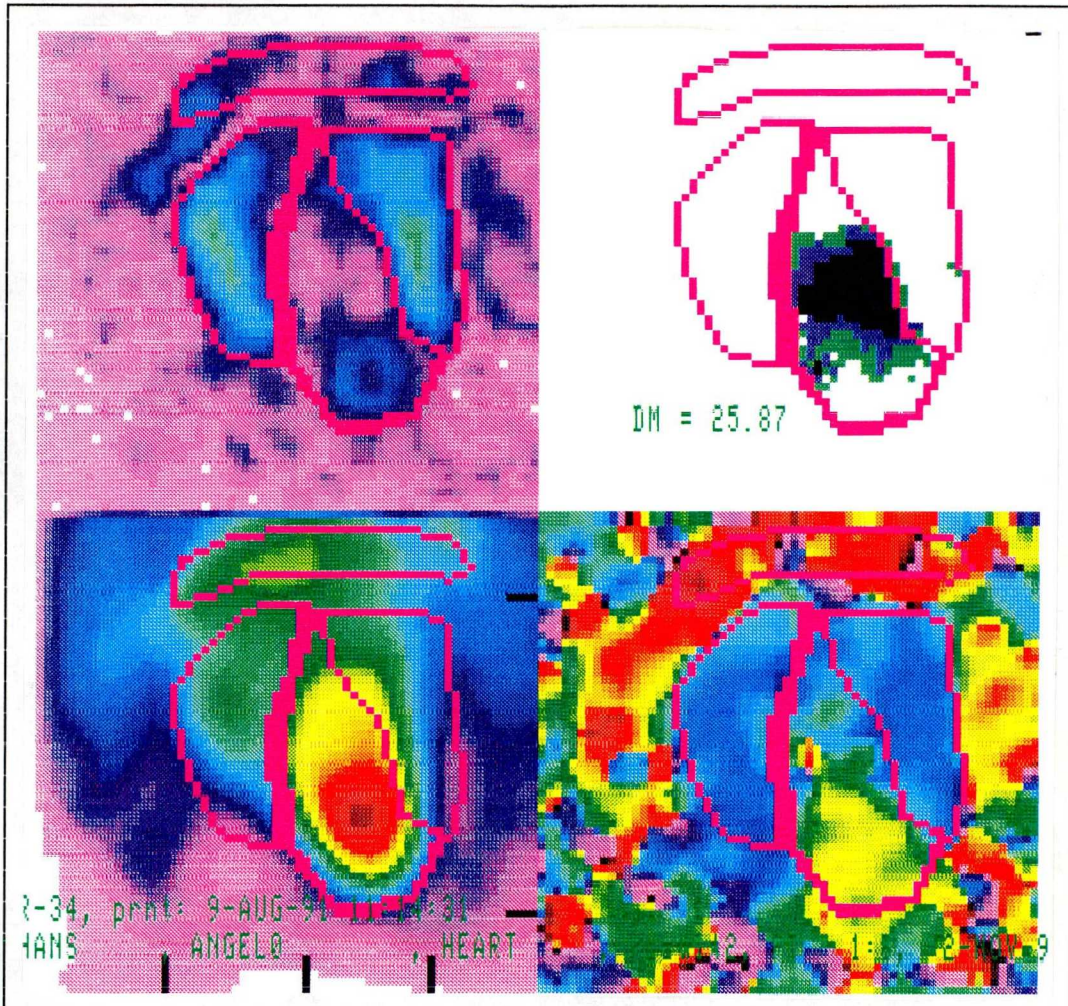


Fig. 33 : Example of a quantification of a amplitude defect in a 4 chamber view of a gaspect study. Left upper corner amplitude image, right upper corner defect quantification with green 1 SD, blue 2 SD and black more than 3 SD amplitude depression with respect to a normal reference out of 5 studies, left lower corner untriggered activity image and right lower corner Fourier phase image.

5 Brain perfusion studies with HMPAO

5.1 Introduction

Conventional radioisotope brain scanning used polar radiopharmaceuticals such as ^{99m}Tc pertechnetate which did not penetrate the normal brain. They images brain pathology by crossing the damaged blood brain barrier. This disadvantages of this agent and the success of positron emission tomography in brain function imaging, led to the search for agents which can cross the blood brain barrier and provide information on regional cerebral blood flow using conventional gamma camera and SPECT imaging. In order to cross the blood brain barrier a substance need to be uncharged, lipophilic and of low molecular weight. However the ideal tracer needs not only to cross the blood brain barrier but remain with a fixed distribution within the brain for a sufficient long time to allow the acquisition of data for reconstruction of tomographic images. A substance which came close to these requirements was found with the ^{99m}Tc complex of hexamethylpropylene amine oxime (HMPAO) which is taken into the brain and shows a long term retention.

5.2 Acquisition

The patient should be placed in a quiet room for a few minutes. Then 350- 500 MBQ of this substance are injected intravenously. 10 min after injection of the tracer, SPECT imaging can be performed using a rotating gamma-camera with a low energy, high resolution collimator. Sixty-four frames of 30 sec each were acquired. Transaxial sli-

ces are calculated on the fly by a filtered back-projection algorithm with a 1-2-1 interslice weighting and a sheep-hanning-logan filter with a cut-off of .4.

5.3 Data processing

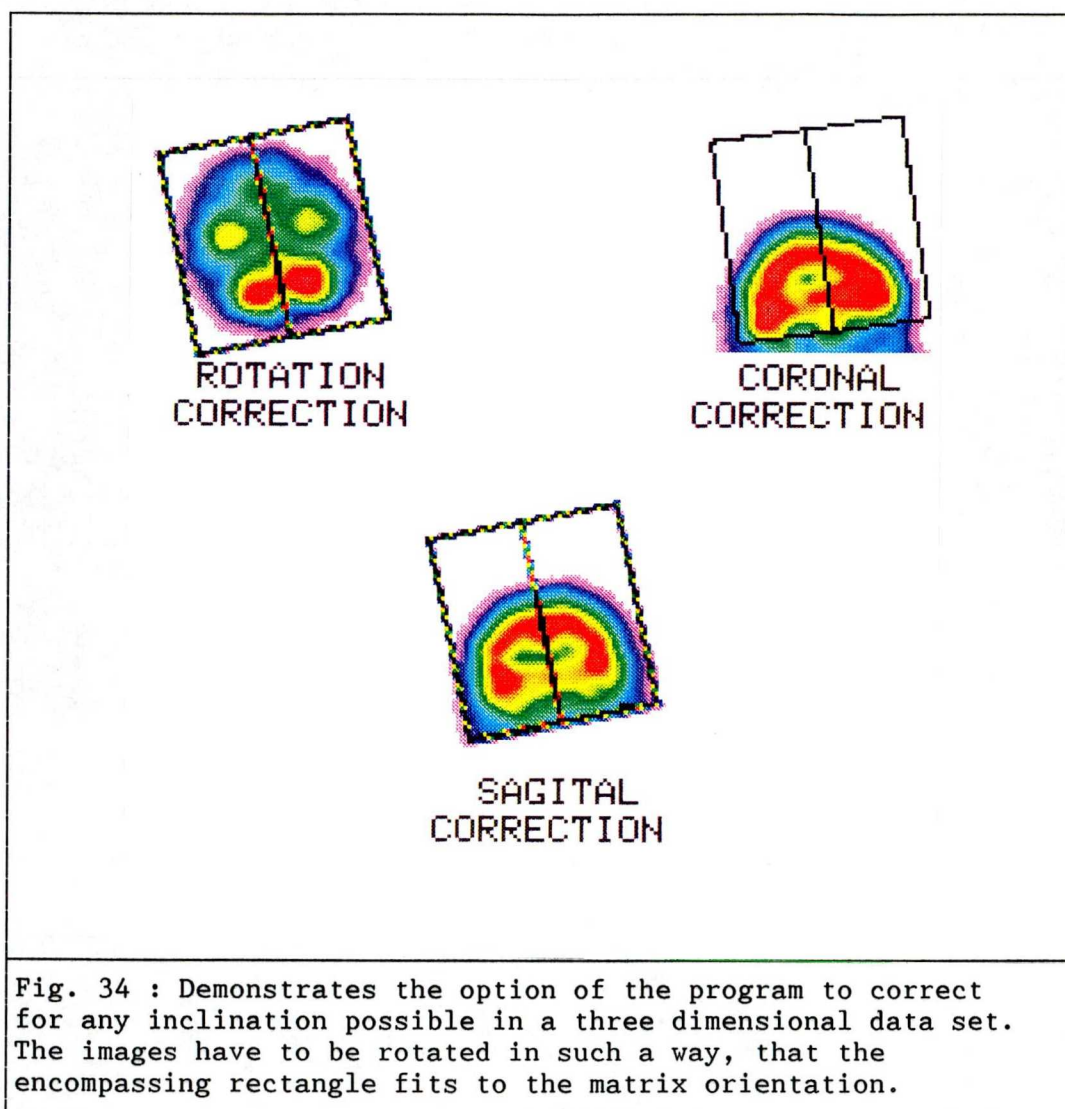
There are a number of commercially available programs on the market which allow manually or semi-automatic quantification of relative Hmpao uptake. However, quantification of regional findings of SPECT-studies of the brain is difficult and is usually performed by comparing left and right side count rate differences by regions drawn manually in selected slices. To overcome these shortcomings a method was developed, that allows quantification of findings in tomographic brain studies in comparison to the distribution of a normal data base, including the dedicated standard deviations. The basic steps of this application consist of 5 points:

- 1 the reorientation of tomographic information, including calculation of oblique slices and the relation of data to anatomical structures.
- 2 Transformation to a circle data set by radiant interpolation.
- 3 the comparison of each circle with a normal reference including the possibility to create normal pattern.
- 4 the classification of the defect by observing the statistical conditions
- 5 retransformation into the organ shape to maintain a adequate presentation of the results.

This algorithm requires a modified application of circle reference method on tomographic studies.

5.3.1 Reorientation of the tomographic data-set

One of the problems when obtaining a standardized and aligned set of tomograms from an individual study is the fact that a data set as a result of a Spect-acquisition and reconstruction algorithm is always oriented with respect to rotation axis. However, if fixed ROIs should be used and if automatic processing should take place, the data should be oriented with respect to characteristic organ landmarks. Therefore a procedure has been developed that corrects for mispositioning of patient's head. An angle-correction for each of the possible inclinations in a cubic set of data was implemented to maintain the reference of the slices onto a anatomical relevant and reproducible plane, which is the meatoorbital plane in our program. (Fig. 34)



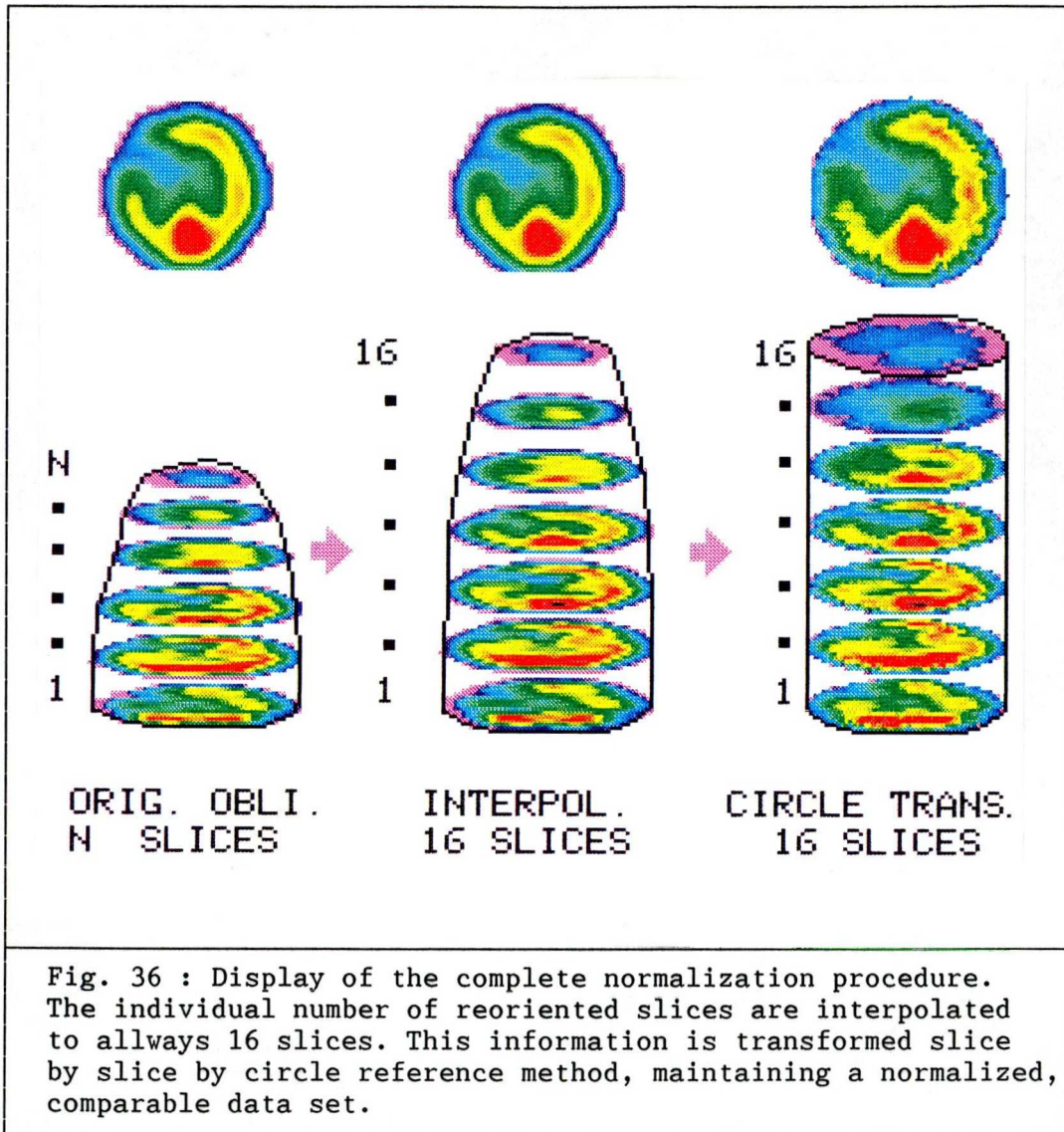
5.3.2 Axial normalization

Aim of the procedure is to maintain a fully comparable tomographic data set. As a consequence of the individual size of the brain an individual number of organ slices is provided by the reconstruction algorithm. A second normalization step is involved which transforms the individual number of slices into 16 standard slices by a simple interslice interpolation. (Fig. 35). This completes the

normalization in one dimension. The normalization of the other two dimensions are accomplished by the documented circle-reference-method.

5.3.3 Application of CRF-method in brain spect studies

The resulting 16 slices were now transformed slice by slice into a comparable form by the circle-reference method. Therefore an edge detection algorithm was included to outline regions of brain in each of the 16 slices. This was done by a relatively simple procedure, because the target to background ratio in such a study is high. The points of gravity were determined inside all of the 16 slices. From these points, the count density profiles of the radii, which are of various length, were obtained in 360 sampling angles and were transformed into a 64 by 64 matrix, with the diameter of the standard circle being 60 pixel in size. The profiles of each angle were transferred into the equivalent radius profile of the reference circle, resulting in a cylindric presentation of the tomographic data set. (Fig. 35). It should be mentioned that the normalization procedure even to that point is fully reversible.



5.3.4 The standardization of the data set

In contrast to positron emission tomography Spect do not deliver absolute values in terms of blood-flow/volume-/time, but only relative values of tracer uptake. To maintain a quantification of the data set a standardization has to be performed to get rid of individual acquisition

parameters like injected dose, individual, physiological Hmpao-uptake variation, absorption differences in different patients, camera sensitivity differences and others. These potential influences were eliminated by a standardization of the count rate on three different target values.

The first normalization procedure keeps the counts in all 16 slices constant, this was called the total count standardization.

The second procedure was to keep the maximal voxel count in the region of cerebellum constant, this was called the cerebellum normalization method. This step was chosen to handle with situations where a general perfusion depression of the cerebrum is masked by a total count standardization.

The third procedure was to keep the counts of each of the 16 slices constant, this was called the slice standardization method.

It is obvious that only data sets standardized with the same procedure can be compared numerically. Therefore for each standardization philosophy separate normal pattern and normal values have to be maintained.

5.3.5 Creation of normal pattern and statistics

One major advantage of this method is the possibility of creation a normal reference data set. This procedure can be performed in any laboratory to calculate its own data base of normal brain perfusion. In our institution out of our data base 11 HMPAO-studies of patients having with a high probability normal perfused brains were transformed into the reference circles 16 slices each. After applying the different normalization and standardization procedures the information is superimposed and added. The three re-

sulting data sets were then divided by the number of normal subjects resulting in a voxel by voxel "mean" image set as normal references. (Fig. 37). The same procedure allows computing of the belonging three sets of standard deviation image for each tomograph and for each normalization procedure. (Fig. 37). (Ref. 50)

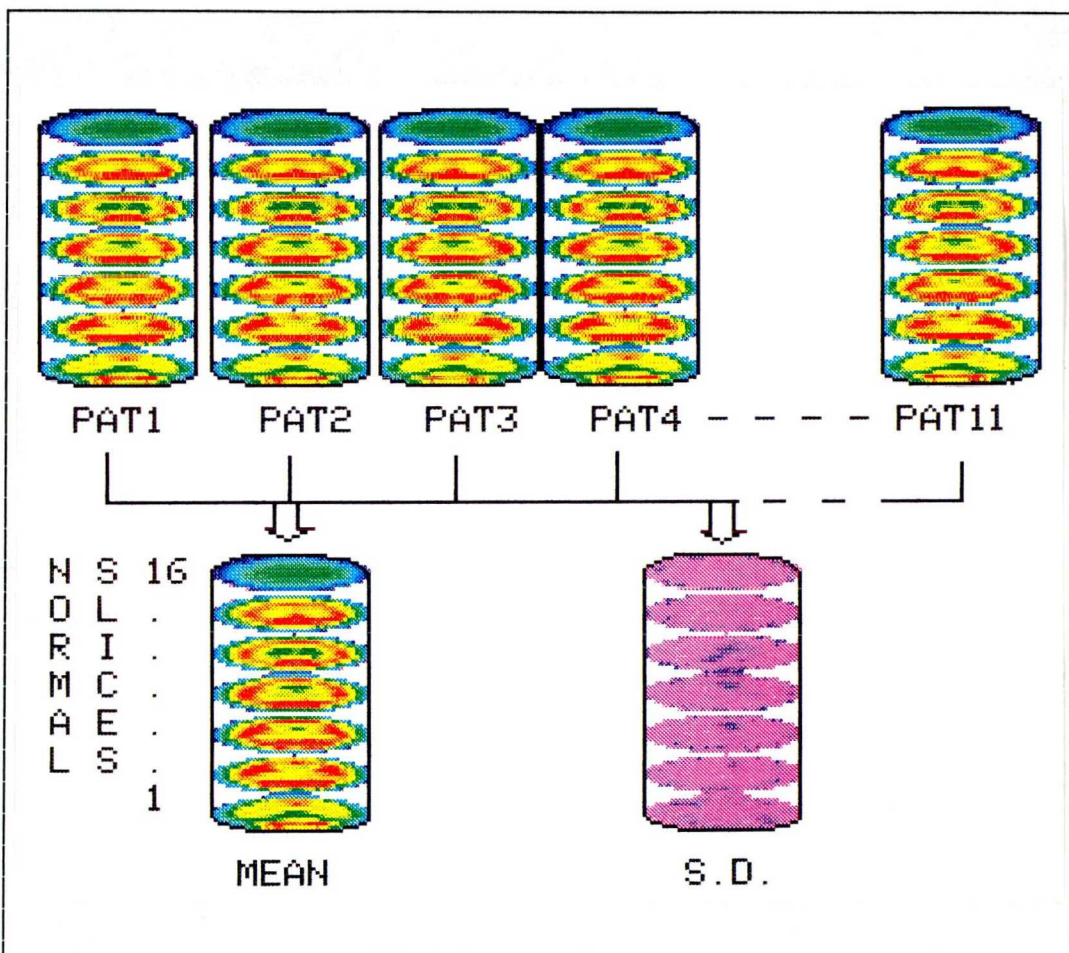
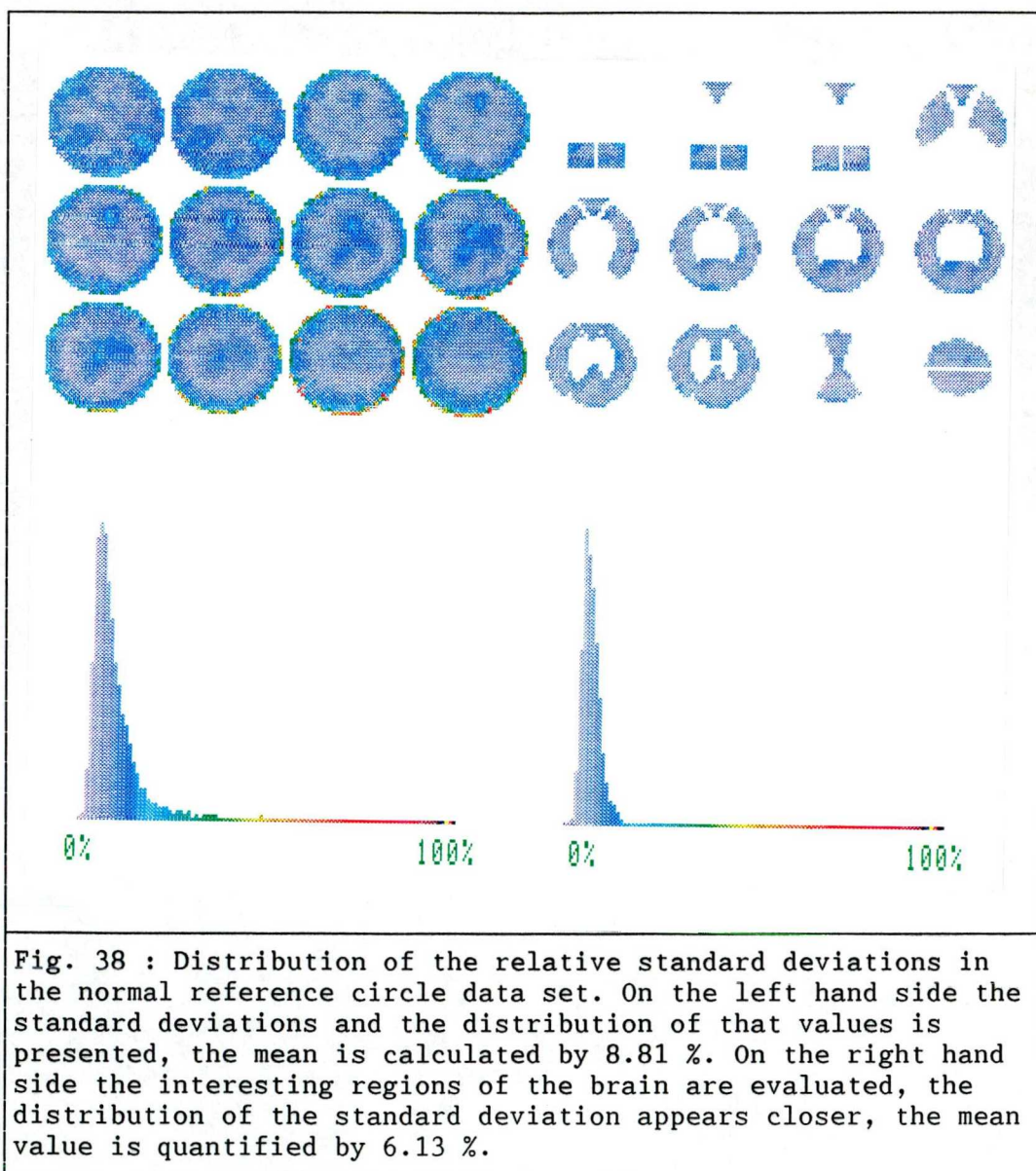


Fig. 37 : Creation of a normal reference set against which any individual study can be compared. 11 studies of normal subjects are transformed in the circle presentation. The mean values and the standard deviation values are calculated voxel by voxel and stored to a database of normal.



5.3.6 The error of the method

It is difficult to identify characteristic landmarks and known structures in the brain perfusion scan. However the quality of quantification depends on that definition. Therefore an important sign of the method compliance is the relative standard deviations of the normal data set. Large standard deviations mean that the overlay of the structures is insufficient or that the individual variation in brain perfusion is too extensive to find a reasonable normal pattern. Fig. 38 shows the histogram of the relative standard deviations of each voxel in the normal reference data set. For the total count standardization the mean of the standard deviation is 8.81 % and in the defined ROIs of the brain the standard deviation calculates to 6.13 %. In conclusion, each voxel in the circle transformed data set has a normal count value and a standard deviation range as a statistical description, and these values are in a range which allows sensitive recognition of depressed perfusion of the brain. (Fig. 38)



5.3.7 ROI definition in circle reference data set

Another way of quantification is provided by defining sectorial ROI's in the circle dimension according to the blood flow distribution of the major brain arteries. Again the major advantages of this method are obvious, because the ROIs once defined in the circle presentation can be used for automatic processing of any individual brain study. (Fig. 39)

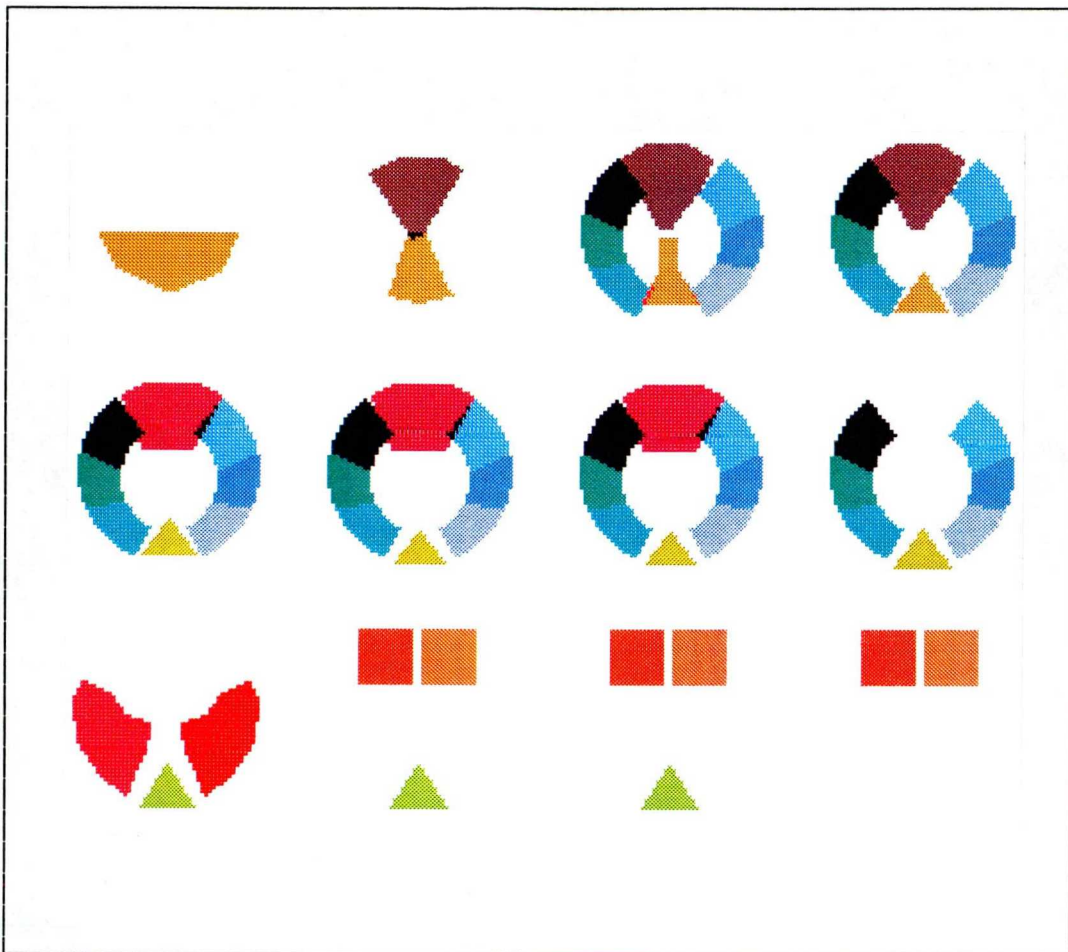


Fig. 39 : Presentation of the once defined regions of interest in the circle dimension. These regions can be applied on any individual study, processed with the same method.

For that purpose regions are defined through different slices of the circle reference data set by an experienced nuclear medicine physician. These ROIs describe coherent anatomical structures in the brain, some referring to different slices. These regions once defined may be used for any individual study because the anatomical link is done in the same way. By the values of these regions it is now possible to obtain normal values of Hmpao-uptake for

each region defined within the standard 16 circles. Values of any individual study may then be compared against the values of normal and the standard deviation in ROIs.

Tab. 10 - 12 show the counts in the defined regions together with their standard deviations for all three normalization procedures.

TABLE 10

Normal values and standard deviations of the normal reference
Total count standardization

Region of interest	N	MEAN	S.D.	C.V.
Cer.med. ri. front.	11	8330760	267041	3.205
Cer.med. ri. media.	11	8376096	221782	2.648
Cer.med. ri. occip.	11	10806263	269522	2.494
Cer.med. le. front.	11	8349751	354385	4.244
Cer.med. le. media.	11	8249234	228314	2.768
Cer.med. le. occip.	11	10957118	270186	2.466
cer.ant. caudal	11	3224114	133586	4.143
cer.ant. medial	11	3245034	158469	4.883
Cer.ant. cranial	11	8857760	460453	5.198
Cerebellum ri.	11	6903182	256931	3.722
Cerebellum le.	11	6927360	332540	4.800
Cer.med. ri. caudal	11	4089437	111750	2.733
Cer.med. le. caudal	11	3949378	79962	2.025
Cer.post. caudal	11	12490490	449823	3.601
Cer.post. cranial	11	15497772	268629	1.733
Cer.media. ri. total	11	27513120	451222	1.640
Cer.media. le. total	11	27556104	642449	2.331
Cer.ant. total	11	15326909	692150	4.516
Cer.post. total	11	27988263	637939	2.279

N = number of observations
C.V. = Coefficient of variance in [%]
all other values in counts

TABLE 11
Normal values and standard deviations of the normal reference
cerebellum standardization

Region of interest	N	MEAN	S.D.	C.V.
Cer.med. ri. front.	11	8875114	479976	5.408
Cer.med. ri. media.	11	8919653	369328	4.141
Cer.med. ri. occip.	11	11508209	490696	4.264
Cer.med. le. front.	11	8896784	561859	6.315
Cer.med. le. media.	11	8787240	435374	4.955
Cer.med. le. occip.	11	11666572	431566	3.699
Cer.ant. caudal	11	3435220	212830	6.196
Cer.ant. medial	11	3458453	248851	7.195
Cer.ant. cranial	11	9437791	654254	6.932
Cerebellum ri.	11	7346468	233226	3.175
Cerebellum le.	11	7369721	255666	3.469
Cer.med. ri. caudal	11	4355422	197884	4.543
Cer.med. le. caudal	11	4205341	151191	3.595
Cer.post. caudal	11	13300881	642659	4.832
Cer.post. cranial	11	16501518	575575	3.488
Cer.media. ri. total	11	29302977	1188130	4.055
Cer.media. le. total	11	29350597	1327715	4.524
Cer.ant. total	11	16331466	1070568	6.555
Cer.post. total	11	29802400	1152474	3.867

N = number of observations

C.V. = Coefficient of variance in [%]

all other values in counts

TABLE 12
Normal values and standard deviations of the normal reference
slice standardization

Region of interest	N	MEAN	S.D.	C.V.
Cer.med. ri. front.	11	8194074	324246	3.957
Cer.med. ri. media.	11	8219327	268767	3.270
Cer.med. ri. occip.	11	10602063	159218	1.502
Cer.med. le. front.	11	8192542	326685	3.988
Cer.med. le. media.	11	8092789	184187	2.276
Cer.med. le. occip.	11	10750745	176489	1.642
Cer.ant. caudal	11	3124772	134657	4.309
Cer.ant. medial	11	3167207	145327	4.589
Cer.ant. cranial	11	9448800	569188	6.024
Cerebellum ri.	11	6972811	257946	3.699
Cerebellum le.	11	6997800	317938	4.543
Cer.med. ri. caudal	11	3854576	112298	2.913
Cer.med. le. caudal	11	3721454	73712	1.981
Cer.post. caudal	11	12288409	334391	2.700
Cer.post. cranial	11	16110781	339492	2.107
Cer.media. ri. total	11	27015465	489320	1.811
Cer.media. le. total	11	27036077	442793	1.638
Cer.ant. total	11	15740780	759979	4.828
Cer.post. total	11	28399190	625865	2.204

N = number of observations
C.V. = Coefficient of variance in [%]
all other values in counts

The perfusion in terms of share of the total perfusion now can be calculated and is listed in tab. 13 . No significant difference in the values for the three standardization procedures was found, therefore only

numbers of total count standardization are presented. These values are dependent on the defined ROIs and on the method, but represent a consistent normal target for any processed study. All individual studies processed with this program are expected to have the same perfusion distribution in the predefined ROIs, if they should be expected to be normal.

Table 13
Perfusion share on total perfusion

Region of interest	share at total brain perfusion
Cer.med. ri. front.	6.92 ± .221
Cer.med. ri. media.	6.96 ± .183
Cer.med. ri. occip.	8.98 ± .223
Cer.med. le. front.	6.94 ± .294
Cer.med. le. media.	6.86 ± .189
Cer.med. le. occip.	9.11 ± .224
Cerebellum ri.	5.74 ± .275
Cerebellum le.	5.76 ± .157
Cer.media. ri. total	22.88 ± .375
Cer.media. le. total	22.91 ± .534
Cer.ant. total	12.74 ± .573
Cer.post. total	23.27 ± .524

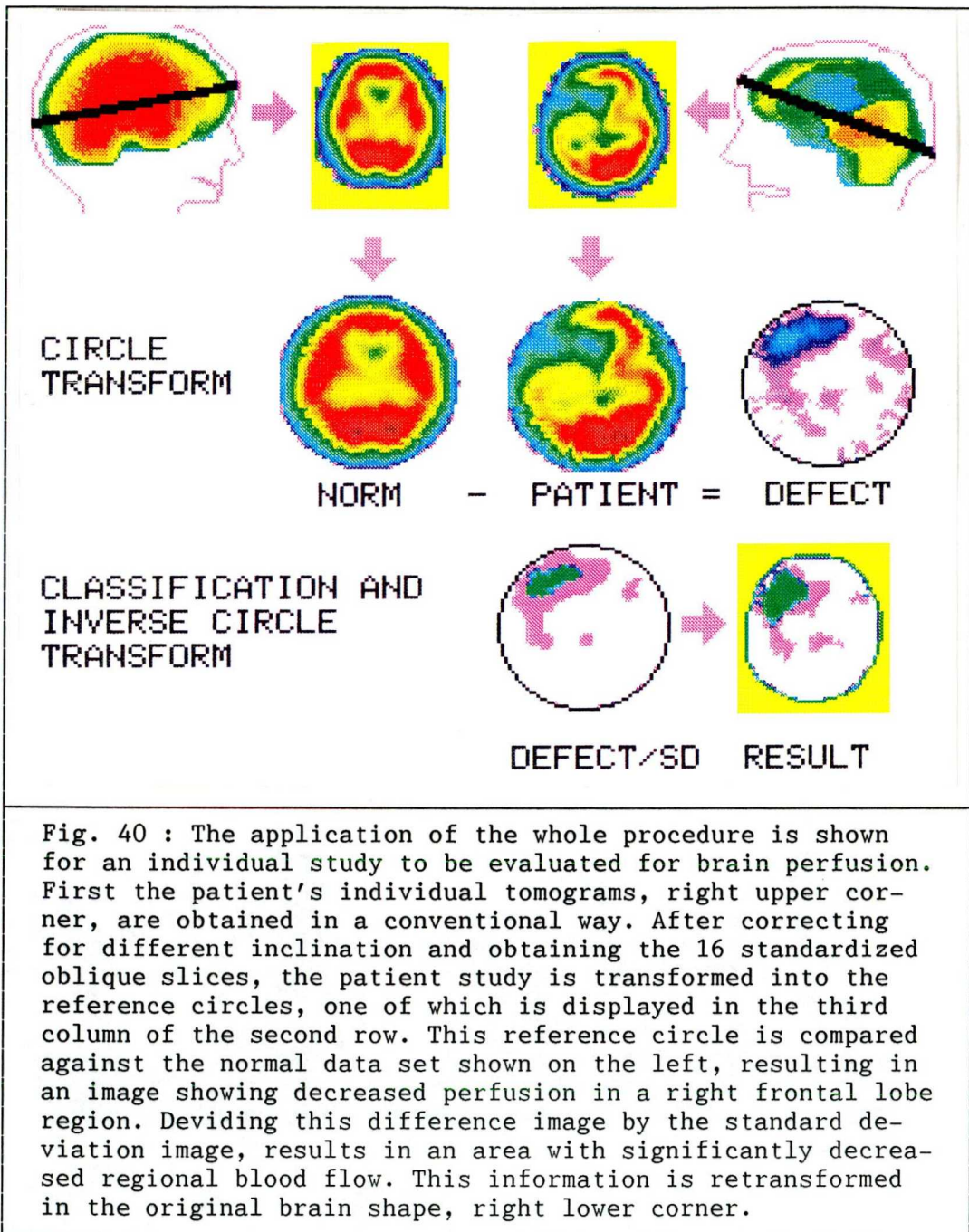
The coefficient of variance (C.V.) is defined as the relative standard deviation in the interesting regions describing the homogeneity of the circle transformed data

sets of the 11 normal subjects. This was calculated for each of the three data sets, provided by the specific normalization procedure. In individual patient studies numerical values can be obtained in terms of percent HMPAO-uptake compared to the mean values in the same region for all three normalization procedures as shown in tab. 10 - 12. The coefficient of variance given in the table outline the range of normal for each ROI.

With respect to voxel quantification, deviation from the normal are observed as significant if voxel count rate is depressed in the mean by more than two standard deviations with respect to normal value. By this application voxel count depression in the brain region of about 12 % are detected to be significant. This is a low value compared to other methods of ROI-quantification where normal ranges of ROI-values are of this order. (Ref. 48)

5.4 Application of the method in an individual study

In an individual study the transverse slice information is obtained by on the fly backprojection algorithm, including observation of correction for inhomogeneity and center of rotation errors. This information is reorientated relatively to the manually given meato-orbital plane. These oblique slices undergo the normalization procedure. The result consists of a standardized and normalized circle reference data set of 16 slices compared to a normal reference. The deviation to the normal can be weighted by the according standard deviation voxel by voxel. To maintain an adequate presentation the information of the defect circles is retransformed to original shape of the organ. (Fig. 40)



It is likely to retransform the normal reference to the individual patient's organ shape as demonstrated in Fig. 41 . By that method the comparison between individual and

normal pattern could be done easily by simple subtraction of the images. However, it is not possible, due to mathematical reasons, to retransform the standard deviation values. Therefore a quantification of the defect with that procedure is not possible.

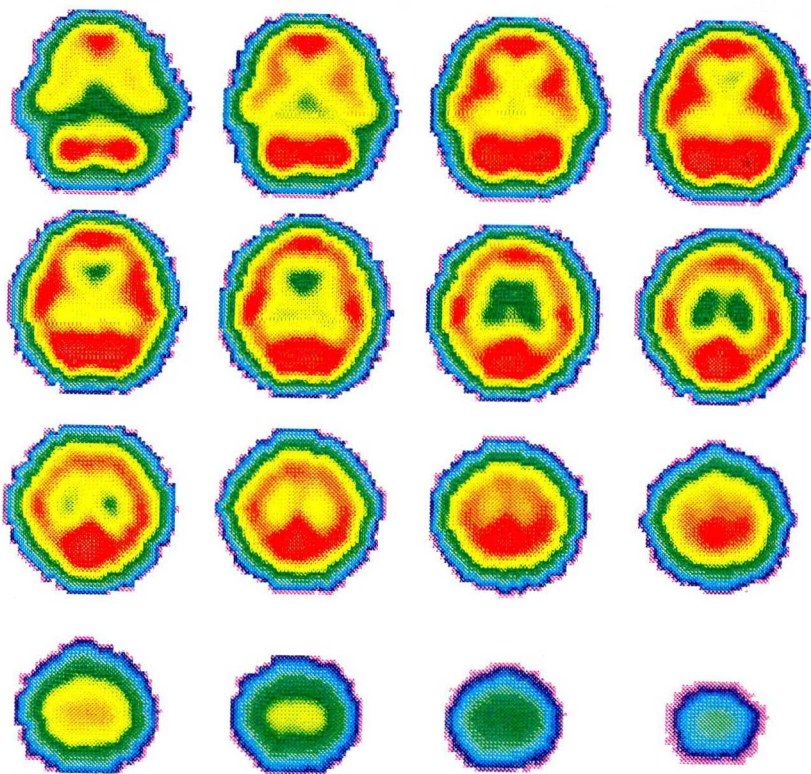


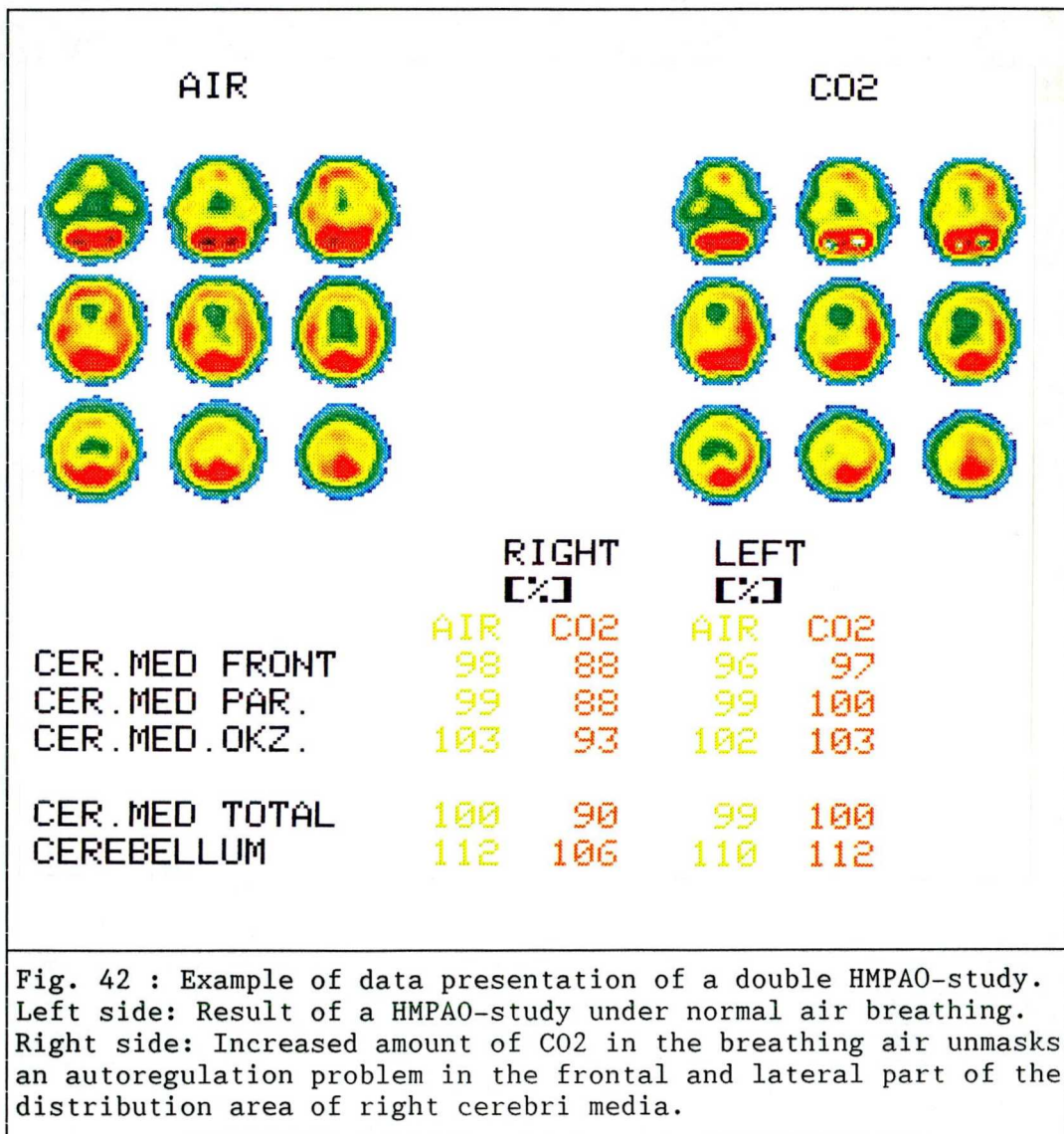
Fig. 41 : Normal reference data set consisting of the information of 11 normal brain perfusion studies retransformed into an individual patient's brain shape.

5.5 Recent and published applications of the method

Cerebral autoregulation protects the brain against changes in systemic blood pressure. If autoregulation was not present, an otherwise trivial fall in the blood pressure e.g. during sleep might cause tissue ischaemia and possible cell damage. Likewise a sudden rise in arterial pressure, e.g. during isometric muscular work would in absence of autoregulation lead to passive vasodilatation of arterioles and capillaries and a potential for development of brain oedema. Moreover, autoregulation of cerebral blood flow is a physiological regulatory mechanism of major importance for the daily regulation of cerebral perfusion. Although, the mechanism of the autoregulation remains obscure, it is obvious that its reaction can be provoked by increasing the amount of CO² in the breath air. The reaction on this provocation can be measured by transcranial Doppler ultrasound. Widder et. al. created a method to quantify the relative increase of blood flow by Doppler ultrasound technique and thus classifying the degree of autoregulation depression.(Ref. 52,53).

A group of patients (n=34) were investigated in cooperation with the neurological department to evaluate disturbances in cerebral autoregulation. HMPAO-Spect studies were performed on patients with known stenosis of the internal cerebral artery during breathing normal air and in a second session during breathing air with increased CO². The difference in HMPAO-uptake were quantified with the method described above and compared to transcranial Doppler results. (Fig. 42).The HMPAO-Spect technique with air and CO² breathing could classify the patients with a sensitivity of 89 % and a specificity of 84 % in comparison to the nonperfect ultrasound technique. Furthermore region of

depressed perfusion, as defined by depressed HMPAO-uptake, could be outlined in opposite to the global observation of the neurological routine method. (Ref. 49).



6. Conclusion

One major subject of nuclear medicine is the evaluation of reproducible, comparable and quantified results by diagnostic radiotracer tests. The quality of the results, however, depends on the performance of the hardware and on the used programmes and algorithms. To further complicate the matter, the results are often produced and significantly influenced by interactions of persons with different training and skill level. Aim of this study was therefore to build up methods with minimized manual interaction. So far, individual influences of the investigators person on the results can be kept under control.

The first method built up to fulfill the previously described requirements is the so called onion-skin-method. It allows the calculation of ejection fractions and the evaluation of background counts without defining a background region. The error of the results are observed carefully with regard to statistical influences and to the relevance of the calculated background contamination to be projected to the object area.

The results are verified by computer simulation and physical modelling. The method has been applied to RNV-studies and the results correlated to angiography, came up with a strong correlation ($r = 0.945$). Values were also calculated from a normal group of patients, specifying values of reasonable ranges for the left and the right ventricle in stress and in rest. The application to the newly developed Gaspect-method is demonstrated. The ejection fraction calculated in three different views are correlated to planar RNV values. The correlation to the left ventricle

EF turned out to be excellent in all three views ($r = 0.941$ to 0.947). Correlation between Gaspect and RNV results was weak for the right ventricle ($r = 0.476$ to 0.655), thus these values remain subject for further improvements and should be verified by a right ventricle ejection fraction gold standard.

Absolute quantification in nuclear medicine faces difficulties because of the the individual shape, size and position of human organs. In the second method a general data processing procedure is presented that allows inter-individual comparison and definition of normal count density pattern of unevenly shaped scintigraphic structures. This new method is demonstrated on Fourier amplitude images of gated heart studies. The information contained in the irregularly shaped left ventricular amplitude scans was transformed into a standard sized circle by interpolating the radiant profiles of varying length from the original left ventricular ROI into the radii of the standard circle. The method was applied to 20 normal amplitude studies, which were transferred into the standard circle, allowing the statistical definition of a normal reference image. Against that database individual left ventricular amplitude images may be compared for documenting areas of significantly depressed amplitudes quantitatively. The method was applied as an example to left ventricle amplitude scan of 4 chamber view of Gaspect study. A normal scan was created out of 5 patients supposed to have normal amplitude pattern. All Gaspect studies were quantified with respect to this "normal reference". The defect score was calculated to quantify regional wall motion abnormalities globally in the different views and the results were correlated to the defect score evaluated by planar RNV.

Although the database of the normal pattern consists of only 5 cases the correlation to the planar RNV proved to be fairly close. ($r = 0.862$)

In a last step it is demonstrated, that the circle-reference-method, developed in our laboratory for heart studies is applicable also to tomographic brain studies provided a standardized correction for inclination and for the number of tomograms is performed. Normal values and pattern of HMPAO-uptake are presented with normal ranges. These values underline that the circle reference method can be used to quantify regionally planar and tomographic data.

ABREVIATIONS

BG	Background
CRF	Circle Reference Method
CT	Computer Tomography
DM	Defect Score
ED	End Diastole
EF	Ejection Fraction
ES	End Systole
FDG	Fluor DesoxyGlucose
Gaspect	Gated SPECT
HMPAO	HexaMethylPropylene Amine Oxime
LA	Long Axis
LAO	Left Anterior Oblique
LR	Left to Right Ratio of Stroke Volumes
LVEF	Left Ventricle Ejection Fraction
MBQ	MegaBeQuerel
MI	Myocardial Infarction
NMR	Nuclear Magnetic Resonance
PACS	Picture Archiving and Communicating System
PET	Positron Emission Tomography
RNV	RadioNuclide Ventriculography
ROI	Region Of Interest
RVEF	Right Ventricle Ejection Fraction
RWMA	Regional Wall Motion Abnormality
Ref	Reference
SA	Short Axis
SD	Standard Deviation
SDU	Standard Deviation Unit
SPECT	Single Photon Emission Computer Tomography
WMA	Wall Motion Abnormality
4CH	Four Chamber

Acknowledgment

The author would like to express his gratitude to Prof. Csernay and his team of the University of Szeged, especially Dr. Mester, for the possibility to present this dissertation and for the chance of cooperation, thus overcoming borders of departments and borders of countries.

Furthermore I would like to thank Prof. Adam for his way of guidance through the pitfalls of science by gentle critics and by encouraging questions.

Very special thanks to Dr. Clausen, for the years of fruitful cooperation and for giving me always the feeling to be a valuable member of the scientific team.

I would like to thank Dr. Bitter for patiently tolerating that a lot of necessary work hasn't been done, because of this dissertation.

Furthermore, the author would like to acknowledge the contribution of the late Horst Geffers, who introduced Fourier analysis to nuclear medicine and who gave the basic idea to the onion-skin-method.

References:

1. Green MV, Brody WR, Douglas MA, et al.: Ejection Fraction by Count Rate from Gated Images. J Nucl Med 19:880-883, 1978
2. Geffers H, Adam WE, Bitter F, et al.: Data processing and functional imaging in radionuclide ventriculography. Information Processing in Medical Imaging. Proceed. 4. International Conference on Data Processing and Medical Imaging. Nashville, Tennessee (1977)
3. Bitter F, Adam WE, Geffers H, et al.: Nuclear Medicine: Synchronized steady state heart investigations. Int. Symp. on Fundamentals in Technical Progress, Cmt. rend., III, press. University Liege (1979)
4. Borer JS, Bacharach SL, Green MV, et al. Real-time radionuclide cineangiography in the noninvasive evaluation of global and regional left ventricular function at rest and during exercise in patients with coronary heart disease. N Eng J Med 296:839, 1977
5. Bickel JB, Doksum KA, Linear Models Regression and Analysis of variance. In: Lehmann EL, ed. Mathematical Statistics, Oakland, Cal.: Holden-Day, INC; 1977:249-310
6. Clausen M, Henze E, Mack S et al.: Integrated display of all pertinent results of radionuclide ventriculography including a human interface adapted to the needs of technician. NucCompact 22(1990):80-84

-
7. Luig H.: Funktionsszintigraphie der linken Herzkammer. Nuklearmedizinische Erfassung schneller Funktionsabläufe zur Bestimmung der linksventrikulären Volumenkurve. Thieme Stuttgart-New York, 1984. S 186 - 201.
 8. Hör G, Schicha H, Standke R. Normwerte der Äquilibrium-Radionuklidventrikulographie. Nucl.-Med. 1990;29:186-194
 9. Goris LM, Briandet PA, Target Detection. In: Goris ML, Briandet PA, eds. A Clinical and Mathematical Introduction to Computer Processing of Scintigraphic Images. New York:Raven-Press;1983:170-201
 10. Garcia E, VanTrain KF, Maddahi J, et al. Quantification of rotational thallium-201 myocardial tomography. J Nucl Med 1985; 26: 17 - 26 .
 11. Stirner H, Buell U, Kleinhans E. Three-dimensional ROI based quantification of rest/stress Tl-201 myocardial SPECT
Nuklearmedizin 1986; 4: 128 - 133
 12. DePasquale EE, Nody AC, DePuey EG, et al. Quantitative rotational thallium-201 tomography for identifying and localizing coronary artery disease.
Circulation 1988; 77: 316 - 327
 13. Clausen M, Weller R, Henze E, et al. Separate display and quantification of myocardial scar versus ischemia in polar coordinates for myocardial ECT.
NucCompact 1988; 19: 50 - 52

-
14. Winkler C, Knoop R. Computerscintigraphischer Nachweis von Hirntumoren durch statistische Vergleichskalkulation anhand einer Normmatrix. In: Camera-Scintigraphie, DKFZ Bericht, Heidelberg, 1968, pp 44 - 49
 15. Adam WE, Tarkowska A, Bitter F, et al. Equilibrium (gated) radionuclide ventriculography. Cardiovasc Radiol 1979; 2: 161 - 170
 16. Henze E, Tymiec A, Delagardelle C, Adam WE, Bitter F, Stauch M. Specification of regional wall motion abnormalities by phase analysis of radionuclide angiograms in coronary artery disease and non-coronary artery disease patients. J Nucl Med 1986; 27: 781 - 787
 17. Douglas KH, Links JM, Chen DCP, et al. Linear discriminant analysis of regional ejection fraction in the diagnostic of coronary artery disease. Eur J Nucl Med 1987; 12: 602 - 604
 18. Bonow RO, Viale OF, Bacharach SL, et al. Asynchronous left ventricular regional function and impaired global diastolic filling in patients with coronary artery disease: reversal after coronary angioplasty. Circulation 1985; 71: 287 - 307
 19. Pavel DG, Byrom E, Lam W, et al. Detection of regional wall motion abnormalities using phase analysis of gated cardiac studies. Clin Nucl Med 1983; 8: 315 - 32

-
20. Standke R, Hoer G, Maul FD. Fully automated sectorial equilibrium radionuclide ventriculography. Proposal of a method for routine use.
Eur J Nucl Med 1983; 8: 77 - 83
21. Podreka I, Suess E, Goldenberg G, et al. Initial experience with Tc-99m HMPAO brain SPECT.
J Nucl Med 1987; 28: 1657 - 1666
22. Perani D, Di Piero, Vallar G, et al. Technetium-99m HMPAO-SPECT study of regional cerebral perfusion in early Alzheimer's disease.
J Nucl Med 1988; 29: 1507 - 1514
23. Clausen M, Weller R, Henze E, Bitter F, Adam WE:
Differenzierende Darstellung und Quantifizierung der Myokardnarbe und der Belastungsischämie im Polarkoordinaten für die Myokard-ECT.
NucCompact 19,50-52 (1988)
24. Weller R, Clausen M, Henze E, Sigmund E, Bitter F, Adam WE:
A general processing method for SPECT and PET-Studies of the brain using reference-circle-method.
NE:Schmidt, Helmut A.E.(Hrsg.); European Nuclear Medicine Congress<1989, Straßbourg>
Nuclearmedicine/Supplementum
25. Henze E, Hildebrand P, Hellwig D, Clausen M, Weller R, Wanjura D, Kress P, Bitter F, Adam WE:
Differentiation between infarction and cardiomyopathy in left bundle branch block by parametric radionuclide imaging.
Am J Physiol Imaging 3:121-127 (1988)

-
- 26 Clausen M, Henze E, Mack S, Langhans J, Weller R, Ost W, Mester J, Adam WE:
Integrated display of all pertinent RNV results of radionuclide ventriculography including a human interface adapted to the needs of the technician.
NucCompact 22 (1990):80-84
- 27 Clausen M, Weller R, Henze E, Bitter F, Adam WE:
Differenzierende Darstellung und Quantifizierung der Myokardnarbe und der Belastungsischämie im Polarkoordinaten für die Myokard-ECT.
NucCompact 19:50-(1988)
- 28 Clausen M, Henze E, Schmidt A, Lietzenmayer R, Weller R, Stauch M, Hombach V, Adam WE: The contraction fraction (CF) in myocardial studies with Technetium-99m-isonitrit (MIBI) - correlations with radionuclide ventriculography and infarct size measured by SPECT.
Eur J Nucl Med 15:661-664 (1989)
- 29 Weissmüller P, Clausen M, Henze E, Weller R, Mayer U, Ostrhues H, Richter P, Kochs M, Adam WE, Hombach V:
Lokalisation vorzeitiger und ektopter ventrikulärer Erregung mittels einer neuen nuklearmedizinischen Schichttechnik
ZKardiologie 79:529-534(1990)
- 30 Mester J, Henze E, Clausen M, Weller R, Holtmeier S, Bitter F, Bair HJ, Adam WE: Amplitudendefekt bei Patienten mit Aorteninsuffizienz. Pathologie oder Artefakt?
NucCompact 20:202-205 (1989)
- 31 Mester J, Clausen M, Henze E, Ochsenkühn R, Lietzenmayer R, Weller R, Adam WE: Einfluß einer dreidimensionalen Datenstabilisierung in der Radionuklidventrikulographie

-
- auf den statistischen Zählfehler der Ejektionsfraktion.
Nucl.-Med. 1990;29:109-112
- 32 Clausen M, Henze E, Weller R, Graf G, Weissmüller P, Lietzenmayer R, Kress P, Weritz D, Mack S, Ochsenkühn R, Mester J, Adam WE: Tomographische Radionuklidventrikulographie (RNV) mit rekonstruierten planaren Ansichten senkrecht zur Körperachse (ISPECT).
NucCompact 21 (1990):95-99
- 33 Clausen M, Weismüller P, Weller R, et al: Doppelangulierte, integrale Emissionscomputertomographie (DA-ISPECT) bei der Radionuklidventrikulographie (RNV) mit rekonstruierten planaren Ansichten ausgerichtet zur langen Herzachse.
NucCompact 21 (1990):167-170
- 34 Clausen M, Henze E, Mack S, Langhans J, Weller R, Ost W, Mester J, Adam WE: Integrierte Darstellung der Ergebnisse der Radionuklidventrikulographie bei einfacher Benutzeroberfläche, geeignet zur Auswertung durch die MTA.
NucCompact 22:80-84 (1990)
- 35 Tarkowska A, Bitter F, Weller R, Adam WE: Normalization of Fourier Amplitudes of ECG-Gated Radionuclide Ventriculography. Comparison of two methods.
NucCompact 22 (1990):50-55
- 36 Tarkowska A, Bitter F, Weller R, Henze E, Adam WE: Quantification of Fourier Amplitudes Using the Reference Circle Method.
NucCompact 21 (1990): 172-176
- 37 Clausen M, Weismüller P, Henze E, Weller R, Mester J, Graf G, Lietzenmayer R, Leutloff U, Kochs M, Hombach V, Adam

-
- WE: Integrated emission computed tomography (ISPECT) during radionuclide ventriculography (RNV) for detection of WPW-syndrome.
- NE: Schmidt, Helmut A.E.(Hrsg.); European Nuclear Medicine Congress<1990 Amsterdam>
Nuclearmedicine/Supplementum
- 38 Clausen M, Weismüller P, Henze E, Weller R, Lietzenmayer R, Kress P, Leutloff U, Kochs M, Hombach V, Adam WE:
Lokalisation vorzeitiger und ektooper ventrikulärer Erregung mittels einer neuen nuklearmedizinischen Schichttechnik.
Radioaktive Isotope in Klinik und Forschung. 19. Internationales Symposium Badgastein. Jan 1990
Schattauer Verlag
- 39 Goris ML, Daspit SG, McLaughlin P et. al.: Interpolative background subtraction.
J Nucl Med 17:744-747 1976
- 40 Bitter BA, Bitter F, Weller R, Tarkowska A, Henze E, Kress P, Clausen M, Adam WE:
Image resemblance, a direct approach on a pixel base.
Eur J Nucl Med 16:515 (1990)
- 41 2nd Report of TACARD: Collective data on nuclear cardiology
Eur J Nucl Med 18:A9-A12 (1991)
- 42 Fishmann AJ, Moore RH, Gill JB, Strauss HW.
Gated blood pool tomography: A technology whose time has come.
Sem Nucl Med 1989;21:13-219.

-
- 43 Corbett JR, Jansen DE, Lewis SE, et. al.:
Tomographic gated blood pool radionuclide
ventriculography: analysis of wall motion and left volume
ventricular volumes in patients with coronary artery
disease.
J Am Coll Cardiol 1985;6:349-358
- 44 Gill JB, Moore RH, Tamaki N, et. al.:
Multigated blood-pool tomography: New method for the
assessment of left ventricular function.
J Nucl Med 1986;27:1916-1924
- 45 Graf G, Mester J, Clausen M, et. al.:
Reconstruction of Fourier Coefficients: A fast method to
get polar amplitude and phase images of gated SPECT.
J Nucl Med 1990;31:1856-1861
- 46 Moore LM, Murphy PH, Burdine JA.
ECG-gated-emissions-computed tomography of the cardiac
blood pool.
Radiology 1980;134:233-235.
- 47 Itti R, Casset F, Phillippe L, Fauchier JP, P. Cosnay,
Huguet R:
Characterization of right or left ventricular contraction
heterogeneity using Fourier phase analysis.
Eur J Nucl Med 14 (1988):196-202
- 48 Podreka I, Baumgartner C, Suess E et. al.:
Quantification of Regional Cerebral Blood Flow with
IMP-SPECT. Reproducibility and Clinical Relevance of Flow
values.
Stroke 1989; 20:183-191

-
- 50 Clausen M, Henze E, Widder B, Weller R, Lietzenmayer R, Kornhuber H, Adam WE:
Regionale Differenzierung dopplersonographischer Befunde im Bereich der Cerebri Media unter CO₂ Atmung mit Hilfe der Tc-99m-HMPAO SPECT.
Nucl.-Med. 2:10-11 (1989)
- 51 Weller R, Clausen M, Mester J, Henze E, Adam WE:
Normal pattern and region values of HMPAO-uptake and the statistical description in a group of normals.
Eur J Nucl Med 16:475 (1990)
- 52 Widder B:
The doppler CO₂-test to exclude patients not in need of extracranial/intracranial bypass surgery.
Journal of Neurology, Neurosurgery and Psychiatrie 52,38-42 (1989)
- 53 Widder. B:
Transcranial Doppler CO₂-Test for the Detection of Hemodynamically Critical Carotid Artery Stenoses and Occlusions
Eur Arch Psychiatr Neurol Sci 236, 162-168 (1986)

